Performance Evaluation of Transmit Diversity Techniques in the CDMA2000 Standard

by

Murali S. Vajapeyam

Submitted to the Department of Electrical Engineering and Computer Science

in Partial Fulfillment of the Requirements for the Degree of

Master of Engineering in Electrical Engineering and Computer Science

at the Massachusetts Institute of Technology

August 17, 2004

Author_____
Department of Electrical Engineering and Computer Science
August 17, 2004

Certified by_____
Levent Aydin
Senior Staff Engineer/Manager
VI-A Company Thesis Supervisor

Certified by_____
Lizhong Zheng
Assistant Professor of Electrical Engineering
M.I.T. Thesis Supervisor

Accepted by_____
Arthur C. Smith
Chairman, Department Committee on Graduate Theses

Performance Evaluation of Transmit Diversity Techniques in the CDMA2000 Standard

by

Murali S. Vajapeyam

Submitted to the

Department of Electrical Engineering and Computer Science

August 17, 2004

In Partial Fulfillment of the Requirements for the Degree of

Master of Engineering in Electrical Engineering and Computer Science

ABSTRACT

This thesis evaluates the performance of two forward-link transmit diversity techniques in the CDMA2000 standard: Space-Time Spreading (STS) and Phase-Sweep Transmit Diversity (PSTD). For each technique, the evaluation consists of conducting 9.6 kbps Markov calls in the field and measuring the mean forward-link fundamental-channel (F-FCH) transmit power required to achieve a 1% frame error-rate (FER) at the mobile receiver. The required transmit power is used to compute an estimate of cell capacity as measured by the number of supported users, assuming a fixed total transmit power at the base station. It is observed that enabling STS increases capacity by up to 80% if all mobiles support STS, but capacity is reduced by up to 20% when fewer than 35% of the mobiles support the technique. The capacity loss results from interference of the diversity-antenna signal on mobiles that do not support STS; such interference causes an F-FCH transmit power increase of up to 1.5 dB in multipath Rayleigh-faded channels, as observed in lab experiments. PSTD, which does not require mobile-specific support, was found to improve cell capacity by 12% according to the field experiments.

VI-A Company Thesis Supervisor: Dr. Levent Aydin

Title: Senior Staff Engineer/Manager, Qualcomm Incorporated

M.I.T. Thesis Supervisor: Dr. Lizhong Zheng

Title: Assistant Professor, Dept. of Electrical Engineering and Computer Science, MIT

Acknowledgements

I would first like to thank Dr. Lizhong Zheng, my MIT thesis supervisor. His coaching was crucial in helping me establish the connections between the research I did at Qualcomm and the existing academic literature. I particularly appreciate his willingness to spend hours at a time discussing various topics with me and clearing my misconceptions. Furthermore, his high standards always pushed me to work harder, contributing to improve both the quality of the thesis and my knowledge in the field.

I would also especially like to thank Dr. Levent Aydin, Senior Staff Engineer at Qualcomm. As project supervisor, he was responsible for tutoring and directing me through the entire course of the project, being always prompt in answering my questions both during the research stage and during the thesis writeup stage. Regarding the latter, his extensive feedback on the initial draft of the thesis was invaluable in guiding me towards the final version.

In addition, I would like to thank various Qualcomm employees whose help was crucial in the successful completion of this project. In particular, I would like to thank Shim Patel (Senior Staff Engineer/Manager) for having tutored me during the first month of my stay and getting me up to speed on the existing research; Mohan Kanthaswamy (Senior Engineer) for having performed much of the lab and field testing at the initial stages, and later teaching me how to do it; Johnny Lim (Field Technician) and Lucky Vorarath (Driver) for performing over 100 drives (!) along the field routes in the data-collection process; Walid Hamdy (Director of Engineering) for following the project closely throughout and giving valuable suggestions; all other Qualcomm employees who directly or indirectly contributed to the project at various stages.

Finally, I would like to thank Dr. Kenneth Stevens, my academic advisor, for his continuous support for my ambitious academic endeavors. Last but not least, I would like to thank my brother and my parents for their constant moral support; their help ensured that I never lacked the motivation to work hard and bring the project to a successful conclusion.

Table of Contents

Introduction

A wireless channel typically presents multiple propagation paths – *multipaths* – for the signal to travel from the transmitter to the receiver. Each multipath acts as a separate channel, applying an attenuation and phase shift to the transmitted signal. As a consequence, a receiver in a wireless system typically sees different replicas of the transmitted signal with various amplitudes and phases. In addition, these amplitudes and phases are continuously changing due to movement of the transmitter, receiver or surrounding structures; as a result, the signal replicas change from adding constructively to adding destructively at the receiver, and vice-versa. The consequence is a phenomenon known as *fading*, consisting of a rapid fluctuation of the received signal strength over short periods of time.

In a fading channel, the probability of low signal-to-noise ratio (SNR) at the receiver is much larger than in a non-fading channel. As a result, for any particular transmit scheme, a fading channel demands significantly larger transmitted power to achieve a target error-rate, compared to a non-fading channel.

In order to reduce this gap in required transmitted signal power, communication systems often support some form of diversity in the signal. *Diversity* consists of providing the receiver with multiple samples of the signal in such a way that the fading processes for the different samples are mutually uncorrelated. If the different fading processes are indeed uncorrelated, the probability of low SNR at the receiver is greatly reduced, and so is the performance gap between a fading channel and a non-fading channel.

Various diversity techniques are already deployed in today's communication systems. Three important types of diversity are time diversity, frequency diversity and antenna diversity**.**

Time diversity techniques typically consist of transmitting multiple coded samples of the signal over time. This method requires that the different samples be transmitted sufficiently far apart in time so that they undergo uncorrelated fading processes. As such, time diversity can be ineffective in *slow-fading* channels where deep fades persist for extended periods of time. Increasing the time gap between the different samples is not always an option, especially in applications with tight latency constraints (such as voice calls).

Frequency diversity techniques attempt to place multiple coded samples of the signal at various frequencies, or alternatively, attempt to spread the signal across a wide frequency band; in particular, the latter is the technique used by spread-spectrum systems such as IS-95 and cdma2000. For frequency diversity to be effective, the utilized spectrum has to be broad enough to ensure that fading is uncorrelated at the different frequencies; in other words, frequency diversity is of little help if the channel applies the same fade across the entire signal bandwidth (a channel scenario known as *flat fading*).

Antenna diversity is a technique that attempts to achieve diversity by using multiple antennas at either the transmitter or the receiver, giving rise to *transmit diversity* and *receive diversity* techniques, respectively. This form of diversity relies on the assumption that if the antennas are located sufficiently far apart, the signals from or to the individual antennas face uncorrelated fading processes. Antenna diversity can be especially useful in slow and flat fading scenarios, where time and frequency diversity techniques are less effective.

The objective of this thesis is to evaluate the performance of 2-antenna transmit diversity techniques in the forward-link, for mobiles and base-stations complying with the cdma2000 standard; these techniques employ two transmitter antennas at the base base-station, with one antenna being denominated *common antenna* (or *main antenna*) and the other being denominated *diversity antenna*. The two techniques evaluated in this thesis are *Space-Time Spread* (STS) and *Phase-Sweep Transmit Diversity* (PSTD); the performance of these two techniques are compared against the performance of the standard one-transmit antenna case, referred to as *No-Transmit Diversity* (NTD).

Space-Time Spread (STS) was originally proposed in [9] and is essentially an adaptation of Alamouti's scheme (originally proposed in [8]) for the cdma2000 standard. In this scheme, each symbol is transmitted from both antennas. The mobile, on its turn, decodes the symbols from each antenna separately, and combines them for improved diversity.

Phase-Sweep Transmit Diversity (PSTD) is a heuristic approach that attempts to artificially accelerate the channel's fading process, thereby avoiding extended periods of deep fade that result in degraded performance. The technique consists in transmitting the same signal from both antennas, but applying a small frequency offset (equivalently, a phase-sweep) to the diversity-antenna signal with respect to the common-antenna signal; the purpose of the phase-sweep is to artificially "fast-fade" the channel and improve the benefits of time diversity.

From the point of view of the mobile receiver, a PSTD cell is identical to a NTD cell; as such, PSTD does not require mobile-specific support and can be deployed at the discretion of the base-station. STS, on the other hand, requires mobile-specific support; therefore, legacy mobiles cannot take advantage of the technique. Even worse, enabling STS can actually result in a significant degradation to legacy NTD mobiles. One dimension of this study is the quantification of this degradation under different cell configurations and channel scenarios.

While simulation results have shown that both STS and PSTD provide substantial improvement compared to NTD, no study has quantified this improvement based on actual field data; such field-based evaluation is the main focus of this thesis. Another important dimension of the study is to use the field results to come up with realistic estimates of the improvement in forward-link capacity brought by the use of STS and

PSTD. These estimates should help service providers determine whether it is advantageous to deploy transmit diversity in cdma2000 cells.

The chapters in this thesis are organized as follows: chapter 1 explains basic concepts related to multipath fading and diversity, and explains the Alamouti and PSTD schemes. Chapter 2 explains the basic structure of the cdma2000 system, as well as the STS adaptation of the Alamouti scheme. Chapter 3 presents the results of simulations quantifying the potential benefits of the different transmit diversity techniques. Chapter 4 explains the lab and field testing methodology. Chapter 5 establishes a model for STS interference to legacy NTD mobiles, and presents the results of lab tests designed to quantify this interference under well-known models. Finally, chapter 6 presents the results of the field tests.

Chapter 1: Multipath fading and transmit diversity

This chapter starts by explaining basic parameters used to characterize a wireless multipath fading channel. It subsequently describes the concept of transmit diversity, and how the technique can be used to mitigate the negative effects of fading in a wireless channel. Finally, the chapter explains the two transmit diversity techniques that will be studied in this thesis: Alamouti scheme and Phase-Sweep Transmit Diversity (PSTD).

1.1 The wireless channel

1.1.1 A linear time-varying channel model

A wireless channel is commonly modeled as a multipath channel; as the name suggests, such a channel is characterized by the existence of multiple physical paths between the transmitter and the receiver. Due to the presence of scatterers in the channel (such as tree leaves), the number of paths is assumed to be infinite, and spaced closely apart.

Each path carries a replica of the transmitted signal, with each replica having a particular attenuation and arriving at the receiver at a particular time delay. Thus, in a typical wireless channel, an impulse transmitted at time zero is received as a train of impulses with different attenuations and arriving at different time delays (as Figure 1 illustrates).

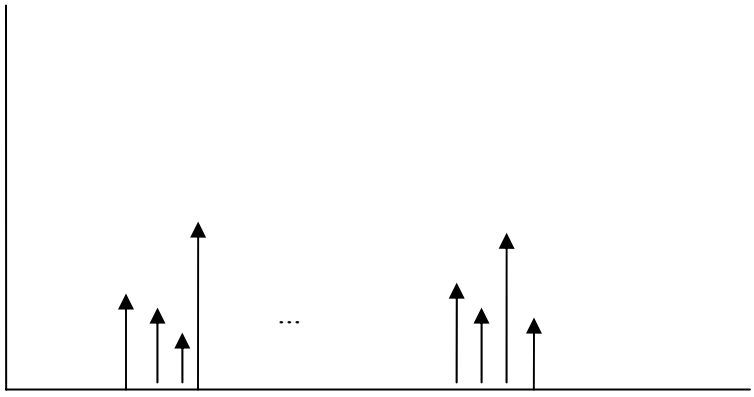

Figure 1: Received signal corresponding to a transmitted impulse on a multipath channel.

A wireless channel is generally modeled as a linear channel. On the other hand, it is not a time-invariant channel because relative movement between the transmitter and the receiver[1] causes the multipaths to change over time. This means that the attenuation and delay of each multipath are time-varying.

Such a channel can be uniquely characterized by a time-varying impulse response $c(\tau;t)$. More precisely, $c(\tau;t)$ is the channel coefficient at delay τ for an impulse transmitted at time t. For a channel with discrete multipaths (such as the one presented in figure 1), the impulse response can be written as:

$$c(\tau,t) = \sum_n a_n(t)\delta\left[t - \tau_n(t)\right] \quad (1.1)$$

where the summation ranges over the multipaths in the channel. Assuming a low-pass channel model, each $a_n(t)$ is a complex number, imposing both an attenuation and a phase-shift on the signal. On the other hand, for a channel with continuous multipaths $c(\tau;t)$ is finite for every τ and non-zero for a continuous range of τ.

The received signal is given by the convolution of the transmitted low-pass signal $s(t)$ and the time-varying impulse response:

$$s'(t) = \int_{-\infty}^{\infty} c(\tau,t)s(t-\tau)d\tau \quad (1.2)$$

In particular, for the discrete-path case the low-pass output can be written as:

$$s'(t) = \sum_n a_n(t)\exp(-j2\pi f_c\tau_n(t))\ \ s(t-\tau_n) \qquad (1.3)$$

where f_c is the carrier frequency.

1.1.2 Fading

It is widely assumed that the coefficients $a_n(t)$ in (1.3) are uncorrelated at different delays. This property causes a phenomenon denominated *fading*, or a rapid fluctuation of the received signal strength over time. Equation (1.3) illustrates why this so: in a simple case, let the transmitted signal be the unmodulated frequency carrier – that is, let $s(t) = 1$ for all t. Equation (1.3) then becomes:

$$s'(t) = \sum_n a_n(t)\exp(-j2\pi f_c\tau_n(t)) \qquad (1.4)$$

[1] As well as movement of other physical structures present in the channel

Equation (1.4) is the sum of phasors of different amplitudes and phases. The amplitudes of the complex coefficients $a_n(t)$ are assumed to change slowly with time; on the other hand, due to the high values of f_c, a small change in $\tau_n(t)$ is enough to turn a phasor from completely in-phase to completely out-of-phase with the sum of the other phasors. For example, a reasonable value for the carrier frequency is 2GHz [2]: at such a frequency, a delay change of 0.25 nanoseconds is enough to cause a 180-degree switch in phase. Equation (1.4) thus shows that as the multipath structure changes with time, the replicas of the transmitted signal change from adding constructively to adding destructively (or vice-versa), resulting in variation of the received signal strength (fading).

Assuming a large number of paths, the law of large numbers can be used. In such a case, the fading channel is typically modeled as a complex Gaussian process. If the Gaussian process is zero-mean – implying that no path is consistently stronger than the others - the amplitude r of the channel gain is said to follow a *Rayleigh* distribution given by the pdf:

$$p(r) = \frac{2r}{\Omega}\exp(\frac{-r^2}{\Omega}) \quad , r \geq 0$$

where $\Omega = E(r^2)$.

In case of a channel where one path is consistently stronger than the others, the complex Gaussian process is no longer zero-mean. The amplitude of the channel fading coefficient then follows a *Rice* distribution [1]. This model is more adequate for a channel with continuous line-of-sight between the transmitter and the receiver, or a channel with a strong static reflector.

1.1.3 Properties of the impulse response

The impulse response $c(\tau;t)$ is a stochastic process in the τ and t variables, with autocorrelation function given by:

$$\phi_c(\tau_1, \tau_2; \Delta t) = \frac{1}{2} E[c^*(\tau_1; t)c(\tau_2; t + \Delta t)] \qquad (1.5)$$

It is generally assumed that this process is wide-sense stationary, and that the channel responses for different delays are uncorrelated. Therefore, (1.5) reduces to:

$$\phi_c(\tau_1, \tau_2; \Delta t) = \phi_c(\tau_1; \Delta t)\delta(\tau_1 - \tau_2) \qquad (1.6)$$

In particular, $\phi_c(\tau_1;0)$ gives the average power at delay τ_1, being termed the *delay power spectrum* of the channel. The range of τ_1 for which $\phi_c(\tau_1;0)$ is non-zero is the *multipath*

[2] In fact, the tests described in chapters 5 and 6 used a carrier frequency of 1.945GHz.

spread of the channel and is denoted by T_m. The quantity T_m can also be seen as the largest delay between the transmitted signal and any of the replicas arriving at the receiver.

The stochastic process *c(τ;t)* can also be characterized in the frequency domain by taking the Fourier transform of the impulse response:

$$C(f;t) = \int_{-\infty}^{\infty} c(\tau,t)\exp(-j2\pi f\tau)d\tau \quad (1.7)$$

Since the time-domain impulse response is time-varying, the frequency-domain impulse-response *C(f;t)* is also time-varying (as equation (1.7) illustrates). Therefore, *C(f;t)* is itself a stochastic process with autocorrelation given by:

$$\phi_C(f_1,f_2;\Delta t) = \frac{1}{2}E[C^*(f_1;t)C(f_2;t+\Delta t)] \quad (1.8)$$

By plugging (1.7) in (1.8) and using (1.6), it can be shown that:

$$\phi_C(f_1,f_2;\Delta t) = \int_{-\infty}^{\infty}\phi_c(\tau;\Delta t)\exp\left[-j2\pi\left(f_2-f_1\right)\tau\right]d\tau = \phi_C(\Delta f;\Delta t) \quad (1.9)$$

where $\Delta f = f_2 - f_1$.

Thus, the process can be said to be stationary in frequency since the frequency correlation only depends on the difference between the frequencies. The function $\phi_C(\Delta f;\Delta t)$ is called the *spaced-frequency, spaced-time correlation function* of the channel; its frequency-correlation and time-correlation properties will be discussed next.

1.1.3.1 Frequency correlation: flat-fading and frequency-selective fading

Setting $\Delta t = 0$ in (1.9) gives the frequency correlation of the channel, which is simply the Fourier transform of the delay power spectrum. As such, the delay power-spectrum and the frequency-correlation function have dual properties; in particular, a larger value for the multipath spread T_m implies a narrower non-zero range for $\phi_C(\Delta f;\Delta t)$ and thus a smaller frequency correlation. This motivates the definition of *coherence bandwidth* of a channel:

$$\left(\Delta f\right)_c \approx \frac{1}{T_m}$$

Intuitively, the wireless channel can be said to impose approximately the same attenuation and phase shift to any two frequencies separated by less than $(\Delta f)_c$, the coherence bandwidth.

Of particular interest is a scenario in which $(\Delta f)_c$ is greater than the bandwidth of the transmitted signal. In this case, all frequencies contained in the transmitted signal are equally faded; hence, this scenario is termed *flat fading*. In a flat-faded channel the multipath spread is smaller than the inverse of the signal bandwidth, so the individual paths cannot be resolved at the receiver. Thus, the receiver effectively sees only one signal consisting of the sum of (un-resolvable) signal replicas at close time delays; from the point of view of the receiver, this resulting signal can be modeled as a single path multiplied by a fading coefficient.

The case where $(\Delta f)_c$ is smaller than the signal bandwidth is denominated *frequency-selective* fading. In such channels, different frequency components of the signal suffer different attenuations, possibly resulting in symbol distortion and degraded performance. At the same time, a frequency selective channel presents multiple resolvable paths to the receiver - unlike the flat-fading scenario. As will be seen in chapter 2, spread-spectrum systems like cdma2000 take advantage of multiple resolvable paths to increase the received signal-to-noise (SNR) ratio and improve receiver performance.

Figure 2 illustrates the classification of a fading channel according to frequency coherence (*W* is the signal bandwidth).

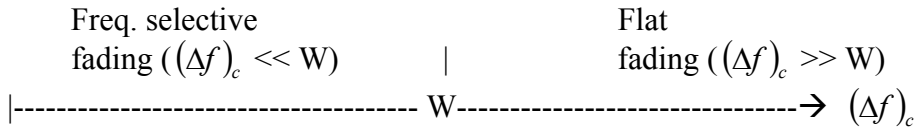

Figure 2: Flat fading and frequency selective fading

1.1.3.2 Time correlation: slow fading and fast fading

The time variation of a wireless channel results from relative movement between transmitter and receiver, as well as movement of surrounding physical structures; such movement alters the multipath structure of the channel. This effect is generally modeled as a Doppler spread, since the relative speeds effectively shift the frequency seen by the receiver.

Equivalently, the Doppler spread can be seen as a range of frequencies λ (centered at zero) such that there is a non-zero signal energy at a frequency shift of λ at either end of the signal bandwidth. More precisely, the power received at Doppler frequency λ is given by:

$$S_C(\lambda) = \int_{-\infty}^{\infty} \phi_C(0;\Delta t)\exp\left(-j2\pi\lambda\Delta t\right)\, d\Delta t \qquad (1.10)$$

The function $S_C(\lambda)$ is denoted the *Doppler power spectrum* of the channel, and the *Doppler spread* B_d is defined as the range of λ for which $S_C(\lambda)$ is non-zero. As (1.10) shows, the Doppler power spectrum is the Fourier transform of the time correlation of the channel at any given frequency. Thus, time correlation and Doppler power spectrum are also dual properties: a longer time correlation implies a narrower Doppler spread, and vice-versa. Therefore, the *coherence time* of the channel can be defined as:

$$\left(\Delta t\right)_c \approx \frac{1}{B_d} \qquad (1.11)$$

Intuitively, the attenuation and phase-shift at any particular delay are highly correlated for two instants separated by less than $\left(\Delta t\right)_c$.

Equation (1.11) shows that a time-invariant channel corresponds to an infinite coherence time and zero Doppler spread – that is, no relative movement between transmitter and receiver. Similarly, a zero-coherence time (white channel) corresponds to an infinite Doppler spread, and can only be achieved at infinite speeds. Due to the duality between time coherence and relative speed between transmitter and receiver, the time coherence of a channel is often specified via the receiver speed and assuming the transmitter to be stationary (case of a mobile station and a base station, respectively).

A wireless channel can be classified as *slow-fading* or *fast-fading* depending on whether the coherence time is much larger or much smaller than the symbol duration, respectively (see figure 3). A fast-fading channel is generally undesirable because it applies a non-uniform attenuation/phase shift to each symbol, resulting in signal distortion. At the same time, very slow fading channels have a disadvantage: if at any given time the channel imposes a high attenuation (or *deep fade*) to the signal, the deep fade could span several symbols and degrade performance. Such a scenario is the primary motivation for the use of transmit diversity, as will be explained in section 1.2.

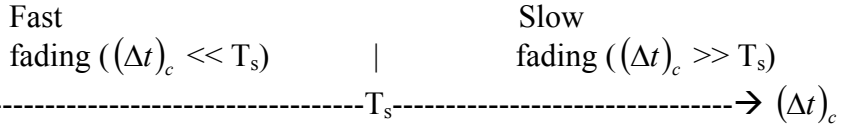

Figure 3: Slow fading and fast fading. T_s is the symbol duration

1.1.4 A tapped-delay channel model

Section 1.1.3.1 explained that a flat fading channel can be modeled as a multiplicative channel in which the transmitted signal is multiplied by a time-varying

fading coefficient at a time-varying delay. This section expands the model for a frequency-selective channel.

Let W be the bandwidth of the transmitted signal. Based on the sampling theorem, the (low-pass) transmitted signal can be written as:

$$s(t) = \sum_{n=-\infty}^{\infty} s(\frac{n}{W}) \operatorname{sinc}\left(t - \frac{n}{W} \right)$$

where

$$sinc(x) = \frac{\sin(\pi W x)}{\pi W x}$$

In the frequency domain, the signal can be written as:

$$S(f) = \frac{1}{W} \sum_{n=-\infty}^{\infty} s(\frac{n}{W}) \exp(-j2\pi f n / W), \quad |f| \le \frac{1}{2} W$$

$$0 \qquad\qquad\qquad\qquad \text{otherwise}$$

The received time-domain signal $r(t)$ can be recovered from $S(f)$ via an inverse Fourier transform of the frequency-domain output:

$$s'(t) = \int_{-\infty}^{\infty} C(f;t) S(f) \exp(j2\pi f t) df = \frac{1}{W} \sum_{n=-\infty}^{\infty} s(\frac{n}{W}) \int_{-\infty}^{\infty} C(f;t) \exp\left[- j2\pi f (t - n/W) \right] df$$

$$= \frac{1}{W} \sum_{n=-\infty}^{\infty} s(\frac{n}{W}) c(t - n/W; t)$$

where the last equality follows from (1.7) and considering the inverse Fourier tranform. Incidentally, the condition $|f| \le \frac{1}{2} W$ for $S(f)$ was dropped since it is assumed (without loss of generality) that $C(f;t)$ is non-zero only in that range.

Finally, the last identity can be written as (after swapping indices in the convolution sum):

$$s'(t) = \frac{1}{W} \sum_{n=-\infty}^{\infty} s(t - \frac{n}{W}) \; c(n/W; t) \qquad (1.12)$$

Despite equation (11.12) suggesting infinitely many signal replicas, in practice the number of replicas is limited due to the finite multipath spread. The number of possible paths is $L = T_m W$, giving rise to the L-tap channel model:

$$s'(t) = \sum_{n=1}^{L} h_i \; s(t - \frac{n}{W}) \qquad (1.13)$$

with $h_i = (1/W)\, c(n/W;t)$. A flat fading channel is a particular case of (1.13) with $L = 1$.

Intuitively, equation (1.13) shows that the large number of paths between the transmitter and the receiver can be grouped into a discrete set of clusters. Within a given cluster, the multipaths have close time delays - less than the inverse of the signal bandwidth - and cannot be individually resolved at the receiver. And because the attenuations and time delays are time-varying for the multipaths within a cluster, the superposition of these paths looks random to the receiver. Therefore, the signal for each cluster can be viewed as coming from a single path, with an associated channel gain represented as a random fading process.

The set of all transmitter-receiver multipaths, on its turn, can be viewed as a discrete set of resolvable taps (one for each cluster), each with its own channel gain represented as a fading process. Since the fading processes for paths at different delays are uncorrelated, the fading processes for different taps are also assumed to be uncorrelated.

1.2 Diversity

The previous section explained that the multipath nature of a wireless channel causes a phenomenon known as fading, or a fluctuation of the channel gain over time. In particular, a fading channel presents a significant probability of *deep fade*, or low channel gain with respect to the transmitted signal SNR. It can be shown [2] that for a fading channel, the bit-error probability is dominated by:

$$P(deep\ \ fade) \approx \frac{1}{SNR}$$

for high SNR values. For simple transmission schemes, the bit-error probability is proportional to 1/SNR, a polynomial decrease with increasing SNR; this contrasts with the exponential decrease in bit-error probability with increasing SNR experienced in a non-fading channel.

A common solution to deal with the problem is to provide the receiver with *diversity*, defined as multiple signal replicas facing mutually uncorrelated fading processes. In a system with diversity, the received signal energy is small only if the fading coefficients are small for all replicas; uncorrelated fading ensures that the probability of this occurrence is much smaller than in a system with no diversity.

In particular, let L be the number of uncorrelated signal replicas at the receiver, with each replica having $1/L$ of the power of the single replica in a no-diversity case. It can be shown [2] that the bit-error probability is dominated by:

$$P(deep\ \ fade) \approx \frac{1}{SNR^L}$$

for high SNR. The quantity L - the number of uncorrelated signal replicas - is the *diversity order* of the system. It can be thus seen than the required SNR (in dB) for an L-order diversity system is L times smaller than in a system with no diversity.

Diversity can be provided across various dimensions; two of these, *time diversity* and *frequency diversity*, are extensively exploited in today's communication systems, as explained in the following subsections.

1.2.1 Time diversity

Time diversity attempts to take advantage of the low correlation of fading coefficients across sufficiently long time intervals. This is typically achieved by coding bits for redundancy and interleaving the coded symbols so that the information for each bit is spread out in time. Yet, in order to ensure uncorrelated fading the symbols must be interleaved over time frames longer than the coherence time of the channel. This characteristic significantly limits the ability of delay-constrained applications (such as voice applications) to take advantage of time diversity in slow fading channels.

1.2.2 Frequency diversity

Frequency diversity attempts to provide diversity by spreading the signal information across different frequencies. In order to ensure uncorrelated fading, the frequency range must be larger than the coherence bandwidth of the channel.

The simplest technique for achieving frequency diversity is to transmit the signal simultaneously at different carrier frequencies, with each pair of frequencies separated by a gap larger than the coherence bandwidth. A slightly more sophisticated technique is *frequency-hopping*, which consists of changing (hopping) the carrier frequency periodically over time.

A different technique, employed by *direct-sequence spread-spectrum* systems such as cdma2000, consists in spreading the transmitted signal with a spreading sequence so that the signal bandwidth is larger than the coherence bandwidth of the channel; in such a system, the receiver is able to resolve the signal components from different taps and obtain *multipath diversity*. Such a technique for obtaining frequency diversity is, however, less effective in flat-fading (or one-tap-delay) channels.

1.2.3 Antenna diversity: transmit and receive diversity

The previous two subsections showed that a scenario of slow and flat fading can result in poor signal reception. In this scenario, both time and frequency diversity are of little help; without any other form of diversity, the transmitter must add power to the signal to ensure satisfactory SNR and bit-error rates at the receiver.

Antenna diversity is an alternative technique designed mainly to provide diversity gains in slow and flat fading channels, and consists of using multiple antennas for transmission or reception of the signals. With antenna diversity, each transmit-receive antenna pair can be viewed as a separate channel. It is assumed that if the antennas are separated by at least 10 carrier wavelengths, the fading processes for each transmit-receive antenna channel are uncorrelated [7]. Thus, each transmit-receive antenna channel provides uncorrelated replicas, and hence diversity, to the receiver.

Antenna diversity is easier to implement in the base-station than in the mobile, for two reasons:

1. The antenna separation required to ensure uncorrelated fading is easier to achieve on the base-station side.

2. Base stations can more easily absorb the costs resulting from the increased complexity due to antenna diversity.

Antenna diversity can be classified as *transmit diversity* or *receive diversity* depending on whether multiple antennas are used for transmission or reception. While the techniques are both designed to provide diversity gains, receive diversity has the advantage of also providing power gain; after all, increasing the number of receive antennas effectively increases the received power. In addition, receive diversity typically requires no changes in the transmitter implementation; on the other hand, many transmit diversity techniques require receiver-specific support due to their reliance on space-time codes for transmission across multiple antennas. Due to the more pronounced benefits of receive diversity and their relative ease of implementation on the base-station side, receive diversity is already employed by cdma2000 base stations to help in the reception of mobile (reverse link) signals.

On the forward link, diversity gains can be obtained by applying either transmit diversity at the base station or receive diversity at the mobile, or a combination of both. Neither technique is commercially deployed yet, but both are topics of active current research. The study of mobile receive diversity is outside the scope of this thesis; instead, this study focuses on base-station transmit diversity, or more specifically, on techniques that use 2 transmit antennas at the base station.

1.3 Two-antenna forward-link transmit diversity

The most basic form of transmit diversity (TD) at the forward link employs one receiver antenna at the mobile and two transmitter antennas at the base station. One transmit antenna is denoted the *common* or *main* antenna, and the other is denoted the *diversity* antenna.

This thesis evaluates two 2-antenna transmit diversity techniques: the *Alamouti scheme*, and *Phase-Sweep Transmit Diversity* (PSTD). The following sections describe these schemes (for reference, the conventional technique that uses only one antenna is denominated *No Transmit Diversity***,** or NTD).

1.3.1 Alamouti Scheme

The Alamouti scheme was proposed in [8], and is designed for coherent detection at the mobile receiver; in other words, it assumes that the mobile can demodulate the signals from each antenna individually, and that it can reliably estimate the channel gains from each transmit antenna.

The scheme works as follows: let u_1 and u_2 be the *n*-th odd and *n*-th even transmitted symbols under a *NTD* cell, respectively. In the Alamouti scheme, the *n*-th odd and *n*-th even symbols (x_1 and x_2) transmitted by the common and diversity antenna are given by the matrix:

$$\begin{bmatrix} x_1 \\ x_2 \end{bmatrix} = \begin{bmatrix} u_1 & -u_2^* \\ u_2 & u_1^* \end{bmatrix}$$

where the first row contains the *n*-th odd and *n*-th even symbols transmitted from the main antenna, while the second row contains the the *n*-th odd and *n*-th even symbols transmitted from the diversity antenna.

It is assumed that h_1 and h_2, the channel gains from the common and the diversity antenna, do not change between two consecutive symbols. With this assumption, the received signal from each antenna (y_1, y_2) can be written as:

$$\begin{bmatrix} y_1 & y_2 \end{bmatrix} = \begin{bmatrix} h_1 & h_2 \end{bmatrix} \begin{bmatrix} u_1 & -u_2^* \\ u_2 & u_1^* \end{bmatrix} + \begin{bmatrix} w_1 & w_2 \end{bmatrix}$$

where w_1 and w_2 are the noise components, assumed to be independent zero-mean complex Gaussian processes.

The mobile recovers the even and odd symbols from y_1 and y_2 as follows:

$$h_1^* y_1 + h_2 y_2^* = \left(\ |h_1|^2 + |h_2|^2 \ \right) u_1 + h_1^* w_1 + h_2 w_2^*$$

$$h_2^* y_1 - h_1 y_2^* = \left(\ |h_1|^2 + |h_2|^2 \ \right) u_2 + h_2^* w_1 - h_1 w_2^*$$

Each of u_1, u_2 carries only half the symbol energy - or $E_s/2$ - since each is transmitted from both antennas. Now, assuming w_1 and w_2 to be uncorrelated Gaussian random variables with standard deviation σ^2, the above expressions imply a received SNR of:

$$SNR' = \frac{\left(\ |h_1|^2 + |h_2|^2 \ \right)^2 \frac{E_s}{2}}{\sigma^2 \left(\ |h_1|^2 + |h_2|^2 \ \right)} = \frac{E_s}{\sigma^2} \frac{\left(\ |h_1|^2 + |h_2|^2 \ \right)}{2}$$

compared to $SNR' = \frac{E_s}{\sigma^2} |h|^2$ for the one-antenna case. As can be seen, in the Alamouti scheme full diversity gain – 2 equal-power uncorrelated replicas at the receiver - is realizable.

1.3.2 Phase-Sweep Transmit Diversity (PSTD)

Phase-Sweep Transmit Diversity (PSTD) is a heuristic approach designed specifically to cope with a slow and flat fading channel. The flat fading in mitigated by multipaths from the diversity antenna; on the other hand, slow fading is mitigated by artificially "fast-fading" the channel and reducing the likelihood of extended deep fades.

The mechanism by which PSTD fast-fades the channel is by creating a Doppler spread directly in the transmitted signal instead of relying on the channel to do so. In this scheme, both antennas transmit the same low-pass signal; however, the base-station applies a small frequency offset to one antenna signal with respect to the other. More precisely: if *s(t)* is the low-pass complex waveform, the low-pass signals transmitted by the antennas are:

Common antenna: *s(t)*
Diversity antenna: $s(t) * exp(2\pi j f_s t)$

Here, f_s is the phase-sweeping frequency, and typically lies between 0 and 100 Hz. It can be seen that the diversity antenna applies a linear phase sweep to the diversity signal with respect to the common antenna signal.

Let h_1 and h_2 be the complex channel gains from each antenna. Assuming that the values of h_1 and h_2 do not change over the course of a symbol duration, the received mobile signal can be written as:

$$r(t) = s(t)*[h_1 + h_2 * exp(2\pi j f_s t)] \quad (1.14)$$

The mobile cannot determine h_1 and h_2 individually: all it sees is the transmit signal multiplied by a gain consisting of the sum of h_1 and a "phase-swept" h_2; this sum is the effective channel gain seen by the mobile receiver.

The phase-sweep attempts to simulate the effects of a mobile moving at a speed corresponding to a Doppler spread of f_s. As shown in [2], the effective channel given by (1.14) is also the channel seen by a mobile moving with a speed of $c*(f_s/f_c)$ in a 2-tap channel in a one-transmit antenna cell. Here, c is the speed of light and f_c is the carrier frequency; in particular, a phase-sweeping frequency of 100 Hz and a carrier frequency of 2 GHz imply a mobile speed of approximately 54 km/h.

Figure 4 illustrates the effect of PSTD on the Doppler spectrum $S_C(f)$; as can be seen, the spectrum is expanded by f_s on both sides.

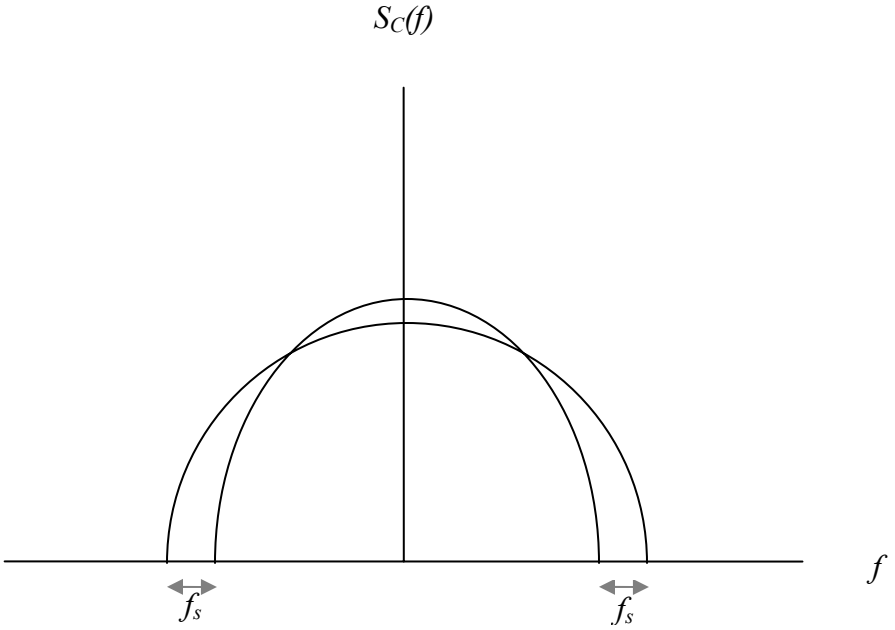

Figure 4: Doppler spectrum broadening due to PSTD. The outward line is the Doppler spectrum with PSTD, the inner line the spectrum without PSTD.

It is important to note that for PSTD to be effective, h_1 and h_2 must have low correlation: otherwise, the phase-sweep effectively causes deep fades in the channel at $1/f_s$ intervals (when the phase-sweep is an odd multiple of π). Due to the low value of f_s, such deep fades are extended, and performance degradation ensues. This result holds, for example, in Rycian channels with a high correlation between the fading coefficients from the two antennas.

An advantage of PSTD over the Alamouti scheme is that it does not require mobile-specific support; the base-station can single-handedly deploy PSTD, and all mobiles in the cell will seamlessly experience the impacts of transmit diversity.

Chapter 2: cdma2000 physical layer

This chapter explains the basic structure of the cdma2000 physical-layer support for voice calls, and focuses on the details that are most relevant to the study of forward-link transmit diversity. More specifically, section 2.1 explains the basic principle behind direct-sequence spread-spectrum systems; section 2.2 explains details of cdma2000 physical-layer operations such as channel-coding, modulation and spreading; section 2.3 explains the cdma2000 implementation of the Alamouti scheme, namely *Space-Time Spreading (STS)*; section 2.4 describes the basic overhead channels and their importance in the system. Finally, sections 2.5, 2.6 and 2.7 explain three concepts of special relevance to direct-sequence spread-spectrum systems: RAKE receivers, power control and soft handoffs.

2.1 Direct-sequence spread-spectrum systems

The cdma2000 system is a *spread-spectrum* system, defined as a system in which the signal bandwidth is much larger than the voice rate. Furthermore, cdma2000 is a *direct-sequence* system because it uses spreading sequences (also known as spreading codes) to expand each user's signal across the entire bandwidth. The higher bandwidth allows for higher spectral redundancy and coding gain in the signal, but comes at the expense of added interference from other users since they all share the same bandwidth.

In order to mitigate interference from other users and provide voice privacy, the codes used for spreading a user's voice signal include user-specific codes; these are designed so that codes for different users have low correlation. In the demodulation process, the receiver de-spreads the total signal received from the base-station using the same user-specific code used for spreading; this step preserves the signal intended for the user while filtering out most interference in the bandwidth.

Figure 1 is an abstract illustration of this property for a spread-spectrum system. It can be seen that the user's voice signal is initially spread to occupy the entire bandwidth. The base-station and the channel subsequently superpose interference and noise across the entire bandwidth. After de-spreading at the receiver, most of this interference and noise remains spread across the bandwidth, whereas the user's voice signal compresses into a narrow region. The voice signal can then be recovered via band-pass filtering.

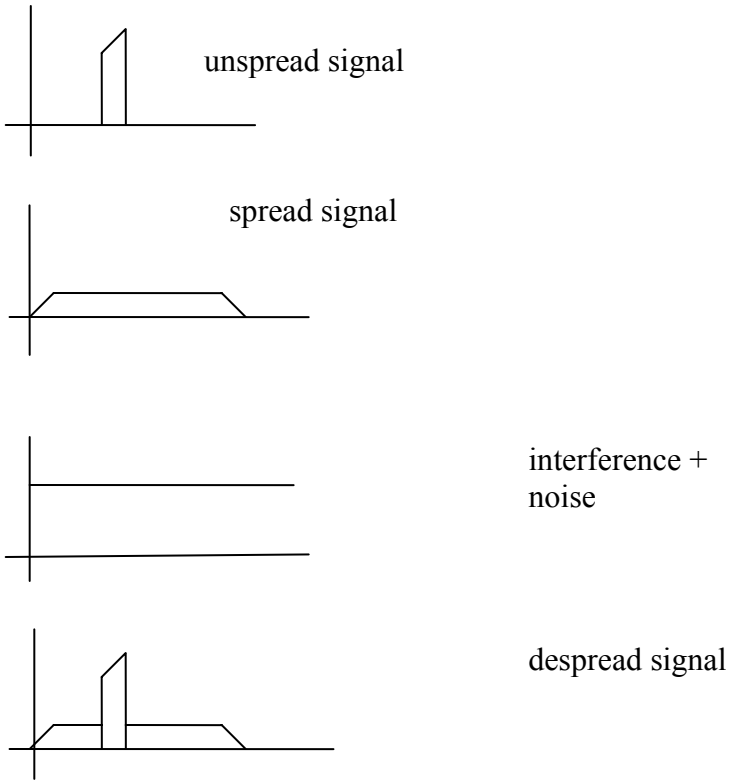

Figure 1: A frequency-domain illustration of the properties of a direct-sequence spread-spectrum system.

2.2 Basic physical layer blocks

Figure 2 presents a basic sketch of the cdma2000 physical layer.

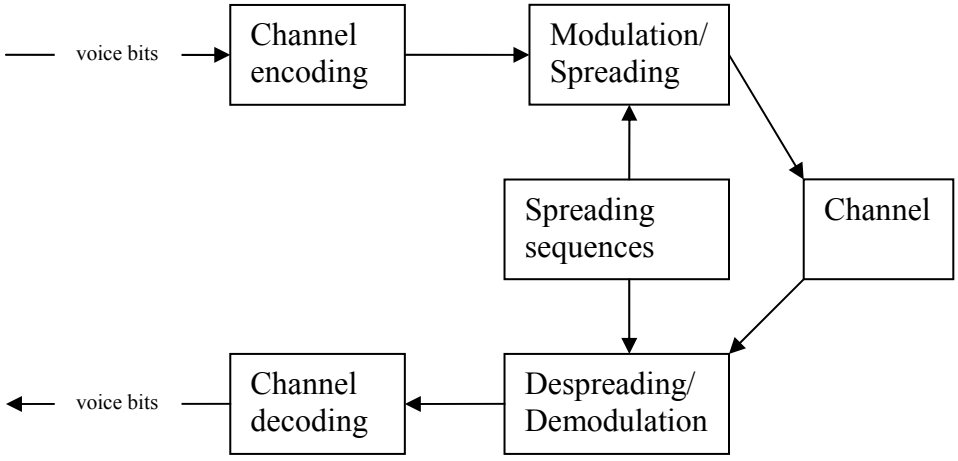

Figure 2: cdma2000 physical layer

The following subsections describe these blocks further. Discussion will be restricted to the transmission and reception of voice bits in structures known as *traffic channels*, or *fundamental channels*[3]; overhead channels will be explained in section 2.4. The discussion focuses mostly on the forward-link; differences in the reverse-link are minor, and where relevant they will be noted explicitly.

2.2.1 Voice bits

In order to efficiently encode various levels of voice activity during a voice call, the cdma2000 system supports four different voice rates for the output of the voice encoder (vocoder): 1.2 kbps (eighth-rate), 2.4 kbps (quarter-rate), 4.8 kbps (half-rate) and 9.6 kbps (full-rate). Higher rates are used during periods of more intense voice activity, and conversely.

2.2.2 Channel encoder/decoder

Figure 3 shows a block sketch of the steps performed during channel coding.

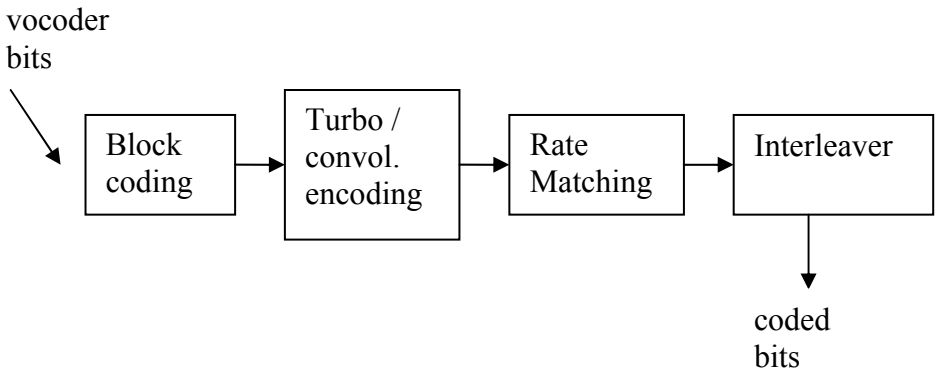

Figure 3: Channel coding steps

The cdma2000 system employs a block coder to compute parity bits and either a convolutional or a turbo encoder for more robust channel coding. The rate of the convolutional/turbo encoder is specified by the *radio configuration* (RC) of the cell, and the standard allows various possible RCs for flexibility. The two radio configurations of interest in this study are RC3 and RC4, as they are the most common configurations currently deployed in cdma2000 cells. With regards to channel coding, RC3 employs a ¼-rate turbo/convolutional encoder while RC4 employs a ½-rate turbo/convolutional encoder.

[3] Traffic channels include supplemental channels that transmit data instead of voice; however, since this study is concerned only with voice calls the distinction will be ignored.

Section 2.2.1 mentioned that the vocoder bit-rate is variable; the transmitted symbol rate, however, is constant. Part of the channel coding process is to perform a process denoted *rate matching*, which matches variable vocoder bit-rates to constant coded-bit rates; this is achieved by repeating the bits for lower data rates - repeating each bit either 2, 4 or 8 times, depending on the data-rate - prior to modulation. Because of redundancy from repeated bits, the required power levels for lower-rate calls are lower than those of full-rate calls.

The last step in channel coding consists in interleaving the coded bits to cope with the possibility of bursty errors, that is, a large number of contiguous bits received in error. If these error bits corresponded to contiguous vocoder coded-bits, the large number of errors would prevent the transducer at the receiver from converting the decoded bits back into voice, degrading the quality of the call. Interleaving, on the other hand, spreads these bit errors in time so that contiguous streams of vocoder coded-bits have a small number of errors; at that level, channel coding typically provides redundancy to detect/correct all errors.

The coded-bits are interleaved within structures called frames; in other words, frames are groupings of channel-coded bits, within which the coded bits can be interleaved. The standard specifies that the frame size can be either 5ms or 20ms for both RC3 and RC4.

2.2.3 Modulation/Spreading

The modulation technique used on forward-link traffic channels is Quadrature Phase-Shift Keying (QPSK). For the reverse-link, Binary Phase-Shift Keying (BPSK) is used. The reason for this choice is that the forward-link has a strong training sequence (pilot channel) for phase coherence and can thus use a higher-dimensionality modulation technique (QPSK); on the other hand, since phase coherence is comparatively poor on the reverse link, the more robust BPSK is used.

The spreading stage is responsible for spreading the QPSK/BPSK-modulated coded bits and converting them into a bandwidth of 1.2288 MHz[4]. Two types of spreading are performed: orthogonal (Walsh) spreading and pseudonoise (PN) spreading[5]. The orthogonal modulation stage converts the coded-bits into a bandwidth of 1.2288 MHz, whereas the PN-spreading stage adds a pseudorandom phase to the spread signal.

The following sections detail the forward-link QPSK modulation and the spreading operations.

[4] A bandwidth of 3.6864 MHz is also allowable by the standards, but this detail will be ignored here.
[5] There are actually two levels of PN-spreading on the forward-link, namely *short PN-spreading* and *long PN-spreading*. The forward-link discussion will focus mostly on short PN-spreading,

2.2.3.1 QPSK modulation

Because forward-link traffic channels employ QPSK modulation, the channel coded bits are first divided in two streams, with the even bits going on one stream and the odd bits on the other. If transmit diversity is enabled (TD mode), each substream is further subdivided in two even-odd - or I/Q - substreams.

Figure 4 illustrates the process; note that each I/Q pair can be viewed as a complex stream of symbols.

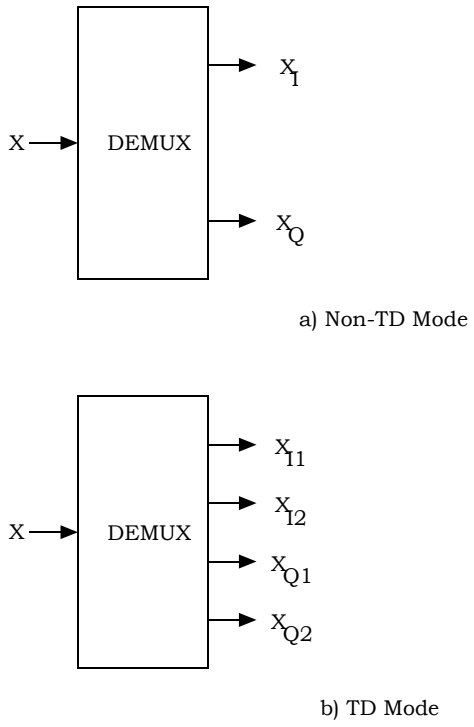

Figure 4: QPSK modulation on the forward-link, without and with transmit diversity.

2.2.3.2 Orthogonal (Walsh) spreading

Orthogonal spreading (also known as Walsh spreading) is the step that spreads the coded bits across the signal bandwidth. This is accomplished by spreading the coded bits with a *Walsh code*, a 2^N-length sequence consisting of the values +1 and -1.

If $w_i(n)$ and $w_j(n)$ are any two distinct 2^N-length Walsh sequences, they satisfy the following property:

$$\sum_{n=1}^{2^N} w_i(n) w_j(n) = 0 \quad \text{for } i \neq j \qquad (2.1)$$

For N=1 the Walsh sequences are given by the following matrix (the i-th row contains the elements of the i-th Walsh sequence):

$$W_1 = \begin{bmatrix} +1 & +1 \\ +1 & -1 \end{bmatrix}$$

Given W_N - the matrix containing the elements of Walsh sequences of length 2^N – the matrix W_{N+1} of Walsh sequences of length 2^{N+1} can be constructed as follows:

$$W_{N+1} = \begin{bmatrix} W_N & W_N \\ W_N & \overline{W_N} \end{bmatrix}$$

where $\overline{W_N}$ is obtained by negating W_N. In particular, it can be seen that there are exactly 2^N possible Walsh sequences of length 2^N.

Let $x(m)$ be the coded bit-stream after assigning all 0-bits to the value +1 and all 1-bits to the value -1, and let $w_k(n)$ be the spreading Walsh sequence (assumed of length L, where L is a power of 2). The Walsh-spread bit-stream is given by:

$$y(n) = \sum_m x(m) \sum_{j=0}^{L-1} w_k(j) \delta[n - mL - j] \qquad (2.2)$$

It is easily seen that if $x(m)$ has a rate of R bits per second, then $y(n)$ has a rate of $L*R$ bits per second; in other words, Walsh spreading increases the bandwidth by a factor of L, where L is the length of the Walsh sequence. Following standard spread-spectrum terminology, from here onwards the post-spreading bits will be referred to as *chips*.

In a given cell, each mobile in a voice call is exclusively assigned one of the L possible Walsh codes, in which to receive forward-links signals[6]. The coded bits for each mobile are spread using the mobile-specific Walsh sequence, and the chips for all mobiles are added together to constitute the full base-station signal.

[6] In reality, some of the Walsh codes are reserved for overhead channels, but this detail will be ignored for now.

In order to recover *x(m)* from *y(n)*, the receiver correlates *y(n)* with $w_k(j)$ and accumulates the result over L chips – a process known as *Walsh de-spreading* of the received signal. Mathematically:

$$x(m) = \frac{1}{L}\sum_{j=0}^{L-1} w_k(j)\ \ y(mL + j) \qquad (2.3)$$

Due to the orthogonality of Walsh codes, de-spreading recovers the mobile's coded bits while filtering out the signals to other mobiles.

Because each Walsh code typically spreads a different signal, each Walsh code is said to be associated with a forward-link *channel*. Since each mobile is assigned a different Walsh code - or equivalently, a dedicated traffic channel - the number of users supported in a cell is limited by L (the total number of Walsh codes of length L).

On the reverse-link, Walsh codes are also used to separate different channels transmitted by a mobile. In this case, however, there is only one traffic channel; the remaining channels are used for overhead, signaling and power control. Unlike the forward-link, the Walsh length differs across channels on the reverse-link.

In non-TD mode[7], the orthogonally-spread chips are subsequently PN-spread (an operation described in the next section), an operation that leaves the chip rate unchanged. Since the bandwidth is 1.2288 MHz and two chips are transmitted at a time on the forward-link (due to QPSK modulation), the received chip rate is 2.4576 MHz. Now, the coded-bit rate for RC3 is 38.4 kbps, implying that the length of the orthogonal spreading sequence must be 2.4576 M/38.4k = 64 chips; similarly, since the coded-bit rate for RC4 is 19.2kbps, the RC4 Walsh-length is 128 chips. In particular, an RC3 cell cannot support more than 64 users, whereas an RC4 cell can support up to 128[8].

The discussion in the previous paragraph illustrates that the rate of the convolutional/turbo encoder must be traded off against the length of the orthogonal spreading code. Higher convolution/encoder rates allow for lower energy-per-bit to achieve a given call quality, while longer orthogonal-spreading codes increase the number of possible supported users in a cell; in the case at hand, RC4 supports a larger number of users per cell at the expense of weaker channel coding.

2.2.3.3 Pseudonoise (PN) spreading

Orthogonal spreading allows for separation of different forward-link channels within a cell. Base-stations and mobiles at neighboring cells, however, use the same Walsh codes for their respective traffic channels. Without any other form of spreading, interference from neighboring cells would seriously hamper communication on the

[7] Discussion of the TD-mode case will be left to section 2.3

[8] In reality these numbers are 61 and 125 after discounting for overhead channels; in practice, they are reduced even further due to handoff overhead.

forward-link. Walsh spreading is also insufficient on the reverse-link because the transmissions from different mobiles are not time-synchronized[9].

In order to reduce interference between base-stations on the forward-link, each base-station spreads its signal using a periodic PN sequence consisting of +1 and -1 values. A PN sequence *b(m)* of period *L* satisfies the following property:

$$\sum_{k=0}^{L-1} b(k)b(k+j) = \begin{cases} L, & j = 0, L, 2L, \ldots \\ -1, & \text{otherwise} \end{cases} \qquad (2.4)$$

Different cells PN-spread their signals using the same PN sequence but starting at different offsets. As can be seen from (2.4), the PN sequence has very low autocorrelation at different offsets; therefore, signals from different cells have very low correlation[10]. Thus, by de-spreading the received signal with the same PN sequence used for spreading, the transmitted signal can be recovered while filtering out most interference from other base-stations.

On the forward-link, each cdma2000 base-station uses two *short PN-codes* for spreading – $PN^{(I)}$ and $PN^{(Q)}$ - both of which have a period of 2^{15}-1 = 32767 elements. If $Y^{(I)}$ and $Y^{(Q)}$ denote the I/Q chip values after Walsh spreading, the PN-spread I/Q chip values are given by:

$$\begin{aligned} Z^{(I)} &= Y^{(I)} * PN^{(I)} - Y^{(Q)} * PN^{(Q)} \\ Z^{(Q)} &= Y^{(I)} * PN^{(Q)} + Y^{(Q)} * PN^{(I)} \end{aligned} \qquad (2.5)$$

Equivalently, by interpreting the I/Q pairs as complex chips – that is, writing $Z = Z^{(I)} + j*Z^{(Q)}$, $Y = Y^{(I)} + j*Y^{(Q)}$ and $PN = PN^{(I)} + j*PN^{(Q)}$, the equations in (2.5) can be compressed as:

$$Z = Y * PN \qquad (2.6)$$

This process is denoted *complex PN-spreading*, and ensures that the mean phase of the complex post-spreading chips is zero. In order to recover Y from Z, the receiver simply performs:

$$Y' = Z' * PN^{*} \qquad (2.7)$$

where PN^{*} denotes the complex conjugate of the PN sequence, or $PN^{(I)} - j* PN^{(Q)}$.

[9] As will be seen in chapter 3, forward-link and reverse-link signals are centered on different carrier frequencies, therefore they interfere little with each other. The text thus ignores forward-link interference on the reverse-link, and vice-versa.

[10] The cells are time-synchronized to ensure that this property holds.

A similar process occurs on the reverse-link, with each mobile spreading its signal with a PN sequence. The sequence is the same for all mobiles, but the starting offset is different for each mobile to ensure both orthogonality and data privacy between users. The code used for PN spreading on the reverse-link is denoted *long PN-code* and has a period 2^{42}-1 chips. Incidentally, the long PN-code is also used for *long PN-spreading* on the forward-link to ensure data privacy between users.

2.3 Transmit diversity: Space-Time Spreading (STS)

The cdma2000 standard supports a 2-transmit-antenna diversity technique denoted *Space-Time Spreading (STS)*; originally proposed in [9], it is essentially an adaptation of Alamouti's scheme for the cdma2000. STS was designed to be backwards compatible with standard non-transmit diversity (NTD) transmission mode; more specifically, both STS and NTD mobiles can coexist in the same cell.

The first difference between STS and NTD is the length of the spreading Walsh code: twice as long for STS mobiles, compared to NTD mobiles. In particular, STS mobiles are assigned 128-chip Walsh codes under RC3 and 256-chip Walsh codes under RC4. In addition, each STS mobile is assigned two dedicated double-length Walsh codes. The two Walsh codes assigned to the same STS mobile are antipodal; denoting by $w_k(n)$ and $w_j(n)$ the two Walsh codes of length $2L$ assigned to the same STS mobile, they satisfy:

$$w_k(n) = w_j(n),\ n = 0, 1, \ldots L-1$$
$$w_k(n) = -w_j(n),\ n = L, L+1, \ldots 2L-1$$

By assigning each STS mobile a pair of antipodal codes, the base-station ensures that a given mobile's STS traffic signal is always orthogonal to both STS and NTD traffic signals of other mobiles; it is this property that allows STS and NTD mobiles to coexist in the same cell.

In line with the notation in figure 4, let X_1 and X_2 denote the two complex I/Q substreams of coded-bits for an STS mobile after the modulation stage. If w_1 and w_2 are the Walsh codes assigned to this STS mobile, the spread chips are given by:

$$Y_1 = X_1 w_1(t) - X_2^* w_2(t) \qquad (2.8)$$
$$Y_2 = X_1^* w_2(t) + X_2 w_1(t)$$

Each Y_1 and Y_2 is then complex PN-spread with the cell's $PN^{(I)}$ and $PN^{(Q)}$ sequences, resulting in PN-spread symbols Z_1 and Z_2 (respectively). Z_1 is then transmitted from antenna 1 while Z_2 is transmitted from antenna 2 (with the same power as Z_1).

Figure 5 presents a block diagram of the transmitter:

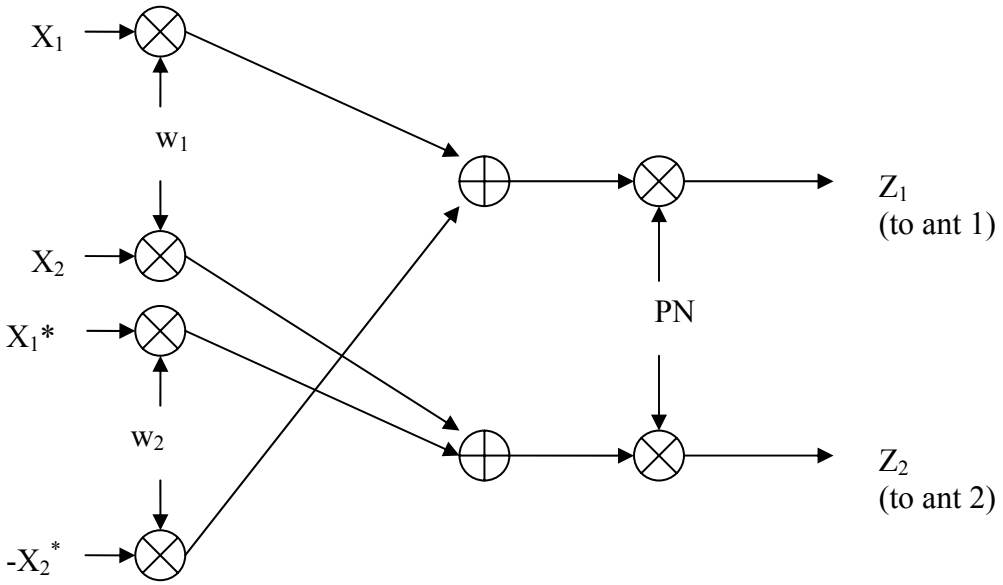

Figure 5: STS scheme

Let h_1 and h_2 be the complex channel gains from antenna 1 and antenna 2, respectively. Assuming that the channel gain and phase remain essentially invariant across a duration of two symbols, the received symbol after PN de-spreading can be expressed as:

$$s'(t) = [X_1 w_1(t) - X_2^* w_2(t)]\, h_1 + [X_1^* w_2(t) + X_2 w_1(t)]\, h_2$$

In order to demodulate $s'(t)$, the mobile first de-spreads it w_1 and w_2. Using (2.1) and (2.3):

$$y_1 = \sum_{j=0}^{L-1} w_1(j)\ s'(j) = L\left(h_1 X_1 + h_2 X_2\right)$$

$$y_2 = \sum_{j=0}^{L-1} w_2(j)\ s'(j) = L\left(h_2 X_1^* - h_1 X_2^*\right)$$

In addition, the mobile obtains estimates of the channel gains h_1 and h_2, and uses them to recover X_1 and X_2 as follows:

$$h_1^* y_1 + h_2 y_2^* = L\,(|h_1|^2 + |h_2|^2)\, X_1$$
$$h_2^* y_1 - h_1 y_2^* = L\,(|h_1|^2 + |h_2|^2)\, X_2$$

like in the Alamouti scheme.

2.4 Forward-link overhead channels

In addition to the traffic channels described in section 2.2, three *overhead channels* are of special importance in the forward-link of the cdma2000 system: *common-pilot channel*, *paging channel* and *synchronization channel*. In addition, it transmit diversity is enabled, a *diversity-pilot channel* is also present.

The following sections describe these overhead channels in more detail, as they will be relevant for the discussion in subsequent chapters.

2.4.1 Common-pilot channel

The common-pilot channel is an uncoded signal consisting entirely of 0-valued bits. The pilot channel undergoes BPSK modulation, which assigns all zero-bits to +1 values. Furthermore, the common-pilot channel is always assigned Walsh-code 0, which consists entirely of +1 values; therefore, the orthogonally-spread common-pilot channel also consists entirely of +1 values. These are finally complex PN-spread, used to modulate the pulse-shaping filter, and transmitted on the carrier.

The baseband common-pilot channel thus consists of the pulse-shaping filter modulated by the PN_I and PN_Q sequences, and transmitted on the cosine and sine of the carrier frequency (respectively). As can be seen from the equations in (2.5), the BPSK-modulated pilot can be seen as a QPSK-modulated signal with a value of 0 for Y_Q.

The common-pilot channel is a strong signal[11] that is continuously transmitted by the main antenna in the base-station. The pilot-channel signal is effectively a training sequence, and serves three main purposes:

1. It permits the mobile receiver to track the strongest multipaths arriving from the main antenna
2. It allows for estimation of the channel amplitude gain and phase shift.
3. It aids the mobile in achieving phase coherence with the base-station.

Section 2.5 describes in more detail how the RAKE receiver performs these functions.

It is worth noting that a pilot is also transmitted on the reverse-link; however, the pilot bits are time-multiplexed with the traffic bits, and both are transmitted on the same reverse-link channel. The reverse-link pilot is an improvement of cdma2000 over the older IS-95 standard, and allows for coherent demodulation and better performance on the reverse-link.

[11] As an illustration: for the tests performed in chapters 5 and 6, roughly 20% of the total base-station power was allocated for the common-pilot channel.

2.4.2 Synchronization and paging channels

The synchronization and paging channels are continuously transmitted by the base-station main-antenna, and like the common-pilot channel are also BPSK-modulated. The synchronization channel is decoded after the pilot-channel is first acquired; once the synchronization channel is acquired, the mobile proceeds to decoding the paging channel.

The synchronization channel informs the mobile about frame boundaries as well as other system information. The paging channel also contains relevant system information; in addition, it is used to page the mobile on the event of an incoming call. The base-station might transmit multiple paging channels, but in general only one is required.

2.4.3 Diversity-pilot channel

When STS is enabled, the mobile needs to track signals from both antennas. Therefore, the diversity antenna must also transmit a pilot sequence so that the mobile can track multipaths, estimate channel gain and perform phase coherence for the signal from the diversity antenna.

The diversity pilot is always transmitted on the 16-th Walsh code. In addition, the cdma2000 standard specifies that the ratio between the diversity-pilot power and the common-pilot power can be either 0dB, -3dB, -6dB and -9dB. Higher diversity-pilot power levels improve phase-coherence, multipath tracking and channel gain estimation from the diversity antenna at the expense of additional power consumption.

2.5 The RAKE receiver

The RAKE receiver is particularly suited for spread-spectrum systems, taking advantage of the high signal bandwidth to decode signals arriving at different multipaths. Because of the fine granularity in multipath resolvability, the use of a RAKE receiver dispenses the use of an equalizing filter; in addition, RAKE receivers are able to effectively exploit the multipath structure of the channel to obtain diversity.

A RAKE receiver has two components, one *searcher* and a set of 4 to 6 *fingers*. The following subsections explain these in more detail:

2.5.1 Searcher

The role of the searcher is to track the delays of the strongest multipaths arriving from the base-station. The searcher relies on the PN-spread pilot signal to achieve this purpose: since the different multipaths delays translate into different PN-offsets for the received signal, the searcher is able to resolve the individual paths by tracking their PN offsets.

Figure 6 presents a block diagram of a cdma2000 searcher:

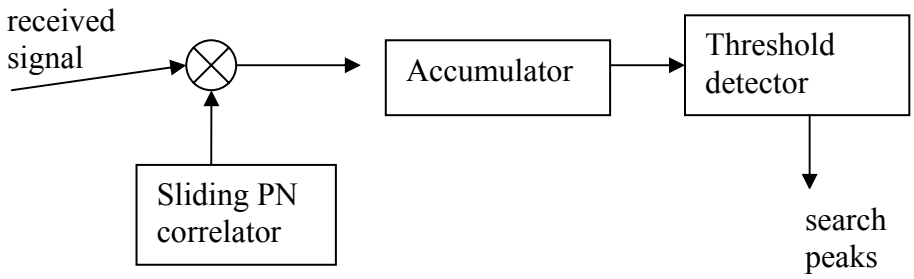

Figure 6: Block diagram of a cdma2000 searcher

As figure 6 shows, the searcher includes a sliding PN correlator: its job is to correlate the received base-station sequence with the PN sequence shifted by various offsets. The accumulator then computes the common-pilot energy and (if STS is enabled) the diversity pilot energy of the correlated signal by de-spreading the correlated signal with the appropriate Walsh codes.

The offsets that result in the largest common-pilot and diversity-pilot energy are separately reported as *searcher peaks* as long as they are above a minimum threshold. Incidentally, it can be seen that a searcher is capable of resolving multipaths within a granularity of 1 chip, or the inverse of the signal bandwidth.

It is worth noting that neighboring-cell PN offsets differ from the serving cell's PN offset by at least 512 chips, a number much larger than the sliding correlator's search window. This prevents signals from neighboring cells to be confused with in-cell multipaths.

2.5.2 Fingers

Once the searcher peaks are determined, it is the job of the RAKE receiver's *fingers* to demodulate the traffic channel signals arriving at each path. Each finger is demodulated by first correlating the received base-station signal with the PN sequence shifted by the searcher-peak offsets; the energy on the mobile's traffic channel is computed by de-spreading the resulting signal with the appropriate Walsh code.

Once the individual fingers are demodulated, the RAKE receiver *combines* their energy by computing a weighted sum of the individual finger energies. A common recombination method is to use *maximal-ratio combining*, which weights individual fingers according to their strength. An alternative method is to use *pilot-based combining*, which weights the fingers according to the received pilot-channel energy received at that particular offset. The pilot-channel energy also gives an estimate of the channel gain.

Figure 7 shows a simple block diagram illustrating finger demodulation and combining.

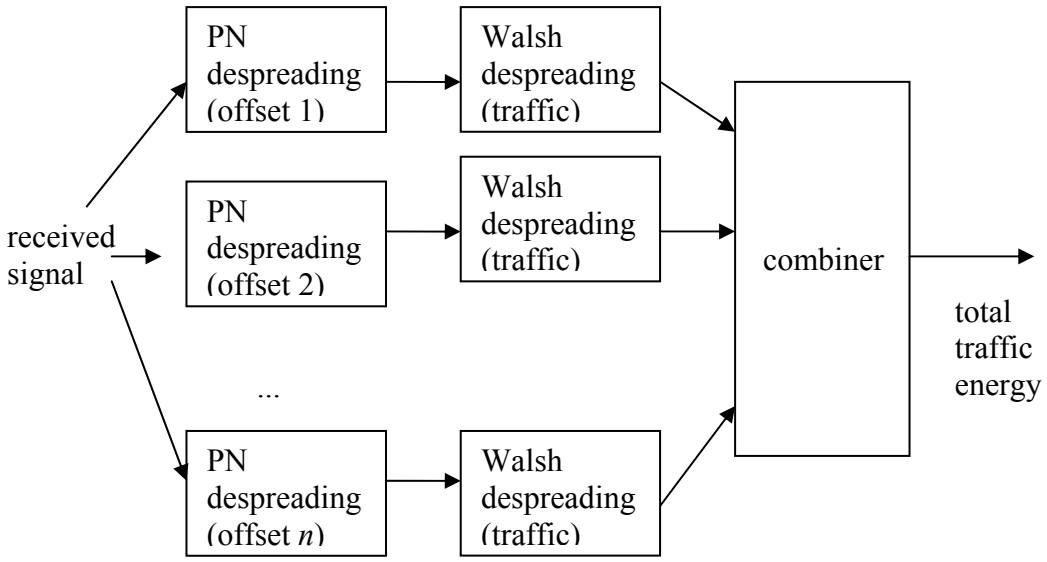

Figure 7: Block diagram of finger combining

Different fingers always use different offsets for PN correlation. In the case of search peaks from the main and the diversity antennas occurring at the same offset, the same finger is used to demodulate the traffic-channel signal at both peaks. The two traffic energies obtained are then combined into an overall finger energy and fed to the combiner, which weights the finger with a combination of main-pilot and diversity-pilot received energy[12].

2.6 Power control

As a direct-sequence spread-spectrum system, cdma2000 is interference-limited rather than power-limited or bandwidth-limited. Because all user signals share a common bandwidth, each user signal poses interference to all other users; as a result, higher power levels for one user imply additional interference to all other users. Power-control is thus crucial for acceptable performance, both on the forward and the reverse-link.

Power control works on the principle of allocating the minimum amount of power necessary to achieve an acceptable quality-of-service (typically measured as a target error-rate for received frames); adherence to this principle not only saves power but also decreases interference to other users.

[12] The algorithm for combining traffic/pilot-channel energy from the two antennas is implementation dependant.

A constant quality of service, or target frame error-rate (FER), is typically achieved by ensuring that the signal arriving at the receiver has approximately constant energy. Therefore, power control has the role of "inverting" the channel effects. There are two main effects at stake: near-far problem and multipath fading. These are addressed by the open-loop and closed-loop stages of power-control (respectively), explained in the following subsections.

2.6.1 Open-loop power control

The open-loop stage of power control addresses the near-far problem on the reverse-link, defined as the varying levels of signal power received from mobiles in the cell due to the varying levels of path loss. More specifically, signals from mobiles located close to the base-station face little path loss attenuation whereas signals from mobiles close to the border of the cell may face large path loss attenuations en route to the base-station.

The mobile transmit power is adjusted once for every new transmitted frame; that is, all symbols in a frame are transmitted with the same power. For each new frame, the mobile's initial estimate for transmit power is essentially the inverse of the total base-station power received at the mobile for the previous frame, plus a correcting factor to account for other-cell interference. The accuracy of this estimate relies on the assumption that channel attenuation due to path loss is highly correlated for the forward and reverse links.

Open-loop power control is not enough to ensure satisfactory performance because it does not compensate for multipath fading; after all, multipath fading is generally uncorrelated between forward-link and reverse-link signals since they are centered at different carrier frequencies. In order to address multipath fading effects, the mobile relies on feedback from the base-station, giving rise to *closed-loop power control* (described next).

2.6.2 Closed-loop power control

Closed-loop power control, unlike open-loop, is mandatory on both forward and reverse-links. It has two components, *inner-loop* and *outer-loop*.

2.6.2.1 Inner-loop

The inner-loop is responsible for verifying whether the received bit-energy-to-noise ratio is above a certain threshold. If the ratio is higher than the threshold, the receiver instructs the transmitter to reduce power; otherwise, the transmitter is instructed to increase power.

The instructions to increase or decrease power are sent via *power control bits*: a value of 0 for the power control bit instructs the transmitter to increase power, whereas a value of 1 instructs the transmitter to decrease power. The dB step size is the same for

both increases and decreases in transmitted power, and is specified as part of the base-station configuration.

Incidentally, there is no dedicated channel for transmitting power-control bits for either the forward or reverse-link traffic channels; instead, these bits are punctured into the traffic channel. The frequency with which power-control bits are transmitted constitutes the inner-loop power-control rate; a typical value (used in all tests in chapters 4 and 5) is 800 Hz, or 16 power-control bits for every 20ms frame. The commands from the 16 power control bits are combined and, if applicable, added to the open-loop estimate to determine the transmitted power level for the next frame[13].

2.6.2.2 Closed-loop

The role of closed-loop power-control is to adjust the threshold used by the inner-loop to ensure a target FER; this threshold is also known as the *setpoint*. Assuming that the inner-loop is successful in ensuring that the received signal power is approximately constant, the setpoint serves as a measure of the bit-energy-to-noise ratio required to achieve a target FER at the receiver.

Ideally, closed-loop power control would continuously estimate the received FER by determining the percentage of total frames received in error. It would then either increase or decrease the setpoint, depending on whether the estimated FER was higher or lower than the target. The problem with this approach is that FER estimations based on previous frames are not reliable, as older frames were likely subjected to different channel conditions.

A common implementation for outer-loop power-control relies only on the result of the latest received frame: if it is received in error, the setpoint is increased, otherwise the setpoint is decreased. The step increase and step decrease are not the same; they should be related in such a way that when power-control is stabilized and a constant FER is achieved, the net setpoint increases should equal the net setpoint decreases.

Let x_i be the step increase and x_d be the step decrease. Assuming a 1% FER, the receiver should get roughly 99 good frames for each bad frame. Therefore, the total decrease is $99x_d$, whereas the total increase x_i, giving the relation $x_d/x_i = 1/99$. More generally, x_d/x_i should equal $y/(1-y)$ where y is the target error-rate.

Figure 8 illustrates the evolution of the setpoint in stationary state.

[13] Other factors that influence power levels (such as access probe corrections) are being ignored here.

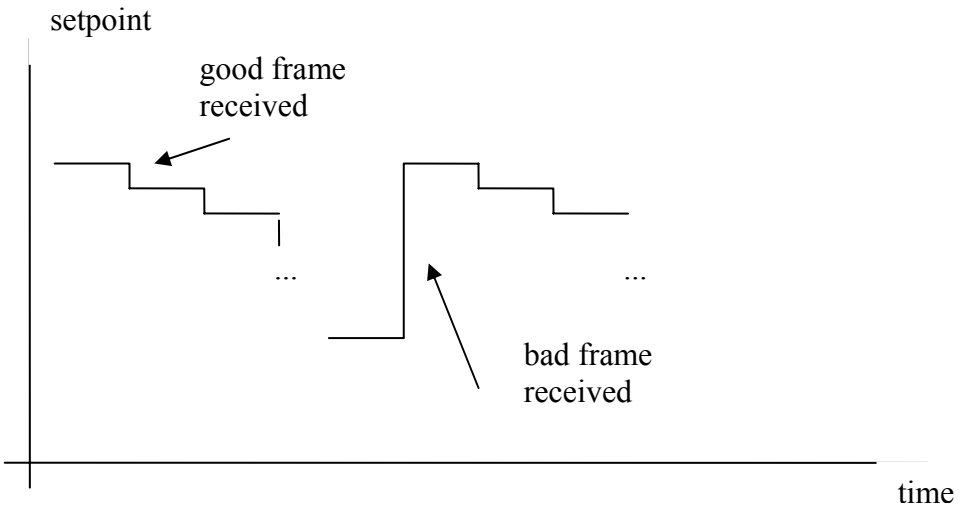

Figure 8: Setpoint evolution in stationary state

It is worth noting that when power-control is enabled, the receiver error-rate is constant. Therefore, the required transmitted power – instead of the error-rate – serves as a measure of system performance. This measure will be used both in simulations and in field results to compare the performance of the different transmit diversity schemes.

2.7 Soft handoff

Unlike conventional systems, cdma2000 allows a mobile close to the border of a cell to be in *soft handoff*. When in soft handoff, a mobile receives its signal from more than one base-station, contributing to spatial diversity.

The most attractive feature of soft handoff is that it allows a mobile to start communication with a new base-station before interrupting communication with the old one, therefore contributing to a smoother transition between serving cells. The main expense of soft handoff is a reduction in the number of available Walsh codes: because a base-station must be able to perform soft handoff with mobiles in other cells, some fraction of the forward-link channels are reserved for handoff activities. These Walsh codes become thus unavailable for in-cell traffic channels.

Chapter 3: Simulation results

(The results described in this chapter are based on [13], and serve as a reference against which to compare the experimental field results in chapter 6.)

Simulations have shown that *Space-Time Spreading (STS)* and *Phase-Sweep Transmit Diversity (PSTD)* both provide significant link-level improvement compared to *No-Transmit Diversity (NTD)*. This chapter presents some of these simulation results, which were obtained in an attempt to quantify the link-level improvements for an array of different channel models and base-station configurations.

Section 3.1 introduces commonly used terms. Section 3.2 describes the channel models used in the simulations. Section 3.3 details simulation-specific configurations for the transmit diversity schemes. Section 3.4 explains the methodology of evaluation and presents the results. Section 3.5 obtains an estimate of the improvements in cell capacity for each transmit diversity technique.

3.1 Background

Section 3.1.1 introduces the concepts of energy-per-chip (E_c), transmit-signal power density (I_{or}) and normalized transmit power (E_c/I_{or}). Section 3.1.2 describes the sources of noise in the cdma2000 system, defines the *geometry* metric and explains its relevance.

3.1.1 E_c, I_{or} and normalized transmit power (E_c/I_{or})

As described in chapter 2, the pulse-shaping unit in cdma2000 is a *chip.* The chips are the output after the voice/data bits undergo error-coding, interleaving, orthogonal spreading and PN-spreading[14]. Each chip subsequently modulates a pulse for generation of the baseband signal.

Because the chip rate approximately equals the bandwidth of the baseband signal, power spectral density levels are specified in units of *energy-per-chip* (E_c). For any given channel, energy-per-chip (E_c) and energy-per-bit (E_b) are related by:

$$E_b = \frac{R_c}{R_b} E_c = P_g E_c \qquad (3.1)$$

where R_c is the chip rate or signal bandwidth, R_b is the bit rate and $P_g = R_c/R_b$ is the *processing gain*.

[14] As in chapter 2, long PN-spreading will be bypassed in this discussion.

In particular, the power density for the base-station signal (I_{or}) is also specified in units of energy-per-chip[15]. In the case of two antennas, I_{or} is the sum of the power densities from the two antennas:

$$I_{or} = I_{or,1} + I_{or,2} \qquad (3.2)$$

where $I_{or,1}$ and $I_{or,2}$ refer to the transmit power densities for the main and diversity antenna, respectively.

Power levels for individual channels are often specified as a fraction of total base station power. This motivates the definition of *normalized transmit power* (E_c/I_{or}) for a channel, which is simply the energy-per-chip in the channel divided by total base-station transmit-power density. It is worth noting that since both the channel E_c and total I_{or} are specified in units of energy-per-chip, E_c/I_{or} is a-dimensional.

In order to make results comparable, I_{or} is kept constant across different tests. As a consequence, E_c/I_{or} can be used as an absolute measure of power; this will be the case for the results in section 3.4 as well as in chapters 5 and 6.

3.1.2 Noise[16]

In the cdma2000 system, noise consists mainly of three components: receiver thermal noise, other-cell interference and in-cell interference. The receiver thermal noise is caused by the thermal agitation of electrons in the receiver hardware, and is modeled as zero-mean additive white Gaussian noise (AWGN). On the other hand, the modeling of other-cell and in-cell interference is more complex, as it depends on the position of the mobile with respect to surrounding base stations (in the case of other-cell interference) and on the multipath structure of the channel (in the case of in-cell interference).

In addition, the modeling of in-cell and other-cell interference is different for the forward and reverse link; however, since the objective of this thesis is to evaluate the benefits of transmit diversity in the base station, the following discussion will be restricted to forward-link interference in cdma2000.

Forward-link interference, in principle, includes interference caused by mobile-transmitted as well as base-station-transmitted signals. The interference of mobile-transmitted (reverse-link) signals on the forward-link can be neglected, however, because forward-link and reverse-link signals are centered at different carrier frequencies. Hence, from here onwards it is assumed that all forward-link interference is due entirely to base-station (forward-link) signals.

[15] The subscript "or" refers to the mutual orthogonality between the channels in the base station transmit signal.
[16] The distinction between *noise* and *interference* will be ignored in this discussion.

3.1.2.1 Other-cell interference and I_{oc}

Other-cell interference refers to interference from base station signals in nearby cells. Due to universal frequency reuse, neighboring cells typically operate on the same forward-link frequency as the serving cell, magnifying the potential for interference. The level of other-cell interference varies from mobile to mobile within a cell, being higher for mobiles near the cell boundary and often negligible for mobiles close to the center of the cell.

In cdma2000, other-cell interference is mitigated by pseudo-noise (PN) de-spreading. As explained in chapter 2, each base station spreads its signal using a complex PN-sequence starting at a particular offset. Though all base stations use the same spreading PN-sequence, sequences for neighboring cells start at different offsets. Because PN sequences at different offsets have very low correlation, interference from neighboring cells is drastically reduced after PN de-spreading at the mobile receiver.

Other-cell interference can be assumed to have the statistics of AWGN when it comes from many independent sources with approximately equal power. This is usually the case for mobiles located close to the center of an urban or suburban cell, where many surrounding base stations equally contribute to other-cell interference. Since receiver thermal noise is also AWGN and is independent of other-cell interference, it is convenient to couple the two together as a single noise process with power spectral density I_{oc}. Mathematically, if $n(t)$ is a sample function of the noise process, then:

$$E\left\{ \left| n(t) \right|^2 \right\} = I_{oc}\delta(0) \qquad (3.3)$$

where $E(.)$ denotes expectation.

3.1.2.2 In-cell interference

In-cell interference refers to interference due to the other channels in the transmit signal of the serving cell's base station. More precisely, a given mobile's traffic channel can suffer interference from the power in the traffic channels intended for other mobiles, or from the power in other broadcast and shared channels that compose the transmit signal of the serving-cell base-station.

As will be shown in chapter 5, in the case of a single resolvable path from the base station to the mobile all channels in the base station signal are mutually orthogonal and in-cell interference is negligible. On the other hand, in the case of multiple resolvable paths from the base-station transmitter antennas to the mobile receiver antenna, the signals coming from the different paths have different time delays and as such are no longer time-synchronized. The lack of synchronization breaks the orthogonality between the forward-link channels, and in-cell interference ensues.

3.1.2.3 Geometry

Geometry, or mean carrier-to-noise ratio at the receiver, is defined as:

$$G = \frac{\overline{I'_{or}}}{I_{oc}} = \frac{I_{or}\ L}{I_{oc}} \quad (3.4)$$

where

I_{or} = energy-per-chip of the signal transmitted from the serving base-station
$\overline{I'_{or}}$ = mean energy-per-chip received at the mobile
L = mean attenuation from the serving-cell base station to mobile
I_{oc} = power-spectral density of other-cell interference plus thermal noise.

The prime superscript in I_{or}' refers to the quantity as seen by the receiver, thus incorporating the channel gain; the bar indicates that it refers to the mean across many symbols (as opposed to a per-symbol density).

Because L and I_{oc} depend on the mobile's location with respect to the serving and surrounding base stations, it follows that geometry varies from mobile to mobile within a cell. More specifically, geometry is high for mobiles close to the center of the cell, and low for mobiles near the cell boundary[17]; Figure 1 illustrates this. In addition, if a mobile changes location significantly during the course of a call, L and I_{oc} change, so the mobile geometry changes over time as well. On the other hand, since geometry involves only the mean received I_{or}' rather than the distribution, it does not incorporate the channel's fading characteristics but only large-scale attenuation and shadowing effects.

Geometry is a simple metric quantifying the amount of noise and other-cell interference. Higher geometry values correspond to less noise, and consequently less required transmitted power to achieve the same call quality.

[17] Ignoring the effects of soft-handoff.

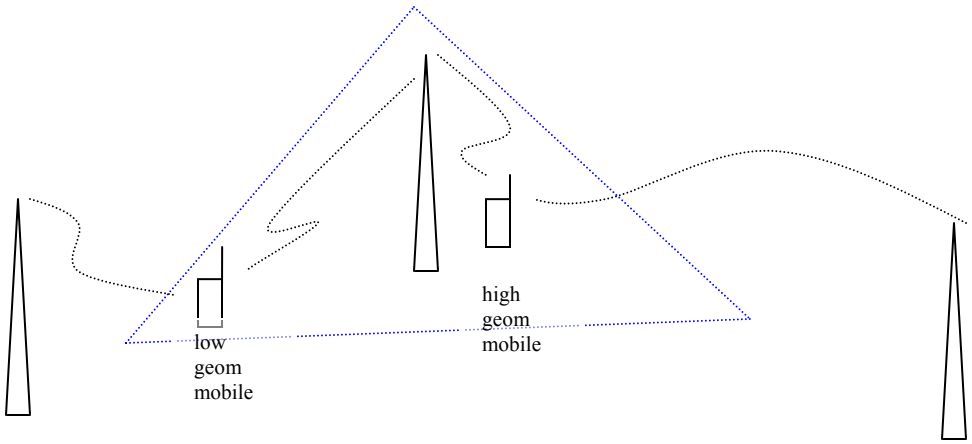

Figure 1: Mobile geometry for different regions in a cell. The curved lines represent base-station transmitted signals, and the straight lines denote cell boundaries.

3.2 Channel models

The following sections describe the different models simulated in an attempt to cover a comprehensive range of possible field scenarios. More specifically, they detail the simulation parameters across the following three dimensions: channel multipath structure/fading model, mobile speed, and geometry. Together, these three dimensions completely characterize the channel according to the models used.

3.2.1 Multipath structure and fading model

The multipath structure is the major determinant of channel behavior in wireless channels, especially in urban and suburban settings. Consequently, in order to evaluate performance under different channel models, it is necessary to consider different channel multipath structures.

As mentioned in chapter 2, the use of PN spreading sequences allows cdma2000 receivers to distinguish paths separated by at least 1 chip (0.813 μs, the inverse of the signal bandwidth). Based on the tap-delay model introduced in chapter 1, the channel multipath structure is modeled as a discrete set of taps, with each tap's delay specified in chips. In addition, the channel coefficient for each tap is modeled as a fading process. Such a model conveniently separates the two opposing effects of multipath: 1) diversity provided by multipath components that are far apart so they can be individually resolved

at the receiver; 2) fading caused by the superposition of closely-spaced multipath components.

As mentioned in chapter 1, it is generally assumed that the fading processes are mutually uncorrelated across different path delays; as such, multiple taps in the channel provide *diversity* to the receiver. Therefore, by simulating multipath structures with different numbers of taps, different levels of *diversity* are being simulated.

The tap-delay channel model incorporates both the path loss attenuation and the fading process into a single coefficient for each tap. The simulation models, on the other hand, separate these two processes. More specifically, they specify for each tap:

1. Time delay (with respect to tap 1)
2. Attenuation, specified as the percentage of the transmit power that goes into the tap.
3. Model for the fading coefficient.

The combination of attenuation and fading coefficient corresponds to the coefficient in the tap-delay model.

Table 1 shows the four different multipath models captured in the simulations. In compliance with standard RAKE-receiver terminology, each tap is termed a *finger*. For each finger, the "Fing(dB)" row says what portion of the transmit power comes at that finger, whereas each "Fing Del (T_c)" row refers to the chip delay of that finger with respect to the smallest-delay finger. The "Unrecovered (dB)" row measures the portion of the signal power that is "lost" because the receiver could not track the corresponding taps. Finally, the "Fading" row specifies the fading model used for the fingers in each channel model. ([1] contains a more detailed description of the Jakes model, a Rayleigh fading model with a particular Doppler power spectrum). In each case, the tap model applies to the channels from both antennas.

Table 1: Multipath channel models [13]

Model	A	B	C	D
ModelName	Pedestrian A	Pedestrian B	Vehicular A	LineOfSight
# Fingers	1	3	2	1
Fing1 (dB)	-0.06	-1.64	-0.9	0
Fing1 Del (Tc)	0	0	0	0
Fing2 (dB)		-7.8	-10.3	
Fing2 Del (Tc)		1.25	1.25	
Fing 3(dB)		-11.7		
Fing3 Del (Tc)		2.75		
Unrecovered(dB)	-18.8606	-10.9151	-10.2759	-Infinite
Fading	Jakes	Jakes	Jakes	K=10, Rician

A more complete justification for these models can be found in [12].

3.2.2 Mobile speed and geometry

As explained in chapter 1, the statistics of a fading model are affected by the relative speed between the transmitter and the receiver. This relative speed establishes a *Doppler spread* and determines a *coherence time* for the channel. Thus, in order to compare the different schemes, different mobile speeds should be simulated. The speeds simulated were: 1 km/h, 3 km/h, 10 km/h, 30 km/h and 100 km/h.

In order to assess performance under different levels of other-cell interference, three geometry values were used in the simulations: 0dB, 4dB and 8dB. These values should give a rough idea of the performance for mobiles in different regions of the cell.

3.3 Transmit diversity schemes

The simulations tested the performance of both *Space-Time Spreading* (STS) and *Phase-Sweep Transmit Diversity* (PSTD), and compared them to the performance of *No-Transmit Diversity* (NTD) as a reference. This section presents simulations-specific details about the different schemes.

3.3.1 No-Transmit Diversity

No-Transmit Diversity (NTD) is the standard technique for transmission in cdma2000 cells, and uses only one transmit antenna. The signal from the antenna contains the broadcast and shared channels as well as the traffic channels for individual mobiles. Once the total base-station transmit power (I_{or}) is fixed, it remains to distribute this power across the different channels – this distribution constitutes the base-station configuration of an NTD cell.

In the simulations, only four types of channels were present: pilot, paging and synchronization channels (collectively termed *overhead* channels), and the fundamental (FCH) traffic channels for individual mobiles[18]. The transmitted power levels of mobile traffic channels are continuously power-controlled in order to achieve a target frame error-rate (FER). The power levels of the overhead channels, on the other hand, are fixed at the base station.

Fixing the power levels of overhead channels involves a tradeoff: higher power results in better acquisition of the channels, but at the expense of the power budget. Since total I_{or} is fixed, higher power levels at the overhead channels imply lower available power for traffic channels, meaning that fewer users can be supported in the cell.

Table 2 shows the power levels used for overhead channels in the simulations. The appropriateness of these values was determined from previous experiments; small

[18] Since only voice calls were simulated, there were no supplemental channels; hence, the only traffic channel present was the fundamental channel.

variations on these values are possible, though they should not affect the results significantly.

Table 2: Power levels of overhead channels

Channel	E_c/I_{or} (dB)
Pilot	-8.5
Paging + synchronization	-7

3.3.2 Space-Time Spreading (STS)

In the *Space-Time Spreading* (STS) scheme, the base station uses two antennas for transmission: one antenna is termed the *common* or *main* antenna, whereas the other antenna is termed the *diversity* antenna. As described in chapter 1, the common antenna transmits overhead channels (pilot, paging, synchronization), full traffic-channel power for non-STS mobiles, and half the traffic-channel power for STS mobiles. The diversity antenna, on the other hand, transmits the diversity pilot and half the traffic-channel power for STS mobiles.

The power levels for the overhead channels in the common antenna are set to the same levels as in the No-Transmit Diversity (NTD) case. And, like in the NTD case, the power levels of the traffic channels are power-controlled so as to achieve a target frame-error rate (FER) and ensure a certain quality to the voice call. Consequently, the only parameter that needs to be specified in STS is the diversity pilot level, set to a fixed value at the base station.

As explained in chapter 2, the cdma2000 standard specifies that the ratio of the diversity pilot to the common pilot can assume any of 4 possible values: 0dB, -3dB, -6dB and -9dB. On one hand, higher power levels imply better diversity pilot acquisition, less required traffic power to achieve a target error-rate, and increased cell capacity. On the other hand, they imply less power available for traffic channels, with a negative influence on cell capacity in terms of number of supported users.

The simulations attempt to quantify the performance of all four flavors of STS: STS-0dB, STS–3dB, STS–6dB and STS-9dB. It is expected that STS-0dB will have the lowest required traffic-channel transmit power due to better diversity pilot acquisition. The simulations should then inform the extent to which reductions in traffic-channel transmit power compensate for the extra power spent in the diversity pilot. In other words, one of the four schemes should represent the optimal tradeoff between satisfactory diversity pilot acquisition and minimal diversity-pilot power consumption.

3.3.3 Phase-Sweep Transmit Diversity (PSTD)

As described in chapter 1, *Phase-Sweep Transmit Diversity* (PSTD) is a two-transmit antenna technique that does not require any mobile-specific support. The channels composing the base station signal are the same as in *No-Transmit Diversity* (NTD), except that the power in each channel is divided in two halves, with one half being transmitted from each antenna. In addition, with respect to the first antenna, the second antenna applies a small frequency offset to the signal (equivalently, a phase sweep) – the phase-sweep essentially "fast-fades" the channel, improving the time-diversity effects brought by interleaving at the transmitter.

In PSTD, the transmit powers for the overhead channels are set to the same levels as in the NTD case. The only additional parameter that needs to be configured is the phase-sweep frequency. In this regard, an important factor is the frame size used for interleaving: 20ms for all simulations. Since coded-bits are only interleaved within a frame, the coherence time of the channel must be smaller than 20ms for time diversity to be of any benefit. Therefore, the phase-sweeping frequency should be at least 1/20 ms = 50Hz between the two antennas, as it guarantees that the channel changes within a frame.

The phase-sweeping frequency should not be very high since fast-fading channels exacerbate receiver imperfections and degrade performance. At the same time, previous simulations have shown that the benefits of phase-sweep are fairly insensitive to the phase-sweep frequency if it is kept low. For the simulations described in this chapter, the phase-sweep frequency was set to 100 Hz.

3.4 Results

Simulations were conducted for each combination of:

1. Multipath profile: A, B, C or D (models described in Table 1)
2. Speed: 1, 3, 10, 30 or 100 km/h
3. Geometry: 0, 4 or 8 dB.
4. Transmit diversity scheme: NTD, PSTD, STS-0dB, STS-3dB, STS-6dB or STS-9dB.

Each simulation corresponded to a full-rate voice-call (rate of 9.6 kbits/s), with power-control set to achieve a fixed 1% FER at the receiver. In all cases, base-station transmit power was set to its maximum value by adding spurious traffic channels.

The mean E_c/I_{or} of the fundamental (FCH) channel served as the performance metric for comparing the different schemes. This metric provides the most direct measure of the effects of transmit diversity: a lower mean E_c/I_{or} for the FCH channel indicates that lower traffic power per mobile is required to achieve the target receiver error-rate, which translates to savings in overall power consumption. Furthermore, if the total base station

transmit power (I_{or}) is capped, a lower FCH E_c/I_{or} per mobile results in increased cell capacity as measured by maximum number of supported users.

3.4.1 Performance across speed

Figure 2 shows the performance of the different schemes for model C, a fixed geometry of 4dB, and varying speeds[19]. The figure shows that all transmit diversity schemes outperform NTD, suggesting that transmit diversity does indeed provide a significant benefit (over 3dB at slow speeds, and up to 1 dB at high speeds). The reduced benefit from transmit diversity at higher speeds is likely due to the added time diversity introduced by faster-fading channels.

The figure illustrates that STS with a larger diversity pilot outperforms STS with a lower diversity pilot. The figure also shows that there is a significant gap between STS-6dB and STS-3dB at low speeds (less than 10 km/h), but that the gap narrows at higher speeds. Meanwhile, it was observed that STS-9dB consistently underperformed other STS schemes at all speeds. STS-0dB was observed to be the top performing scheme, though the difference to STS-3dB was small.

The figure shows that PSTD has a performance comparable to STS-6dB at low speeds; meanwhile, it was observed that PSTD performance is comparable to STS-9dB at high speeds. The figure also shows that the performance of PSTD converges to that of NTD at high speeds. This is expected because at high speeds the channel is already "fast-fading", so the artificial fast-fading induced by PSTD has little noticeable effect.

[19] Similar trends were observed for other geometries and channel models.

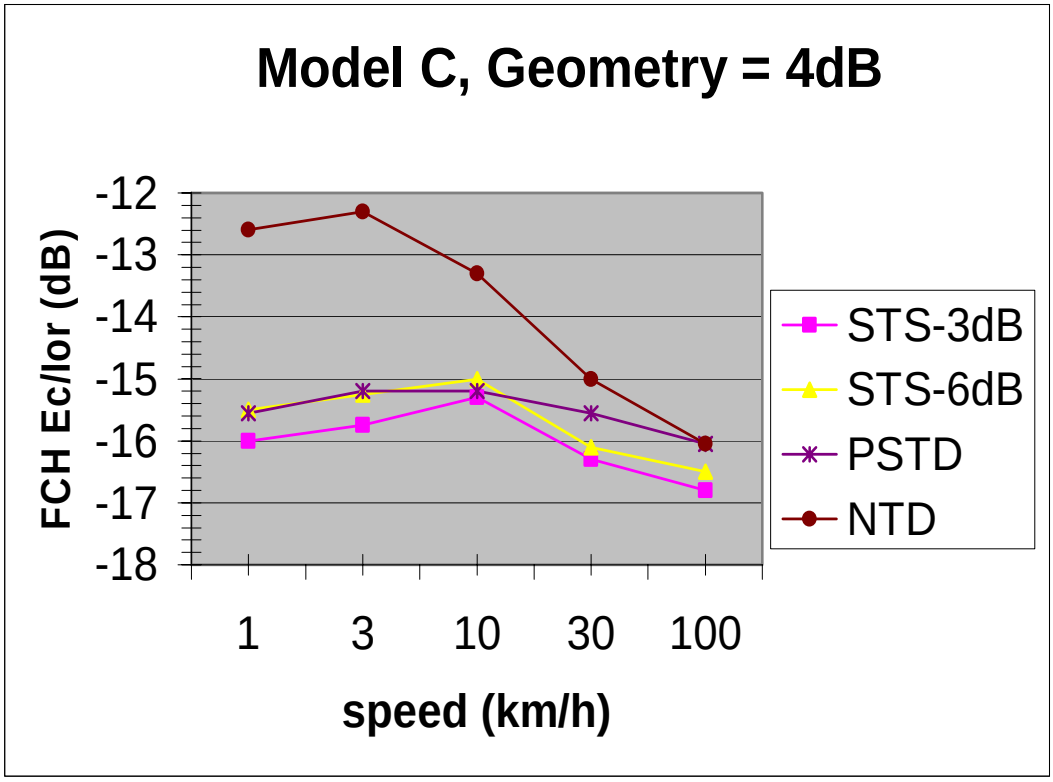

Figure 2: Performance across speed

3.4.2 Performance across multipath/fading model

Figure 3 compares the performance of STS-3dB, STS-6dB and PSTD across different multipath channel models. The figure plots the difference in required FCH E_c/I_{or} compared to the NTD case.

Comparing the Rayleigh models A, B and C, it is clearly seen that all transmit diversity techniques provide the largest benefit - over 3dB - in model A (a one-tap channel) and the smallest benefit - approximately 1dB - in model B (a three-tap channel). The graphs suggest that the multipath diversity (equivalently, frequency-selectivity) in models B and C reduce the potential diversity gain due to transmit diversity.

It can also be seen that the benefits of transmit diversity are lowest for model D. This is explained by the fact that model D is a Rician channel with a high K-factor, or equivalently, a high correlation between the channels from the two antennas. Because of the high correlation, the signals from the diversity antenna provide less diversity and therefore reduced link-level improvements for STS. For PSTD, there is in fact degradation with respect to NTD: as explained in chapter 1, the high correlation between antennas results in extended deep fades in PSTD due to the deterministic phase-sweep between the two transmitted antenna signals; these extended deep fades significantly degrade performance at the mobile receiver.

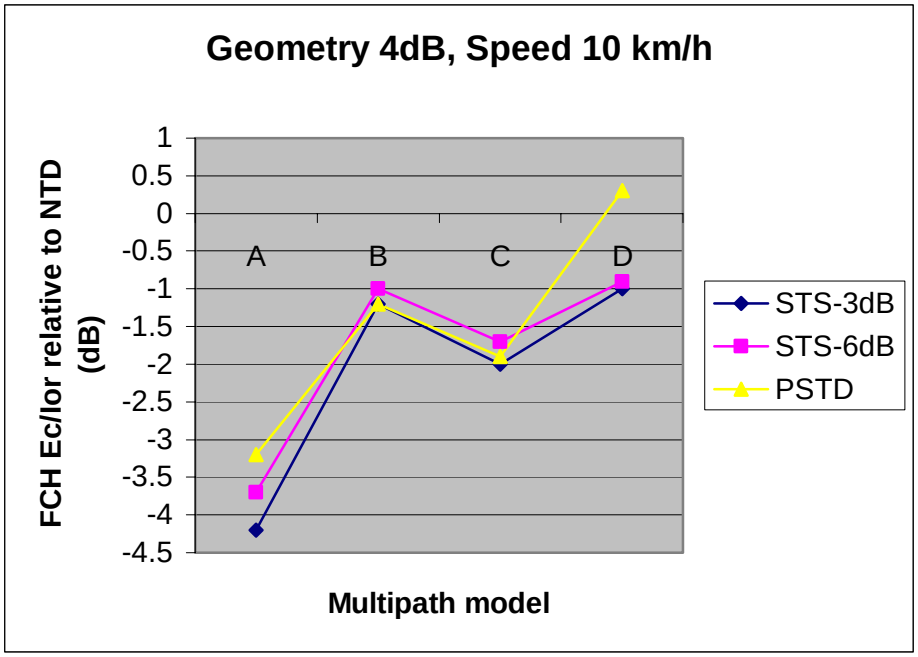

Figure 3: Performance across multipath/fading model

3.4.3 Performance across geometry

Figure 4 compares the performance of STS-3dB, STS-6dB, PSTD and NTD for different channel geometries. The first plot shows the raw FCH E_c/I_{or}, whereas the second plot shows the E_c/I_{or} performance with respect to NTD.

It can be seen that the performance improvements due to transmit diversity are reduced for higher geometries - being approximately 3dB for low geometries and 1.7dB for high geometries. These results corroborate the fact that the main benefits from transmit diversity occur in scenarios of low received signal-to-noise ratio (as explained in chapter 1).

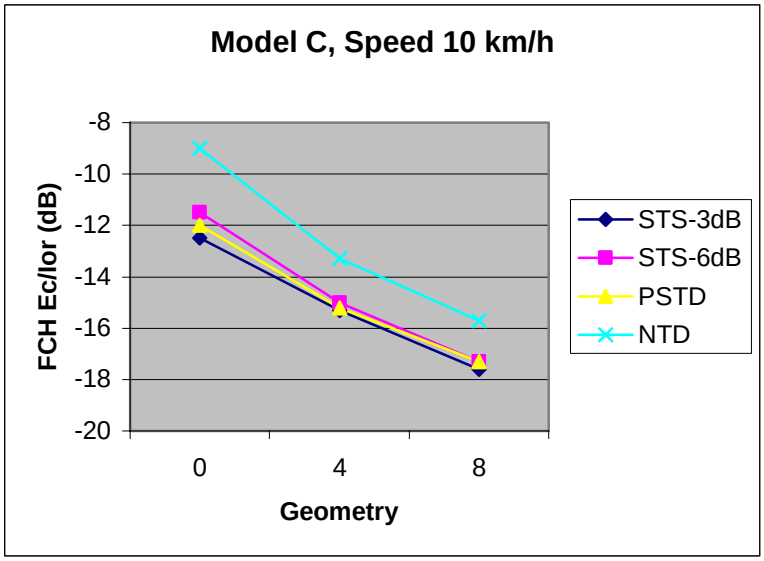

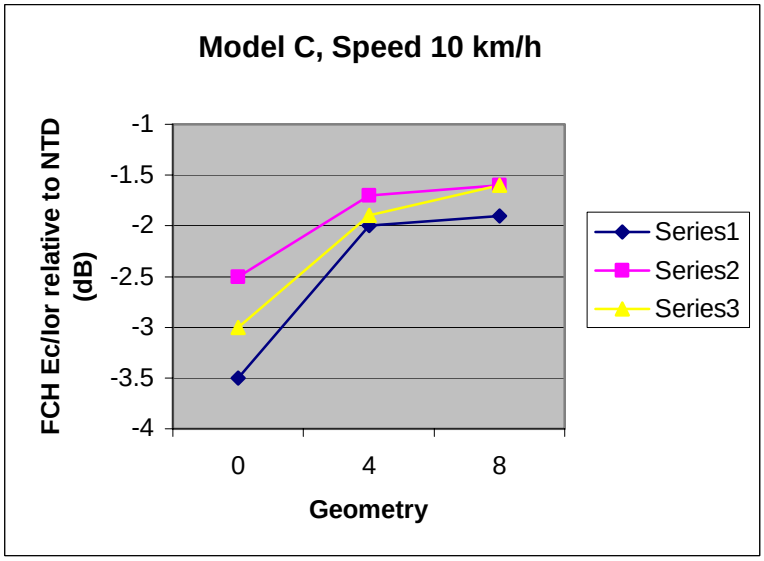

Figure 4: Performance across geometry

3.5 Cell capacity estimation

This section attempts to use the simulation results to obtain an aggregate measure of cell capacity under the different transmit diversity techniques. Here, cell capacity refers to the maximum number of supported users given a fixed amount of base-station transmit power (I_{or}).

The number of supported users in a cell can be estimated by:

$$N = \frac{I_{or} - P_{oh}}{\overline{\left(\frac{E_c}{I_{or}}\right)}} \qquad (3.5)$$

where

N = maximum number of supported users in the cell

P_{oh} = total power in the overhead channels (common pilot, paging, synchronization, and diversity pilot)

$\overline{\left(\frac{E_c}{I_{or}}\right)}$ = FCH E_c/I_{or} required for a mobile to attain the target frame error-rate

The values of I_{or} and P_{oh} are fixed. The E_c/I_{or}, however, varies according to multipath structure, speed and geometry. The approach used here is to compute an aggregate E_c/I_{or} consisting of a weighted average of the required E_c/I_{or} values for different channel scenarios; this aggregate E_c/I_{or} can then be plugged into equation (3.5) to obtain an estimate of cell capacity.

3.5.1 Speed and mobility profiles

Because the required FCH E_c/I_{or} varies with speed, the first step in obtaining an aggregate value is to match a *speed profile* against each channel model in Table 1. In each speed profile, it is assumed that mobiles assume only a discrete set of speeds, and that each speed occurs a certain percentage of the time.

Table 3 shows the speed profiles. Compared to table 1, table 3 has an added model E; this model has the same multipath/fading profile as model A, differing from the latter only in the speed profile. Notice that the numbers in each column in table 3 add to 100%.

The speed profiles in table 3 assume that larger numbers of multipaths tend to occur at intermediate speeds (between 10 km/h and 60 km/h), since the multipath models (B and C) have speed profiles concentrated on that range. The 1-path models (A and D), on the other hand, have speed profiles concentrated on low and high ranges, respectively.

Table 3: Speed profiles for multipath channel models [13]

Model	A	B	C	D	E
1 Km/Hr	30%	0%	0%	0%	0%
3 Km/Hr	40%	30%	0%	0%	0%
10 Km/Hr	30%	40%	30%	0%	0%
30 Km/Hr	0%	30%	60%	40%	40%
100 Km/Hr	0%	0%	10%	60%	60%

The speed profiles allow for the computation of an aggregate E_c/I_{or} for each channel model. In order to encompass these five aggregate values into a single E_c/I_{or} number, a *mobility profile* must be specified detailing what percentage of the mobiles fits each of five profiles (A-E).

Three mobility profiles were defined, and are specified in table 4. For each mobility profile, each entry refers to the percentage of users belonging to a certain speed profile. Low mobility scenarios correspond to larger portions of users at low-speed profiles (A, B), whereas the opposite holds for medium and high mobility scenarios (larger fraction of users under profiles C, D and E). Notice that the numbers in each row in table 4 add to 100%.

Table 4: Mobility profiles [13]

Mobility	Model A	Model B	Model C	Model D	Model E
Low	30%	30%	20%	10%	10%
Medium	20%	20%	20%	20%	20%
High	0%	0%	20%	50%	30%

3.5.2 Geometry profiles

Table 5 defines two *geometry profiles*; notice that the numbers in each row add to 100%.

Table 5: Geometry profiles [13]

Geometry	0dB Ior^/Ioc	4dB Ior^/Ioc	8dB Ior^/Ioc
Low	20%	50%	30%
High	10%	40%	50%

3.5.3 Capacity estimates

The three mobility and two geometry profiles give rise to six cases, each of which specifies what percentage of mobiles in the cell fall under each combination of multipath model, mobile speed and geometry. In each of the six cases, the aggregate FCH E_c/I_{or} is obtained by a weighted mean of the individual E_c/I_{or} values – obtained via simulation - for each multipath/speed/geometry combination. The weights are simply the percentages of mobiles in the cell under each particular combination (as specified by tables 1, 3, 4 and 5).

Figure 5 shows the results. The figure illustrates that NTD always has the worst performance. It also confirms that STS performance is better the stronger the diversity pilot. The performance of PSTD lies between STS-6dB and STS-9dB, being worse than STS-9dB at higher mobility scenarios.

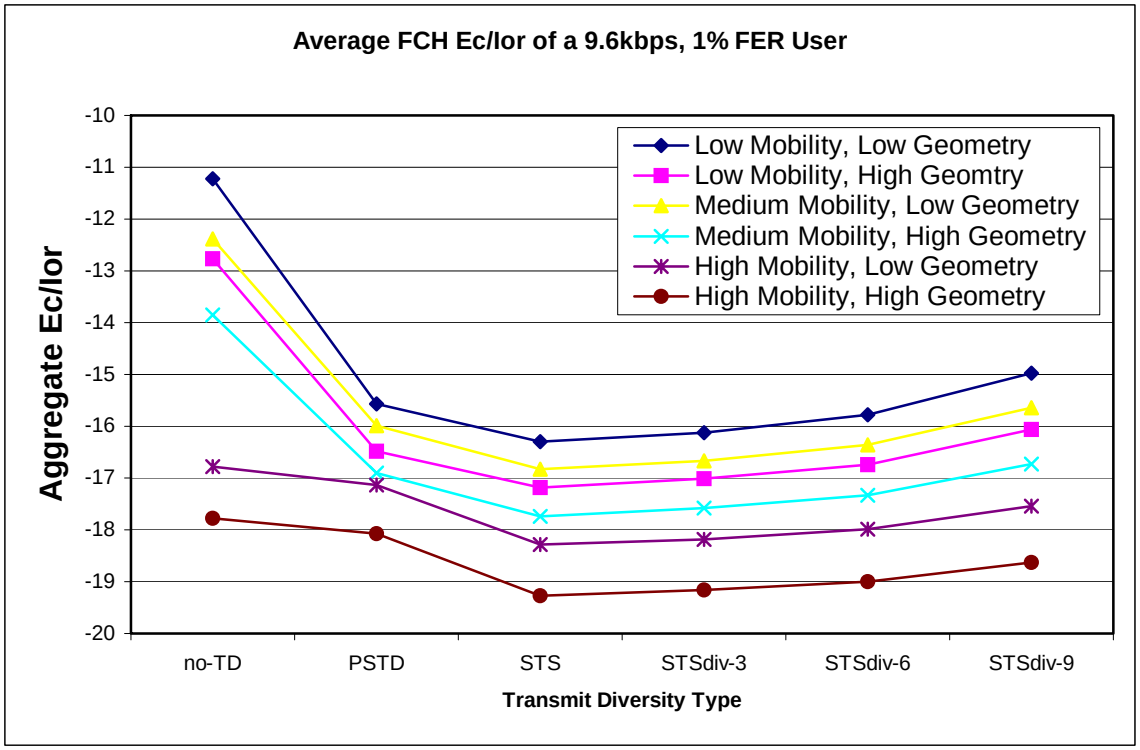

Figure 5: Average FCH E_c/I_{or} for different mobility-geometry scenarios [13]

Figure 6 displays the cell capacity estimates for all six combinations of mobility and geometry (after plugging the aggregate FCH E_c/I_{or} in figure 5). As can be seen from the histogram, the capacity of STS-0dB is consistently lower than the capacities of STS-3dB and STS-6dB, showing that the improved performance of STS-0dB (as measured by a lower required FCH E_c/I_{or}) does not compensate for the extra power spent on the diversity pilot. In high mobility scenarios, even a -3dB diversity pilot appears high, as STS-6dB has a higher capacity.

The capacity of PSTD is comparable to STS-3dB and STS-6dB, except in high mobility scenarios. Despite underperforming STS-3dB and STS-6dB in most cases (according to figure 5), PSTD has a comparable capacity because it does not incur the overhead of a diversity pilot channel. In addition, PSTD has another advantage not captured in the simulations: it does not require mobile-specific support and hence benefits all mobiles, whereas legacy mobiles do not support and hence cannot benefit from STS.

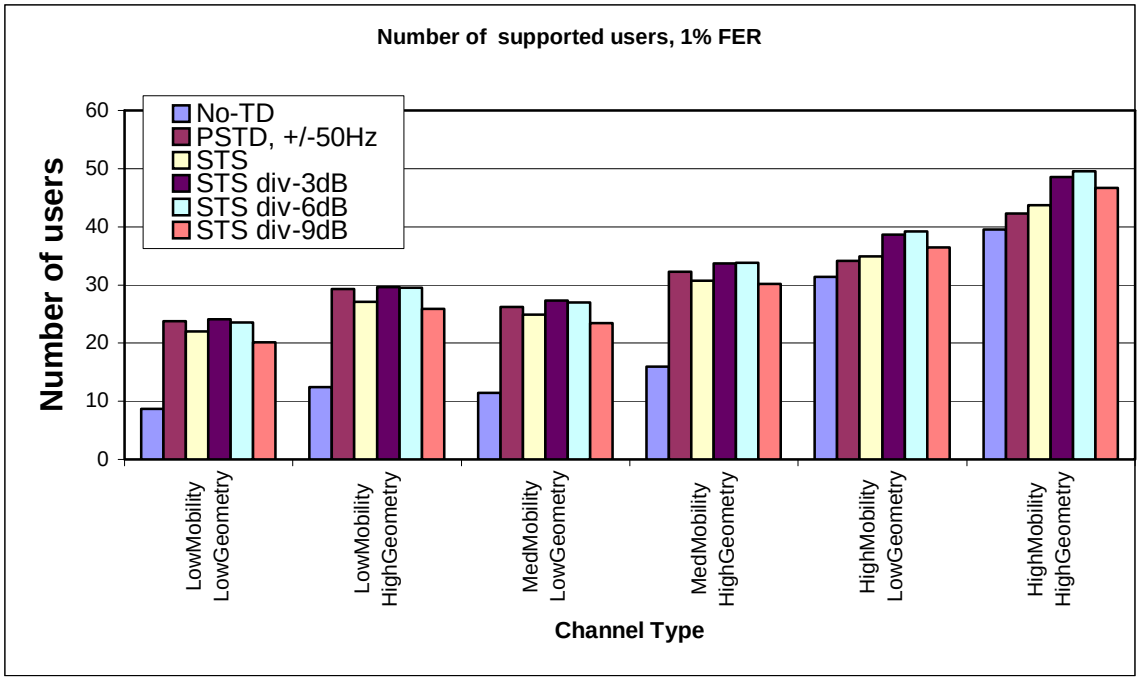

Figure 6: Base station capacity estimates [13]

Summarizing: simulations indicate that both PSTD and STS seem to provide significant capacity improvements in terms of maximum number of users supported. In scenarios of low mobility, PSTD, STS-3dB and STS-6dB seem to provide the largest improvement, while STS-3dB and STS-6dB outperform other schemes in scenarios of higher mobility.

Chapter 4: Testing methodology

Chapter 3 presented simulation results quantifying the link-level improvements of *Space-Time Spreading (STS)* and *Phase-Sweep Transmit Diversity (PSTD)* over *No-Transmit Diversity (NTD)*. There is no guarantee, however, that the models used in the simulations adequately mimic real channel conditions: rather, an analysis of link-level improvements based on actual field data is necessary to determine whether transmit diversity is beneficial in practice. Such field-based data analysis is the main focus of this thesis.

The simulations in chapter 3 had another limitation: they tested the three schemes (STS, PSTD, NTD) in isolation. As a consequence, the cell capacity estimates obtained correspond to cells in which all mobiles support the same scheme. In a realistic field scenario, however, a cell could be populated with a mix of mobiles supporting different schemes; such coexistence raises interference issues not captured in the simulations. Quantifying the effects of such coexistence-related interference, both under well-known channel models and in the field, is another focus of this research.

This chapter describes the methodology used for evaluating the transmit diversity schemes in the field[20]. Section 4.1 presents a global picture of the forward-link physical layer blocks relevant to the field tests. Section 4.2 describes metrics related to these building blocks; these metrics were computed from the field data in an attempt to evaluate the link-level improvements brought by transmit diversity. Section 4.3 contains descriptions of the different cell configurations that were tested in the field; these configurations attempt to capture scenarios with different mixes of mobiles across the different schemes. The approach described throughout the chapter was used not only in the field, but also in lab experiments designed to quantify the impacts of coexistence-based interference on receiver performance.

4.1 System overview

4.1.1 Transmitter

Figure 1 presents a block diagram of the forward-link STS transmitter system[21] after the modulation/spreading stage. In the figure, X_m denotes one frame of post-spreading QPSK symbols of a mobile's fundamental channel, transmitted from the main antenna. X_d is analogous to X_m and consists of the fundamental-channel symbols transmitted from the diversity antenna, for the same mobile.

[20] Results will be presented in chapter 6.
[21] The NTD and PSTD diagrams are simpler, thus not pictured.

X_{mp} and X_{dp} are the main-pilot and diversity-pilot symbols, respectively. Finally, O_m and O_d are the sum of the complex symbols transmitted from the main-antenna and diversity-antenna (respectively) on all other forward-link channels.

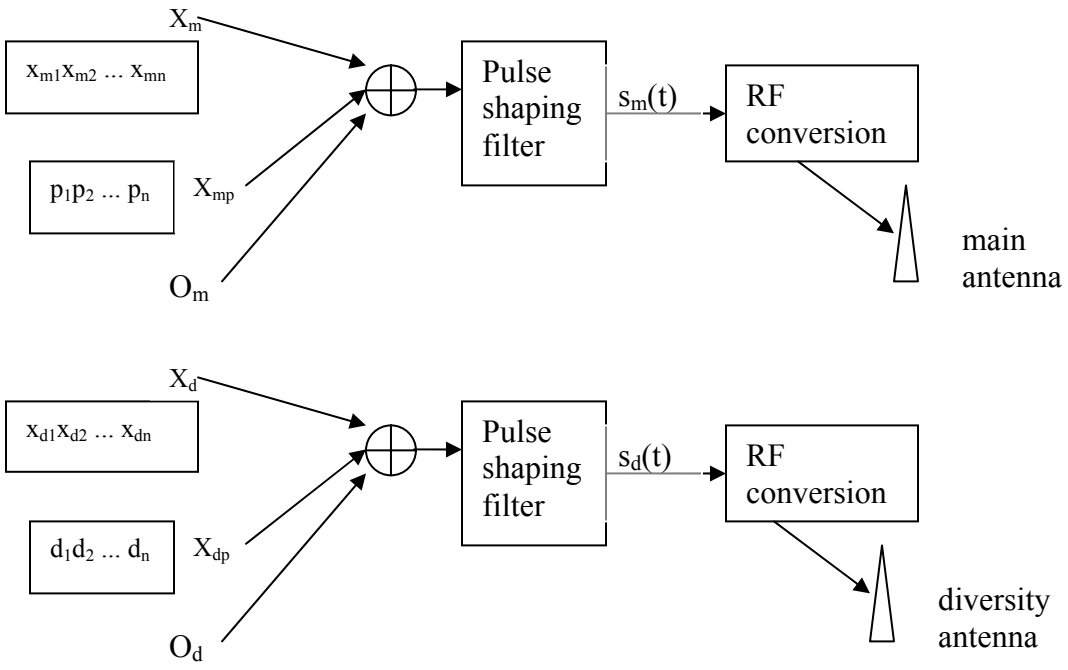

Figure 1: STS transmitter scheme

Since transmitted power is constant across a frame and across antennas, all symbols x_{mi} and x_{di} have the same power. Therefore, the energy-per-chip of the fundamental channel ($E_{c,FCH}$) can be written as:

$$E_{c,FCH} = \frac{1}{L}\frac{\|X_m\|^2 + \|X_d\|^2}{n} = \frac{2}{L}\frac{\|X_m\|^2}{n} \qquad (4.1)$$

where $\|X\|$ denotes the energy in vector X, L denotes the length of the spreading Walsh sequence and n denotes the number of symbols in a frame. Similarly, the energy-per-chip of the main-pilot ($E_{c,mp}$) and diversity-pilot ($E_{c,dp}$) channels can be written as:

$$E_{c,mp} = \frac{1}{L}\frac{\|X_{mp}\|^2}{n} \qquad (4.2)$$

$$E_{c,dp} = \frac{1}{L}\frac{\|X_{dp}\|^2}{n}$$

Finally, the energy-per-chip of the total base-station transmitted power (I_{or}), as well as the energy-per-chip of total transmitted power from the main antenna ($I_{or,1}$) and diversity antenna ($I_{or,2}$) can be written as:

$$I_{or} = \frac{1}{L}\frac{\|X_m\|^2 + \|X_d\|^2 + \|X_{mp}\|^2 + \|X_{dp}\|^2 + \|O_m\|^2 + \|O_d\|^2}{n}$$

$$I_{or,1} = \frac{1}{L}\frac{\|X_m\|^2 + \|X_{mp}\|^2 + \|O_m\|^2}{n} \qquad (4.3)$$

$$I_{or,2} = \frac{1}{L}\frac{\|X_d\|^2 + \|X_{dp}\|^2 + \|O_d\|^2}{n}$$

4.1.2 Receiver

Figure 2 shows a simplified sketch of the receiver system for STS (after down-conversion from carrier frequency):

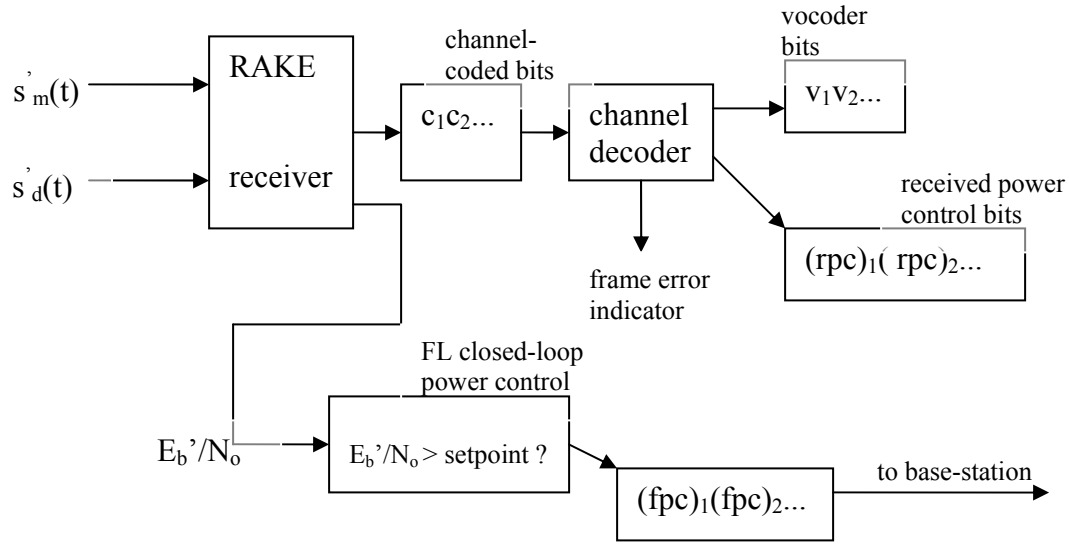

Figure 2: STS receiver scheme

4.1.2.1 Received signal

The channel is assumed to follow a tapped-delay channel model. Therefore, the received low-pass signals $s_m'(t)$ and $s_d'(t)$ can be written as:

$$s_m' = \sum_{i=1}^{N_m} h_i s_m(t - \frac{\Delta i}{W}) + n_m(t) \qquad s_d' = \sum_{j=1}^{N_d} h_j s_d(t - \frac{\Delta j}{W}) + n_d(t) \qquad (4.4)$$

Here, Δi and Δj are the PN offsets for the i-th tap from the common antenna and j-th tap from the diversity antenna (respectively), and h_i and h_j are the tap fading coefficients; N_m and N_d denote the number of taps from the common and diversity antennas, respectively; W denotes the signal bandwidth (1.2288 MHz). Finally, $n_m(t)$ and $n_d(t)$ denote other-cell interference plus thermal noise, modeled as independent zero-mean additive white Gaussian noise (AWGN) processes.

The amplitude of the channel gains from the main and diversity antennas can be written as:

$$|h_m|^2 = \sum_{i=1}^{N_m} |h_i|^2 \qquad |h_d|^2 = \sum_{j=1}^{N_d} |h_j|^2 \qquad (4.5)$$

Therefore, the signal energies received from each antenna can be written as:

$$I_{or,1}' = I_{or,1}|h_m|^2 \qquad I_{or,2}' = I_{or,2}|h_d|^2 \qquad (4.6)$$

Total received base-station power can be written as

$$I_{or}' = I_{or,1}' + I_{or,2}' \qquad (4.7)$$

The power density of other-cell interference and thermal noise (I_{oc}) satisfies:

$$E\left[|n_m(t)|^2 \right] + E\left[|n_d(t)|^2 \right] = I_{oc}\delta(0) \qquad (4.8)$$

Finally, total received power at the mobile is denoted as I_o, and can be written as:

$$I_o = I_{or}' + I_{oc}$$

4.1.2.2 Decoded bits

The RAKE receiver demodulates the received signal into the original channel-coded bits (bar any decoding errors). These channel-coded bits are subsequently fed to

the channel decoder, which recovers both the transmitted vocoder bits and reverse-link closed-loop power-control bits[22]. Regarding the latter, there are 16 power-control bits assuming inner-loop power-control frequency of 800Hz and 20ms frames. The adjustment to mobile transmit power (Tx_{adj}) is then given by:

$$Tx_{adj} = \left[\sum_{i=1}^{16} 1 - 2(pc)_i \right] \Delta step \qquad (4.9)$$

where $\Delta step$ denotes the step change per power-control bit. Finally, the channel-decoder examines whether the frame was received in error; if so, the frame error count is incremented and any information pertaining to the frame (including Tx_{adj} is discarded).

4.1.2.3 Forward-link closed-loop power control

The *setpoint* is the target received bit-energy-to-noise ratio (E_b'/N_o) for a mobile's traffic channel, being periodically adjusted by the outer-loop power control so as to achieve a target frame-error rate (FER) at the receiver. Here, E_b' is received energy-per-bit, and N_o is total noise plus interference, given by:

$$N_o = I_{ic} + I_{oc}$$

where I_{ic} denotes in-cell interference[23] and I_{oc} denotes other-cell interference plus thermal noise.

The received E_b'/N_o is periodically estimated, the period being a configurable parameter of closed-loop power control. As illustrated in figure 2, the received E_b'/N_o is estimated after demodulation at the RAKE receiver, and its value compared to the setpoint. If the setpoint is higher, the inner-loop power-control outputs a 0-bit indicating a need for increase in base-station transmit power; otherwise, it outputs a 1-bit. The set of power control bits output by the inner-loop for the current received frame is transmitted to the base-station in the next frame. Upon receipt of the frame, the base-station decodes the power-control bits and adjusts the transmit power for the mobile's fundamental channel accordingly.

4.2 Performance metrics

During a call, both the mobile and the base station have the ability to log various measurements related to call performance or channel conditions. The metrics described in this section were computed from the measurements in these log files.

[22] As explained in chapter 2, power-control bits from the base-station are punctured into the fundamental channel and transmitted to the mobile.
[23] Modeling of in-cell interference (I_{ic}) is done in chapter 5.

Section 4.2.1 describes mobile metrics, while section 4.2.2 describes base-station metrics. For generality, all metrics are explained for the STS case – the NTD and PSTD cases are analogous, and simpler.

4.2.1 Mobile metrics

Table 1 shows the metrics computed from the mobile logs.

Table 1: Mobile metrics

FL FER	PICH	setpt	# lock	P_cp		Txadj(dBm)	
(%)	Ec'/Io (dB)	(dB)	fing	T_diff = 1/2	T_diff = 1	mean	std

The metrics can be divided in two categories - channel condition metrics and receiver metrics. The channel condition metrics are:

1. Mean number of locking fingers
2. Probability of common-antenna and diversity-antenna fingers occurring at the same delay

The receiver metrics are:

3. Mean normalized pilot-channel received power (PICH E_c'/I_o)
4. Mean mobile setpoint
5. Mean and standard deviation of mobile transmit-adjust (Tx_{adj})
6. Mean forward-link frame-error rate (FL-FER)

The following sections explain each of the metrics in more detail.

4.2.1.1 Number of locking fingers

Section 4.1 showed that the received low-pass signals from the common and the diversity antenna can be written as:

$$s_m' = \sum_{i=1}^{N_m} h_i s_m(t - \frac{\Delta i}{W}) + n_c(t) \qquad s_d' = \sum_{j=1}^{N_d} h_j s_d(t - \frac{\Delta j}{W}) + n_d(t)$$

Ideally, the RAKE receiver would demodulate the signals at all taps. In practice, however, a RAKE receiver cannot distinguish a weak finger from spurious noise. In addition, since the recombination algorithm weights the fingers according to their strength, weak fingers have little influence on the final decision regarding the transmitted symbol. Therefore, it is more practical and efficient to only use a finger in the recombination process if the finger's energy is above a certain threshold; such a finger is said to be in *lock*.

The number of locking fingers detected by the RAKE receiver gives a crude idea of the total number of taps seen by the receiver. This number can be written as $N_m + N_d - N_c$, where N_c is the number of tap delays occurring at both s_m' and s_d'.

4.2.1.2 Probability of common-antenna and diversity-antenna fingers occurring at the same delay[24]

In order to get an idea of the correlation between the channels from the common and the diversity antennas, the following metrics of interest were computed from the STS mobile logs:

1. Conditional probability for the occurrence of path delay Δi in the diversity signal, given its occurrence in the main signal (P_{md}).
2. Conditional probability for the occurrence of path delay Δj in the main signal, given its occurrence in the diversity signal (P_{dm}).

The previous section introduced the quantity N_c, defined as the number of common taps in the received main and diversity signals at a given point in time. The conditional probabilities above can thus be expressed as the expected values of N_c/N_m and N_c/N_d, where N_c and N_d are the number of paths from the main and diversity antennas (respectively).

These probabilities were estimated from the searcher results. As explained in chapter 2, the searcher determines the time delays of the strongest taps from both the main and the diversity antenna; these are reported as *searcher peaks* and specified as chip offsets. Letting $\{P_m\}_t$ and $\{P_d\}_t$ be the set of searcher peaks from the common and diversity antennas (respectively) reported by the searcher algorithm at time t, P_{md} and P_{dm} can be defined as:

$$P_{md} = \Pr\left\{ \exists\ x \in \{P_d\}_t\ \therefore |x - y| \le T_{diff} \ \middle|\ y \in \{P_m\}_t \right\}$$

$$P_{dm} = \Pr\left\{ \exists\ x \in \{P_m\}_t\ \therefore |x - y| \le T_{diff} \ \middle|\ y \in \{P_d\}_t \right\}$$

Here, T_{diff} represents the threshold for minimum offset difference, so that searcher peaks whose delays differ by less than T_{diff} are considered as having the same offset; such peaks will be referred to as *matching* peaks.

In other words, for each searcher peak from the common antenna, P_{md} represents the likelihood that there is a matching searcher peak from the diversity antenna. If Ma_t is the number of common searcher peaks at time t that have matching diversity peaks, and if M_t is the total number of main-antenna search peaks at time t, P_{md} can be estimated as:

[24] Unlike the other metrics, this one is only relevant for STS.

$$P_{md} = \sum_t Ma_t \Big/ \sum_t M_t$$

where the index t ranges over the entire duration of the call. That is, P_{md} is computed by counting the number of common search peaks that have matching diversity peaks, and dividing it by the total number of common search peaks. As table 1 shows, P_{md} was computed for T_{diff} values of half-a-chip and one chip for each voice call. Completely analogous statements can be made about P_{dm}.

A low value for P_{md} or P_{dm} indicates that the common and diversity fingers tend to occur at different offsets. Since it is assumed that tap coefficients are uncorrelated for different offsets, this result would indicate that the overall channel response is also uncorrelated for the two antennas. On the other hand, high values for P_{md} and P_{dm} indicate a higher level of correlation between the two antennas.

4.2.1.3 Mean normalized pilot-channel received power ($E_{c,p}'/I_o$)

This metric is different for NTD and STS phones, so the two cases will be explained separately.

For a NTD mobile, *normalized pilot-channel receive power* refers only to the main-pilot. It is defined as $E_{c,mp}'/I_o$, where $E_{c,mp}'$ is the received main-pilot energy-per-chip and I_o is the spectral density of the received power satisfying $I_o = I_{or}' + I_{oc}$ (with I_{or}' and I_{oc} given by (4.6), (4.7) and (4.8)).

For every received frame, a NTD mobile receiver estimates the $E_{c,mp}'/I_o$ of the main-pilot channel. This metric can be related to the received carrier-to-interference-and-noise ratio I_{or}'/I_{oc}, as the following derivation illustrates:

$$\frac{E_{c,mp}'}{I_o} = \frac{E_{c,mp}'}{I_{or}' + I_{oc}} = \frac{\frac{E_{c,mp}'}{I_{or}'}}{1 + \frac{I_{oc}}{I_{or}'}} \Rightarrow \frac{I_{or}'}{I_{oc}} = \left(\frac{E_{c,mp}' \Big/ I_{or}'}{E_{c,mp}' \Big/ I_o} - 1 \right)^{-1} \qquad (4.10)$$

Section 4.1 defined h_m as the overall channel gain from the base-station main antenna to the mobile antenna, and this gain applies both to the common-pilot and total I_{or}. Therefore, relation (4.1) reduces to:

$$\frac{I_{or}'}{I_{oc}} = \left(\frac{E_{c,mp}' \Big/ I_{or}'}{E_{c,mp}' \Big/ I_o} - 1 \right)^{-1} = \left(\frac{E_{c,mp} |h|^2 \Big/ I_{or} |h|^2}{E_{c,mp}' \Big/ I_o} - 1 \right)^{-1} = \left(\frac{E_{c,mp} \Big/ I_{or}}{E_{c,mp}' \Big/ I_o} - 1 \right)^{-1} \qquad (4.11)$$

Since the mobile knows the value of $I_o = I_{or}' + I_{oc}$, equation (4.11) illustrates that the mobile can estimate both I_{or}' and I_{oc} as long as it knows $E_{c,mp}/I_{or}$ (the normalized transmitted main-pilot energy-per-chip, given by (4.2)). The estimates of I_{or}' and I_{oc} play an important role in the open-loop reverse-link power-control, as they allow the mobile to compensate for other-cell interference in its open-loop estimate for transmit power [5].

An STS mobile receiver, on the other hand, estimates the received energy of both the common and the diversity pilot signals. The $E_{c,p}'/I_o$ metric in this case corresponds to a combination of $E_{c,mp}'/I_o$ and $E_{c,dp}'/I_o$ (the received energies for the common and the diversity pilot), and relation (4.11) no longer applies[25].

For each voice call, the mean pilot $E_{c,p}'/I_o$ was computed over the entire duration of the call. This metric serves mainly as an estimate the quality of the forward-link: a lower $E_{c,p}'/I_o$ implies higher levels of interference and noise with respect to received signal power, and hence higher required transmit power to achieve the same FER. In other words, it gives a rough idea of the geometry of the cell. In addition, since the NTD-mobile $E_{c,p}'/I_o$ includes only the common-pilot whereas the STS-mobile $E_{c,p}'/I_o$ also includes the diversity pilot, a comparison between the two values gives an indication of received diversity-pilot power.

4.2.1.4 Mean mobile setpoint

The setpoint is shown in figure 2 and explained in section 4.1.2.3. Assuming ideal power-control, the mean mobile setpoint represents the theoretical E_b'/N_o required to achieve the target FER. This theoretical value depends only on the modulation scheme and on channel coding, which is common to all the transmit diversity schemes. In practice, however, the setpoint is also affected by the channel because power control is not ideal and does not respond instantaneously to changes in channel conditions.

Power control works best in slow-fading channels, when the power-control response time is smaller than the coherence time of the channel. On the other hand, the power-control loops are less efficacious for tracking changes in faster-fading channels; as a consequence, received E_b'/N_o – and hence the setpoint - typically has a larger variance for such channels. Since the E_b'/N_o vs. FER is a convex function[26], a larger variance for E_b'/N_o implies a larger required mean E_b'/N_o to achieve the same mean FER: thus, faster-fading channels generally correlate with higher mean setpoint values. Through a similar reasoning, it can be inferred that a larger variance for the channel's fading coefficients is also correlated with a higher mean setpoint.

[25] The combination algorithm is implementation-dependent.

[26] Assuming E_b'/N_o on a logarithmic scale and FER on a linear scale – those were the scales used for setpoint and FER averaging.

4.2.1.5 Mean and standard deviation of mobile transmit-adjust (Tx_{adj})

As shown in figure 2 and equation (4.9), the mobile transmit-adjust (Tx_{adj}) is the total adjustment command sent by the base-station as part of closed-loop reverse-link power control. Since Tx_{adj} is determined by power control bits sent on the forward link, forward-link improvements due to transmit diversity can have an impact on reverse-link transmitted power. Thus, inspecting the mean and standard deviation of the Tx_{adj} should indicate whether improved forward-link conditions due to transmit diversity can help the reverse-link as well.

4.2.1.6 Mean forward-link frame error-rate (FL-FER)

This metric represents the mean forward-link frame error-rate (FL-FER) over the duration of a call, obtained simply by counting the number of frames received in error and dividing by the total number of received frames. The purpose of this metric is to indicate whether the mobile receiver successfully achieved the target FER for the call: if the value of the metric is close to the target FER, it is an indication that power control worked effectively; if not, it is an indication that something might have gone wrong with the call and requires further inspection (or repeating the test).

4.2.2 Base station metrics

Table 2 shows the metrics computed from the base station data.

Table 2: Base station metrics

F-FCH Ec/Ior (dB)		RL FER (%)
mean	std	

As table 2 shows, the following metrics were computed:

1. Mean reverse-link frame error-rate (RL-FER)
2. Mean and standard deviation of the normalized-transmit-power of the forward-fundamental channel ($E_{c,FCH}/I_{or}$).

The following subsections explain these metrics in more detail.

4.2.2.1 Mean reverse-Link frame error-rate (RL-FER)

This statistic represents the mean reverse-link frame error-rate (FER) for the duration of the call. The mean reverse-link FER is a verification metric, and its value should be close to the target reverse-link FER. If not, it is an indication that reverse-link power control was not fully effective, meaning that something might have gone wrong with the call and that the test might need to be repeated.

4.2.2.2 Mean and standard deviation of normalized-transmit-power for the fundamental channel ($E_{c,FCH}/I_{or}$)

This statistic represents the mean normalized transmit power for the forward-fundamental channel ($E_{c,FCH}/I_{or}$), and is the major performance metric for a given transmit diversity scheme. If transmit diversity improves the forward link, less traffic channel power is required to achieve the target FER at the receiver. Therefore, any improvement due to transmit diversity should be reflected directly in lower values for this metric.

This metric is related to the received bit-energy-to-noise ratio through the carrier-to-interference-and-noise ratio, $I_{or}^{'}/I_{oc}$. The following derivation illustrates this relationship in the case of one transmitter antenna at the base station:

$$\frac{E_b^{'}}{N_o} = \frac{P_g E_{c,FCH}^{'}}{I_{ic} + I_{oc}} = \frac{P_g \dfrac{E_{c,FCH}^{'}}{I_{or}^{'}}}{\dfrac{I_{ic}}{I_{or}^{'}} + \dfrac{I_{oc}}{I_{or}^{'}}} = \frac{P_g \dfrac{E_{c,FCH}}{I_{or}}}{\dfrac{I_{ic}}{I_{or}^{'}} + \dfrac{I_{oc}}{I_{or}^{'}}} \quad (4.12)$$

where the processing gain P_g is defined as the ratio between the chip rate and the bit rate, and I_{ic} denotes in-cell interference.

As will be shown in chapter 5, in-cell interference is negligible if there is only one tap in the channel, in which case $I_{ic} \approx 0$. Equation (4.12) then simplifies to:

$$\frac{E_b^{'}}{N_o} = P_g * \frac{E_{c,FCH}}{I_{or}} * \frac{I_{or}^{'}}{I_{oc}} \quad (4.13)$$

Equation (4.13) establishes a simple linear relation between received bit-energy-to-noise ratio and $E_{c,FCH}/I_{or}$, with the carrier-to-interference-and-noise ratio ($I_{or}^{'}/I_{oc}$) as a scaling constant.

Section 4.2.1.3 derived a relationship between received $I_{or}^{'}/I_{oc}$ and $E_{c,mp}/I_o$ for the NTD case. That relationship allows for an estimation of in-cell interference. Further development of equation (4.12) and using (4.11) leads to:

$$\frac{E_b^{'}}{N_o} = P_g * \frac{E_{c,FCH}}{I_{or}} * \left(\frac{I_{ic} + I_{oc}}{I_{or}^{'}} \right)^{-1} = P_g * \frac{E_{c,FCH}}{I_{or}} * \left(\frac{I_{ic}}{I_{or}^{'}} + \frac{E_{c,mp} \big/ I_{or}}{E_{c,mp}^{'} \big/ I_o} - 1 \right)^{-1}$$

$$\Rightarrow \frac{I_{ic}}{I'_{or}} = P_g * \frac{E_{c,FCH}/I_{or}}{E'_b/N_o} - \frac{E_{c,mp}/I_{or}}{E'_{c,mp}/I_o} + 1 \qquad (4.14)$$

In addition to the mean, the standard deviation of $E_{c,FCH}/I_{or}$ is also a metric of interest. A higher value for this metric is typically caused by a lower variance of the equivalent channel gain from the base station to the mobile. As mentioned in chapter 1, the main idea behind transmit diversity is to reduce the probability of an extended deep fade; an inspection of the standard deviation should therefore inform whether this goal is indirectly accomplished by reducing the volatility of the channel conditions.

4.3 Cell configuration

As mentioned in the introduction to this chapter, one dimension of this thesis is to evaluate the improvements of transmit diversity (TD) in cells containing a mix of mobiles supporting different TD techniques. Such a scenario would likely occur in the early stages of TD deployment: while new mobiles would automatically support TD, existing mobiles would still be unable to take advantage of it. As a consequence, base stations would be required to support both TD and non-TD mobiles until all cell-phone subscribers upgraded to TD-supporting mobiles.

The following mobile distributions need to be considered:

1) All mobiles are NTD (as a reference against which to compare the improvements brought by the different TD techniques)
2) All mobiles use a certain TD technique (PSTD or STS).
3) Some mobiles use TD and others do not.

All cases were tested under a *fully-loaded* cell, that is, a cell transmitting at maximum power. This was done for three reasons: first, a fully-loaded cell is saturated with mobiles, thus being the scenario where possible capacity increases are most relevant. Second, fully-loaded cells correspond to the highest possible values of in-cell interference, a phenomenon with significant impact on cell capacity. Finally, simulating all cases under the same total transmit power makes results comparable across different tests.

Strictly speaking, full base-station transmit power would require testing with a large number of mobile stations so as to generate the required number of traffic channels. In practice, only one or two mobiles were used in each test, and spurious traffic channels were simulated in order to bring the base-station to full power. The amount of power transmitted in these spurious traffic channels is adjusted on a frame-by-frame basis so that total base station power is constant regardless of forward-link power control on the real traffic channels.

All tests were performed in a single isolated cell sector. As a consequence, individual cell-capacity estimates are exaggerated because there is no other-cell interference or handoff overhead. However, since both of these factors are independent of the TD scheme, the estimates should still present a rough picture of the relative capacity improvements obtainable in realistic cells.

Sections 4.3.1 and 4.3.2 explain the configurable parameters relevant to STS and PSTD, respectively. Section 4.3.3 presents some details regarding the voice calls performed. All sections focus only on parameters that apply both to lab and field testing; the lab-specific and field-specific parameters will be described in chapters 5 and 6.

4.3.1 STS

STS was designed to be backwards compatible with NTD so that STS and NTD mobiles could coexist in the same cell. In a cell with both NTD and STS mobiles, the NTD mobiles demodulate only signals from the main antenna, whereas STS mobiles track pilots and demodulate traffic-channel signals from both antennas. As will be shown in chapter 5, the power coming from the diversity antenna constitutes interference to a NTD mobile if the wireless channel presents multiple resolvable paths; in addition, the larger the power coming from the diversity antenna, the more pronounced is this interference.

Based on the above considerations, it is of interest to evaluate the performance of NTD and STS phones under different levels of diversity-antenna transmitted power; each level constitutes a *loading scenario*. In addition, it is also desirable to evaluate the improvements of STS under different levels of diversity pilot (as was done in the simulations).

Subsection 4.3.1.1 lists the diversity-pilot levels, and 4.3.1.2 details the loading scenarios tested. Section 4.3.1.3 explains how to configure the base-station so as to simulate a given loading scenario for the cell.

4.3.1.1 Diversity pilot level

As explained in chapter 2, the cdma2000 standard specifies four possible values for the diversity pilot with respect to the main pilot: 0dB, -3dB, -6dB and –9dB. The simulation results showed, however, that a diversity pilot of 0dB adds little benefit compared to STS-3dB, resulting in lower cell capacity. The simulations also showed that a -9dB diversity pilot is too weak for reliable diversity-pilot acquisition and phase-tracking of signals coming from the diversity antenna. Thus, due to time and resource constraints, only the -3dB and -6dB values were tested; according to the simulations, these were the diversity pilot values that resulted in the largest improvement in cell capacity.

4.3.1.2 Loading scenario

The loading scenario specifies the amount of base-station transmitted power that comes from the diversity antenna. The diversity antenna transmits only the diversity-pilot channel and half the power in the STS traffic channels[27]; thus, for a given value of diversity pilot, a larger amount of diversity-antenna power is equivalent to a larger amount of STS traffic-channel power, which roughly translates to a larger number of STS mobiles in the cell.

Based on these considerations, parameter *Z* is defined as:

$$Z = X/(X+Y)$$

where:

X = total traffic power transmitted for STS mobiles.
Y = total traffic power transmitted for NTD mobiles.

Equivalently, Z is the ratio between the STS traffic power and total traffic power transmitted by the base station, and serves as an indirect measure of the ratio between the number of STS mobiles and the total number of mobiles in the cell.

Parameter *Z* characterizes the "loading scenario" for the cell, as table 3 illustrates:

Table 3: Loading scenarios and *Z* ratios

Loading scenario	Z = (STS traffic)/(total traffic)	Diversity pilot
1	0	Absent
2	0	Present
3	0.1	Present
4	0.5	Present
5	1	Present

Loading scenario 1 corresponds to a NTD cell in which all mobiles are NTD and no power is transmitted from the diversity antenna[28]. This case provides the NTD reference against which any improvements due to STS can be quantified. The remaining loading scenarios correspond to STS cells, that is, cells in which the diversity pilot is present. As table 3 shows, loading scenarios 2-6 correspond to the following values of *Z*: 0, 0.1, 0.5 and 1. The Z = 0 test represents a cell with no STS mobiles but in which the diversity pilot is still transmitted; the Z = 1 case, on the other hand, represents a cell in which all mobiles are STS, and simulates full STS deployment.

As can be seen from the table, loading scenarios 2 and 3 correspond to low *Z* ratios: 0 and 0.1, respectively. The reason for focusing on small *Z* ratios is to get a better

[27] The other half is transmitted from the common antenna.
[28] In particular, no diversity pilot is transmitted in loading scenario 1.

idea of the initial impact of STS deployment on base station capacity. In cells with a small number of STS mobiles, capacity might actually be reduced if the interference-induced loss incurred by the majority of NTD mobiles is not offset by the gain experienced by the minority STS mobiles. On the other hand, any capacity improvements brought by STS should be more evident under loading scenarios 4 and 5 (corresponding to *Z* ratios of 0.5 and 1, respectively).

4.3.1.3 STS cell configuration

STS configuration consists in specifying the diversity pilot level and the loading scenario. The diversity-pilot level is a parameter that can be specified directly in the base station configuration. The setup of the loading scenario, however, requires using spurious traffic channels to bring the base-station to full transmitted power while maintaining the desired ratio between STS traffic and NTD traffic power.

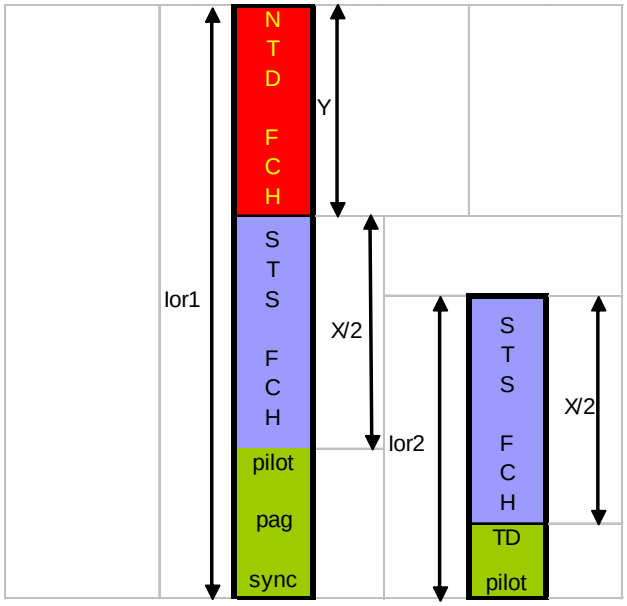

Figure 3: Power distribution on each antenna

Figure 3 illustrates how the power is distributed on each antenna. It is desired to have the following:

$$I_{or} = I_{or,1} + I_{or,2} = I_{max}$$

where I_{max} is the maximum base-station transmitted power.

Some of the power in each antenna is allocated to overhead channels. In the main antenna, the overhead channels are the common-pilot, paging and synchronization channels. In the diversity antenna, the only overhead channel is the diversity pilot. Table 4 depicts the power allocation used for the overhead channels:

Table 4: Power allocation for overhead channels

Channel	E_c/I_{or} (dB)
Common pilot	-7
Paging	-10
Synchronization	-13

The diversity pilot was set to -10 or -13dB depending on whether the desired diversity-pilot level was -3dB or -6dB with respect to the common pilot.

Total traffic power is simply the maximum base-station transmitted power minus the power allocated to overhead channels. The *Z* ratio determines how much of the traffic power is NTD traffic power and how much is STS traffic power - which determines how the traffic power is distributed between the two antennas.

Let *X* be the total STS traffic power, *Y* be total NTD traffic power, O_c be the overhead power in the common antenna and O_d be the overhead power in the diversity antenna[29]. The following relation holds:

$$X + Y = I_{max} - O_c - O_d$$

Based on the relation $Z = X/(X+Y)$, it is easily seen that:

$$X = Z * (I_{max} - O_c - O_d) \qquad (4.15)$$
$$Y = (1-Z) * (I_{max} - O_c - O_d) \qquad (4.16)$$

Finally, as figure 3 illustrates, all of *Y* goes into the common antenna, whereas half of *X* goes into the common and half into the diversity antenna. Thus, spurious traffic power should be added to each antenna so that:

$$I_{or,1} = O_c + X/2 + Y$$
$$I_{or,2} = O_d + X/2$$

with *X* and *Y* given by (4.15) and (4.16). The power in the overhead channels and the *Z* ratio thus completely specify the power distribution in the two antennas.

4.3.2 PSTD

PSTD is an improvement applicable to a regular NTD cell and does not require mobile-specific support. As described in chapter 1, the technique consists of dividing the base-station transmit power in two halves, and transmitting each half from one of the antennas at a small frequency offset from the carrier frequency. As a result, PSTD configuration is entirely dependent on the base station, and its effect is perceived by all the NTD mobiles in a cell.

[29] O_c and O_d can be easily computed from the values in table 4.

The power allocated to the overhead channels was the same as in the NTD-only test (loading 1), with the transmitted power in each channel equally divided between the two antennas. The phase-sweeping frequency was ± 50Hz in all cases.

4.3.3 Test calls

Table 5 summarizes the call parameters common to lab and field testing.

Table 5: Voice call parameters

Frequency	1945 MHz
Bit Rate	9600 bps (full-rate)
Chip Rate	1.2288 Mcps
Inner-loop power-control rate (both forward and reverse link)	800Hz
Outer-loop power control (both forward and reverse link)	1% FER target
Forward-fundamental frame duration	20 ms

Chapter 5: STS interference on NTD

As mentioned in chapter 2, *Space-Time Spreading* (STS) is a two-antenna transmit diversity technique that is backwards-compatible with *No-Transmit Diversity* (NTD). In particular, an STS-supported cell can support both STS mobiles and legacy NTD mobiles. The coexistence of STS and NTD mobiles in the same cell does not, however, come without a loss: in channels with multiple resolvable paths from the transmitter antennas to the receiver, the signal from the diversity antenna can cause a significant degradation to a NTD mobile. The study of this interference is the focus of this chapter.

Section 5.1 introduces the models and develops a qualitative analysis of the interference suffered by a NTD mobile in a cdma2000 cell. Section 5.2 presents the results of lab experiments designed to quantify this interference under a two-path Rayleigh-faded channel.

5.1 Interference to a NTD mobile in a cdma2000 cell

As mentioned in chapter 1, performance degradation in fading channels is dominated by the probability of low received SNR. The objective of this section is to show that for a NTD mobile experiencing a multipath fading channel, the probability of low instantaneous received SNR is higher in an STS-enabled cell than in a regular NTD cell; therefore, NTD mobiles perform worse in STS-enabled cells than in regular NTD cells.

Section 5.1.1 introduces the notation used for cdma2000 forward-link channel signals. Section 5.1.2 establishes properties of the correlator functions for the RAKE receiver. Section 5.1.3 uses these properties to develop an expression for post-demodulation signal-to-noise-ratio (SNR) for a NTD mobile assuming no in-cell interference; section 5.1.4 adds the in-cell interference component and derives two SNR expressions, one for a NTD mobile in a NTD cell and one for a NTD mobile in an STS-enabled cell. Finally, section 5.1.5 compares the two derived SNR expressions assuming both an additive white Gaussian noise (AWGN) channel and a fading channel.

5.1.1 Forward-link channel signals

Four types of forward-link channels were used in the tests, namely: common/diversity pilot, paging, synchronization and fundamental channels. The pilot, paging and synchronization channels use Binary Phase-Shift Keying (BPSK) modulation, whereas the fundamental channel uses Quadrature Phase-Shift Keying (QPSK) modulation. As explained in chapter 2, BPSK modulation can be viewed as QPSK modulation with the Q branch containing only 0's as scalar modulation symbols; hence, there is no loss of generality in assuming that all forward-link channels in consideration are QPSK-modulated.

Let N_c be the Walsh-length, and let $w_k(n)$ be the Walsh sequence (consisting of +1 and -1 values) used to spread the k-th forward-link channel. As shown in chapter 2, both the in-phase and the quadrature components are spread with the same Walsh sequence. After Walsh spreading, the m-th QPSK symbol on the k-th forward-link channel can be written as:

$$Y_{m,k} = \sqrt{2E_{c,k}(m)}x_k(m)\sum_{n_0=0}^{N_c-1} w_k(n_0)\delta[n-n_0]$$

where $E_{c,k}(m)$ is the energy-per-chip[30] and

$$x_k(m) = \frac{x_k^{(I)}(m) + j\ x_k^{(Q)}(m)}{\sqrt{x_k^{(I)}(m)^2 + x_k^{(Q)}(m)^2}}$$

is the unit-energy transmitted QPSK symbol. Here, $x_k^{(I)}(m)$ can assume either the value +1 or -1, and $x_k^{(Q)}(m)$ can assume any of -1, 0 or +1 as a possible value[31].

Let $PN_m(n) = PN_m^{(I)}(n) + j\ PN_m^{(Q)}(n)$, $1 \le n \le N_c$, be the pseudo-noise (PN) spreading sequence for the m-th symbol . More precisely, $PN_m^{(I)}(n)$ and $PN_m^{(Q)}(n)$ are the N_c-chip subsets of the serving cell's PN sequences that happen to spread the m-th symbol[32]. As shown in chapter 2, complex PN-spreading of $Y_{m,k}$ results in:

$$Z_{m,k} = \sqrt{2E_{c,k}(m)}x_k(m)\sum_{n_0=0}^{N_c-1} w_k(n_0)PN_m(n_0)\delta[n-n_0]$$

Thus, if $p(t)$ is the pulse-shaping filter (having duration T_c, the chip duration), the low-pass representation for the m-th symbol in the k-th FL channel is[33]:

$$s_{k,m}(t) = Z_{m,k} * p(t) = \sqrt{2E_{c,k}(m)}x_k(m)\sum_{n=0}^{N_c-1} w_k(n)PN_m(n)p(t-nT_c) =$$

$$= \sqrt{2E_{c,k}(m)}x_k(m)g_{k,m}(t) \qquad (5.1)$$

[30] The factor of 2 before $E_{c,k}(m)$ is due to the fact that $Y_{m,k}$ is a complex low-pass representation of the signal, so the amplitude of $Y_{m,k}$ is twice the square-root of its energy.

[31] The value $x_k^{(Q)} = 0$ occurs in the pilot, paging and synchronization channels as they are BPSK signals viewed as QPSK. For the QPSK-modulated forward-fundamental channel, $x_k^{(Q)}$ can only assume the values ±1.

[32] Note that sequences $PN_m^{(I)}(n)$ and $PN_m^{(Q)}(n)$ both vary with m, repeating every 384 symbols

[33] The $*$ operation in the second expression denotes convolution.

with $g_{k,m}(t) = \sum_{n=0}^{N_c-1} w_k(n) PN_m(n) p(t - nT_c)$ being the pulse-shaping filter shaped by the combination of Walsh and PN-spreading signals.

The total base-station signal for the *m*-th symbol is just the sum of the signals across all forward-link channels:

$$s_{BS,m}(t) = \sum_k s_{k,m}(t) \ , \ 0 \le t \le T_s$$

where $T_s = N_c T_c$ is the symbol duration. The assumption (introduced in chapter 2) that total base-station power is constant implies that the energy-per-chip of the base-station signal, given by:

$$I_{or,m} = \frac{1}{2} \frac{1}{N_c} \int_0^{Ts} s_{BS,m}(t) s_{BS,m}{}^*(t) dt$$

is constant regardless of *m*. Therefore, the quantity will be referred to simply as I_{or} in the rest of this chapter. For notational convenience, from here onwards the symbol index *m* will be dropped; it will be implicitly assumed that all symbol-dependent quantities refer to the *m*-th symbol.

5.1.2 The correlator for the RAKE receiver

Letting channel *k* be the mobile's traffic channel, the RAKE receiver attempts to demodulate the signal $s_k'(t)$, that is, the received signal corresponding to $s_k(t)$ as given by equation (5.1). Equation (5.1) shows that the spreading sequence for the mobile is (after dropping the symbol index *m*):

$$g_k(t) = \sum_{n=0}^{N_c-1} w_k(n) PN(n) p(t - nT_c)$$

Let "finger *i*" denote the finger assigned to demodulate the received base-station signal at a delay of *i* chips. The spreading sequence received at finger *i* can be written as:

$$g_{k,i}(t) = \sum_{n=0}^{N_c-1} w_k(n) PN_{-i}(n) p(t - nT_c) \qquad (5.2)$$

where $PN_{-i}(n)$ denotes the complex PN-sequence right-shifted by *i* chips.

The correlator for the finger *i* is simply $g_{k,i}{}^*(t)$. This correlator performs both PN and Walsh de-spreading in order to filter out signals from different multipaths and from other forward-link channels.

Assuming - without loss of generality - that the pulse-shaping filter has unit energy, the autocorrelation of $g_{k,i}$ is given by:

$$\int_0^{Ts} g_{k,i}(t) g_{k,i}^{*}(t) dt = N_c \qquad (5.3)$$

In addition, the orthogonality of Walsh codes guarantees that for $j \neq k$:

$$\int_0^{Ts} g_{j,i}(t) g_{k,i}^{*}(t) dt = 0 \qquad (5.4)$$

That is, spreading sequences for the same delay but different Walsh codes are completely orthogonal.

Let R_c denote the chip rate, or equivalently, the signal bandwidth. The symbol correlation between $s_k(t-i/R_c)$ - the signal at the k-th channel at a delay of i chips - and $g_{k,i}^{*}(t)$ is given by:

$$\int_0^{Ts} s_k(t - i/R_c) g_{k,i}^{*}(t) dt = \sqrt{2E_{c,k}} x_k \int_0^{Ts} g_{k,i}(t) g_{k,i}^{*}(t) dt = \sqrt{2E_{c,k}} x_k N_c \qquad (5.5)$$

On the other hand, correlating $s_j(t-i/R_c)$ – that is, a signal from a different forward-link channel - with $g_{k,i}^{*}(t)$ results in:

$$\int_0^{Ts} s_j(t - i/R_c) g_{k,i}^{*}(t) dt = \sqrt{2E_{c,j}} x_j \int_0^{Ts} g_{j,i}(t) g_{k,i}^{*}(t) dt = 0 \qquad (5.6)$$

Putting (5.5) and (5.6) together, it can be seen that correlating $g_{k,i}^{*}$ with the total base station signal at a delay of i PN chips results in:

$$\int_0^{Ts} s_{BS}(t - i/R_c) g_{k,i}^{*}(t) dt = \int_0^{Ts} \sum_j s_j(t - i/R_c) g_{k,i}^{*}(t) dt$$

$$= \int_0^{Ts} s_k(t - i/R_c) g_{k,i}^{*}(t) dt + \sum_{j \neq k} \int_0^{Ts} s_j(t - i/R_c) g_{k,i}^{*}(t) dt$$

$$= \sqrt{2E_{c,k}} x_k N_c \qquad (5.7)$$

It can be seen that the PN chips used to spread $s_{BS}(t-i/R_c)$ are the same as the PN chips used to spread $g_{k,i}(t)$; equivalently, it can be said that $s_{BS}(t-i/R_c)$ and $g_{k,i}(t)$ are PN-aligned. As a consequence, all channels in $s_{BS}(t-i/R_c)$ are mutually orthogonal, and Walsh de-spreading after PN de-spreading completely filters out the signals from forward-link channels other than the k-th channel[34].

Finally, define N_i to be the correlation between $n(t)$ and the deterministic signal $g_{k,i}^{*}(t)$, where $n(t)$ is a sample function of a zero-mean AWGN process with power spectral density I_{oc}. It can be seen that:

$$E[N_i] = E\left[\int_0^{Ts} n(t)g_{k,i}^{*}(t)dt\right] = \int_0^{Ts} E\left[n(t)\right]\, g_{k,i}^{*}(t)dt = 0 \qquad (5.8.1)$$

$$Var[N_i] = E\left[\int_0^{Ts}\int_0^{Ts} n(t)n^{*}(\tau)g_{k,i}(t)g_{k,i}^{*}(\tau)d\tau dt\right]$$
$$= \int_0^{Ts}\left(\int_0^{Ts} I_{oc}\ \delta(t-\tau)g_{k,i}(t)g_{k,i}^{*}(\tau)d\tau\right)dt = N_c I_{oc} \qquad (5.8.2)$$

$$E\left[N_j N_i^{*}\right] = \int_0^{Ts}\left(\int_0^{Ts} I_{oc}\ \delta(t-\tau)g_{k,j}(t)g_{k,i}^{*}(\tau)d\tau\right)dt = r_{k,j,k,i}I_{oc},\ i \neq j \qquad (5.8.3)$$

where $r_{l,j,k,i}$ is defined as:

$$r_{l,j,k,i} = \int_0^{Ts} g_{l,j}(t)g_{k,i}^{*}(t)dt \qquad (5.9)$$

The use of PN sequences guarantees that for delays i and j with $i \neq j$ and for any Walsh sequences k and l:

$$r_{l,j,k,i} << N_c$$

The following section will develop the model for the simple case in which $r_{l,j,k,i}$ is assumed to be zero for $i \neq j$. A more general case will be developed in section (5.1.4).

[34] In practice, the received signal and the finger correlator are not perfectly PN-aligned due to small timing misalignments between receiver and transmitter; thus, there is a small amount of co-channel interference after Walsh de-spreading at each finger. This interference term will be assumed negligible compared to other sources of interference.

5.1.3 Post-demodulation SNR: perfectly orthogonal codes (no in-cell interference)

Assuming that the PN sequences are completely orthogonal - that is, $r_{l,j,k,i} = 0$ for $i \neq j$ - implies that $E[N_j N_i^*] = 0$; in other words, equation (5.8.3) shows that different noise components N_i and N_j are orthogonal.

In addition, the correlation between total base-station signal and a spreading sequence at a different delay is also identically zero, as the following development illustrates:

$$\int_0^{Ts} s_{BS}(t - j/R_c) g_{k,i}^*(t)dt = \int_0^{Ts} \sum_l s_l(t - j/R_c) g_{k,i}^*(t)dt = \sum_l \int_0^{Ts} \sqrt{2E_{c,l}}\, x_l g_{l,j}(t) g_{k,i}^*(t)dt$$

$$= \sum_l \sqrt{2E_{c,l}}\, x_l \int_0^{Ts} g_{l,j}(t) g_{k,i}^*(t)dt = \sum_l \sqrt{2E_{c,l}}\, x_l r_{l,j,k,i} = 0 \qquad (5.10)$$

The important implication of this result is that under the assumption of perfect orthogonality for PN codes, finger *i* completely filters out signals from multipaths other than *i*.

For a NTD user in a cell where transmit diversity is not enabled, there is a single channel from the base station to the mobile, namely the channel from the single transmitter antenna to the receiver antenna. Assuming this channel to be an *L*-tap delay channel and ignoring inter-symbol interference[35], the base-station signal received at the mobile can be expressed as:

$$s'_{BS}(t) = \sum_{i=1}^{L} h_{i,1}\ s_{BS}(t - \frac{i}{R_c}) + n(t)\ ,\ 0 \le t \le T_s \qquad (5.11)$$

where $h_{i,1}$ is the channel coefficient for tap *i* from antenna 1 (main antenna), R_c is the chip rate (equivalently, the signal bandwidth) and *n(t)* is a sample function of the other-cell interference plus thermal noise. As explained in chapter 3, *n(t)* can be assumed to be zero mean AWGN with variance I_{oc}.

Assuming an ideal RAKE receiver, the signal received in each of the *L* taps is demodulated by exactly one finger. The expression at the output of finger *i* is given by:

[35] This is a reasonable assumption – for urban and suburban channels, the multipath spread is typically less than $T_s/3$. In such channels, it is assumed that inter-symbol interference is dominated by in-cell and other-cell interference.

$$D_i = \int_0^{Ts} s_{BS}'(t) g_{k,i}{}^*(t)dt + \int_0^{T_s} n(t) g_{k,i}^*(t)dt$$

$$= h_{i,1} \int_0^{Ts} s_{BS}(t - i/R_c) g_{k,i}{}^*(t)dt + \sum_{j=1, j\neq i}^{L} h_{j,1} \int_0^{Ts} s_{BS}(t - j/R_c) g_{k,i}{}^*(t)dt + \int_0^{Ts} n(t) g_{k,i}^*(t)dt$$

$$= h_{i,1}\sqrt{2E_{c,k}}\, x_k N_c + N_i \qquad (5.12)$$

The outputs of the fingers (the D_i values) are subsequently combined in order to reach the final decision variable. A cdma2000 typically implements pilot-based combining[36]: each D_i is weighted by h_i^*, with h_i^* being estimated from the strength of the pilot signal received in finger i. Assuming perfect channel gain estimation at the receiver[37], the combined output of the fingers is:

$$\sum_{i=1}^{L} h_{i,1}^* D_i = \sqrt{2E_{c,k}}\, x_k N_c H + \sum_{i=1}^{L} h_{i,1}^* N_i \qquad (5.13)$$

where the overall coefficient for the signal (H) is given by:

$$H = \sum_{i=1}^{L} |\, h_{i,1}\,|^2 \qquad (5.14)$$

In particular, H is real.

The first term in the summation of (5.13) corresponds to the signal, the second term corresponds to other-cell interference and thermal noise. Given the channel coefficients, the only non-deterministic terms are the N_i values (all of which are zero-mean and independent of the channel coefficients). Thus, for these channel coefficients, the instantaneous post-demodulation SNR can be written as:

$$SNR_{nodiv} = \frac{\left|\sqrt{2E_{c,k}}\, x_k N_c H\right|^2}{E\left[\left|\sum_{i=1}^{L} h_{i,1}^* N_i\right|^2\right]} = \frac{2N_c^2 H^2 E_{c,k}}{E\left[\left|\sum_{i=1}^{L} h_{i,1}^* N_i\right|^2\right]}$$

[36] As stated in [5], pilot-based combining is typically easier to implement than (optimal) maximal-ratio combining, and the performance loss relative to maximum-ratio combining is not significant.

[37] The assumption of perfect channel gain estimation is reasonable because the forward-link pilot channel (from which the channel coefficients are estimated) is a strong signal.

$$= \frac{2N_c^2 H^2 E_{c,k}}{\sum_{i=1}^{L} \left|h_{i,1}\right|^2 Var[N_i] + \sum_{i=1, j=1, i\neq j}^{L} h_{i,1}^* h_{j,1} E[N_i^* N_j]}$$

$$= \frac{2N_c^2 H^2 E_{c,k}}{H \; N_c I_{oc}} \qquad \text{(from (5.8.2), (5.8.3) and the fact that } r_{k,j,k,i} = 0\text{)}$$

$$= \frac{2N_c \; H \frac{E_{c,k}}{I_{or}}}{\frac{I_{oc}}{I_{or}}} = 2N_c \frac{E_{c,k}}{I_{or}} \frac{H \; I_{or}}{I_{oc}}$$

$$= 2N_c \frac{E_{c,k}}{I_{or}} \frac{I_{or}^{'}}{I_{oc}} \qquad (5.15)$$

Expression (5.15) is very similar to (4.13) in chapter 4, and establishes a linear relation between $E_{c,k}/I_{or}$, geometry ($I_{or}^{'}/I_{oc}$) and received SNR.

If STS is enabled, equation (5.11) is instead written as:

$$s^{'}(t) = \sum_{i=1}^{L} h_{i,1} \; s_{BS,1}(t - i/R_c) + \sum_{i=1}^{L} h_{i,2} \; s_{BS,2}(t - i/R_c) + n(t) \;\; 0 \le t \le T_s \qquad (5.16)$$

Signals $s_{BS,1}$ and $s_{BS,2}$ are the components of $s_{BS}(t)$ coming from the common and diversity antennas, respectively; thus, they satisfy the relation $s_{BS,1}(t) + s_{BS,2}(t) = s_{BS}(t)$. On the other hand, $h_{i,1}$ and $h_{i,2}$ are the channel coefficients for the i-th tap from antenna 1 (common antenna) and antenna 2 (diversity antenna), respectively. There is no loss of generality in this model: if the path at delay i/R_c only comes from one of the antennas, one of ($h_{i,1}$, $h_{i,2}$) is zero.

For a NTD user in an STS-enabled cell, only the signal from the common antenna matters. As a consequence, the function $g_{k,i}(t)$ used for correlation at the RAKE receiver is the same as in the one-transmit-antenna case. The in-cell interference must, in principle, include the interference caused by correlating the $s_{BS,2}(t-\tau)$ components with $g_{k,i}^*(t)$. As explained in chapter 2, however, the use of Walsh-code k for a NTD mobile's traffic channel precludes its use on any of the channels transmitted from the diversity antenna. As a consequence, all channels from the diversity antenna are orthogonal to the

NTD mobile's traffic channel and there is no interference from the diversity antenna[38]. Thus, equation (5.15) represents the post-demodulation SNR for this case as well.

5.1.4 Post-demodulation SNR: pseudo-orthogonal codes

The previous section illustrated that under the assumption of perfect PN-code orthogonality, the performance of a NTD phone is the same regardless of whether STS is enabled in the cell; in practice, however, enabling STS significantly hurts the performance of a NTD mobile. In order to understand this phenomenon, the original assumption of perfect orthogonality between PN sequences must be relaxed.

More specifically, it will be assumed that the correlation between two spreading sequences at different delays is a non-zero constant regardless of the Walsh sequences and of the specific delays. That is:

$$r_{l,j,k,i} = \int_0^{Ts} g_{l,j}(t) g_{k,i}{}^{*}(t) dt = r, \quad i \neq j \qquad (5.17)$$

with $r << N_c$ is constant regardless of the delays i and j and the Walsh sequences k and l. Equation (5.8.3) then becomes:

$$E\left[N_i^* N_j\right] = \int_0^{Ts} \left(\int_0^{Ts} I_{oc}\ \delta(t-\tau) g_{k,i}^*(t) g_{k,j}(\tau) d\tau \right) dt = r I_{oc},\ i \neq j$$

Therefore, the expected power coming from other-cell interference and noise is given by:

$$E\left[\left|\sum_{i=1}^{L} h_{i,1}^* N_i\right|^2\right] = \sum_{i=1}^{L} \left|h_{i,1}\right|^2 Var\left[N_i\right] + \sum_{i=1, j=1, i\neq j}^{L} h_{i,1}^* h_{j,1} E\left[N_i^* N_j\right]$$

$$= \left(N_c H + r H_{cr,1}\right) I_{oc} \qquad (5.18)$$

where H is given by (5.14) and

$$H_{cr,1} = \sum_{i=1, j=1, i\neq j}^{L} h_{i,1}^* h_{j,1} = \left|\sum_{i=1}^{L} h_{i,1}\right|^2 - \sum_{i=1}^{L} \left|h_{i,1}\right|^2 \qquad (5.19)$$

is a real number.

[38] Under the assumption (relaxed in the next section) that signals arriving at different tap delays are perfectly orthogonal.

In addition, it will also be assumed that the correlation between total base-station signal $s_{BS}(t)$ and a spreading sequence at a different delay is proportional to the Euclidean norm of the base-station signal. Mathematically, for the one-antenna case:

$$a_{k,i,j} = \frac{1}{\sqrt{I_{or}}} \int_0^{Ts} s_{BS}(t - j/R_c) g_{k,i}^*(t) dt = \frac{1}{\sqrt{I_{or}}} \sum_l \sqrt{2E_{c,l}} x_l \int_0^{Ts} g_{l,j}(t) g_{k,i}^*(t) dt = a \tag{5.20.1}$$

with a constant and small due to the approximate orthogonality between $g_{l,j}(t)$ and $g_{k,i}(t)$.

For the two-antenna case, the assumptions are:

$$a_{k,i,j}^{(1)} = \frac{1}{\sqrt{I_{or,1}}} \int_0^{Ts} s_{BS,1}(t - j/R_c) g_{k,i}^*(t) dt = a$$

$$a_{k,i,j}^{(2)} = \frac{1}{\sqrt{I_{or,2}}} \int_0^{Ts} s_{BS,2}(t - j/R_c) g_{k,i}^*(t) dt = a \tag{5.20.2}$$

The assumptions of $r_{l,j,k,i}$ and $a_{k,i,j}$ being constant, while simplistic, help explain STS degradation on NTD mobiles.

For the one-antenna case, the in-cell interference component of the RAKE receiver output at finger i is given by:

$$\sum_{j=1, j\neq i}^{L} h_{j,1} \int_0^{Ts} s_{BS}(t - j/R_c) g_{k,i}{}^*(t) dt = a\sqrt{I_{or}} \sum_{j=1, j\neq i}^{L} h_{j,1}$$

The recombination algorithm weights the output of finger i by $h_{i,1}{}^*$ and subsequently adds the outputs. As a result, total in-cell interference at the output of the RAKE receiver is given by $a\sqrt{I_{or}} \sum_{j=1, j\neq i}^{L} h_{i,1}^* h_{j,1}$, having power:

$$I_{ic} = \left(a\sqrt{I_{or}} \sum_{j=1, j\neq i}^{L} h_{i,1}^* h_{j,1} \right) \left(a\sqrt{I_{or}} \sum_{j=1, j\neq i}^{L} h_{i,1}^* h_{j,1} \right)^* = a^2 I_{or} H_{cr,1}^2 \tag{5.21}$$

Starting from (5.13) and adding the in-cell interference component, it can be seen that the post-demodulation SNR is given by:

$$SNR_{nodiv} = \frac{2N_c^2 H^2 E_{c,k}}{a^2 I_{or} H_{cr,1}{}^2 + \left(N_c H + rH_{cr,1}\right) I_{oc}} = \frac{2N_c{}^2 H^2 \frac{E_{c,k}}{I_{or}}}{a^2 H_{cr,1}{}^2 + \frac{I_{oc}}{I_{or}} \left(N_c H + rH_{cr,1}\right)}$$

(5.22)

For the two antenna case, received signal energy as well as thermal noise and other-cell interference are the same. On the other hand, total in-cell interference at the output of the RAKE receiver is given by:

$$a\left[\sqrt{I_{or,1}}H_{cr,1}+\sqrt{I_{or,2}}H_{cr,2}\right] \qquad (5.23)$$

with $H_{cr,1}$ given by (5.19) and $H_{cr,2}$ given by:

$$H_{cr,2}=\sum_{i=1,j=1,j\neq i}^{L}h_{i,1}^{*}h_{j,2}=\left(\sum_{i=1}^{L}h_{i,1}^{*}\right)\left(\sum_{j=1}^{L}h_{j,2}\right)-\sum_{i=1}^{L}h_{i,1}^{*}h_{i,2} \qquad (5.24)$$

Note that the *i*-th tap from the diversity antenna does not cause interference on the demodulation of the common-antenna signal at the *i*-th finger; as seen in chapter 2, time-aligned signals from the common and diversity antenna are mutually orthogonal. Hence the summation of $H_{cr,2}$ only includes values of $j \neq i$.

Equation (5.13) thus leads to the following expression for instantaneous post-demodulation SNR (given the channel coefficients):

$$SNR_{div}=\frac{2N_c^2E_{c,k}H^2}{\left|\ a\left(\ \sqrt{I_{or,1}}H_{cr,1}+\sqrt{I_{or,2}}H_{cr,2}\ \right)\right|^2+\left(\ N_cH\ +\ rH_{cr,1}\ \right)I_{oc}}$$

$$=\frac{2N_c^2H^2\dfrac{E_{c,k}}{I_{or}}}{a^2\left[f{H_{cr,1}}^2+(1-f)\left|H_{cr,2}\right|^2+2\sqrt{f(1-f)}H_{cr,1}\,\mathrm{Re}\left\{H_{cr,2}^{*}\right\}\right]+\dfrac{I_{oc}}{I_{or}}{H_N}^2} \qquad (5.25)$$

where

$f = I_{or,1}/I_{or}$
$1\text{-}f = (I_{or} - I_{or,1})/I_{or} = I_{or,2}/I_{or}$
${H_N}^2 = \left(N_cH\ + rH_{cr,1}\right)$

The value of *f* lies between 0.5 and 1 because the power from the diversity antenna ($I_{or,2}$), is strictly less than the power from the common antenna ($I_{or,1}$). The reason for the latter is that any STS traffic power transmitted from the diversity antenna is also transmitted from the common antenna; in addition, the common antenna transmits a larger amount of overhead power (common pilot, paging, synchronization channels) than

the diversity antenna (whose only overhead channel is the diversity pilot). Finally, the common antenna also transmits all the NTD traffic power.

5.1.5 Noise and interference comparison: STS versus NTD

Comparing (5.22) and (5.25), it is clear that the signal energy as well as the other-cell interference and thermal noise are the same for the one-antenna and two-antenna cases. The only difference lies in the in-cell interference terms, which are rewritten here for convenience:

$$\begin{array}{ll} a^2 H_{cr,1}{}^2 & \text{(NTD case)} \\ a^2\left(\; fH_{cr,1}{}^2 + (1-f)\left|H_{cr,2}\right|^2 + 2\sqrt{f(1-f)}H_{cr,1}\,\mathrm{Re}\{H_{cr,2}^*\}\;\right) & \text{(STS case)} \end{array} \qquad (5.26)$$

First of all, it is obvious that if there is only one resolvable path from each transmitting antenna to the receiving antenna, both $H_{cr,1}$ and $H_{cr,2}$ are zero, so in-cell interference is zero in both cases. Thus, in a one resolvable path (flat fading) scenario, there is no additional degradation to a NTD mobile when STS is enabled.

In a multipath scenario, $H_{cr,1}$ and $H_{cr,2}$ - and thus in-cell interference - are not zero. The expressions in (5.26) show that after normalization to I_{or}, the only factors affecting in-cell interference are the channel coefficients and f, which represents the fraction of total power transmitted from the common antenna.

The next two subsections compare the interference for multipath scenarios under stationary and fading channels.

5.1.5.1 Stationary channel, at least two resolvable paths

In this channel, all the coefficients are constant. In this case, the instantaneous SNR expressions (5.22) and (5.25) constitute mean SNR as well. Since the channel is stationary, it is clear that the relative values of in-cell interference for the NTD and STS cases depend on the channel coefficients. In a simple case, assuming $H_{cr,1} = H_{cr,2} = H_{cr}$, equations (5.26) become:

$$a^2 H_{cr}{}^2 \qquad (5.27.1)$$

$$a^2 H_{cr}{}^2\left[1 + 2\sqrt{f(1-f)}\right] \qquad (5.27.2)$$

Equation (5.27.1) can be seen as a particular case of (5.27.2) with $f = 1$ (all power transmitted from the common antenna).

The second term in the summation in (5.27.2) is in-cell interference that is not present in a one-transmit-antenna case. In addition, the product $f(1-f)$ is maximized for $f = 0.5$. Since f is always greater than 0.5, smaller values of f result in a higher value for (5.27.2). Consequently, higher power from the diversity antenna corresponds to higher levels of in-cell interference.

5.1.5.2 Rayleigh fading channel, at least two resolvable paths

Establishing a closed expression for the interference is harder for a fading channel because post-demodulation signal, in-cell interference and other-cell interference are all mutually correlated through the channel coefficients. This section will only present a brief intuitive analysis; a more precise quantification of the impacts of in-cell interference will be relegated to lab experiments, whose results will be presented in section (5.2).

From the expressions (5.22) and (5.25), it is clear that higher absolute values for the channel coefficients result in larger in-cell interference. In the NTD-cell case, however, a high channel coefficient $h_{i,1}$ also contributes to the signal energy – that is, $h_{i,1}$ also appears as part of H in the numerator of (5.22). In the case of a NTD mobile on an STS cell, however, the $h_{j,2}$ channel coefficients from the diversity antenna only appear as interference as part of $H_{cr,2}$ in the denominator of (5.25); as such, they do not contribute to improve SNR. If some of the $h_{j,2}$ values happen to be strong while the $h_{i,1}$ values are weak, the interference from the diversity antenna can be high with respect to received signal power; as a consequence, the probability of low post-demodulation SNR is higher for the STS-enabled cell than for the regular NTD cell. This probability is higher for higher values of diversity-antenna power, since the $h_{j,2}$ coefficients are scaled by $I_{or,2}$; thus - like in the AWGN channel - the performance degradation is expected to be higher for higher values of $I_{or,2}$.

5.2 Performance degradation due to in-cell interference

This section presents results obtained via lab experiments in an attempt to quantify the performance degradation suffered by NTD mobiles under a multipath Rayleigh-faded channel in an STS enabled cell. These results could have been obtained via simulations, like was done in chapter 3; lab measurements, however, have the advantage of incorporating the effects of hardware imperfections in the demodulation process, thereby more closely mimicking the performance of a real mobile in non-ideal channel conditions.

Section 5.2.1 describes the method used to quantify the performance degradation; section 5.2.2 describes the lab setup and the measurement procedures; section 5.2.3 presents the results.

5.2.1 Quantifying STS performance degradation on a NTD mobile

The previous section explained that the level of in-cell interference is partially determined by the power distribution between the two transmitting antennas. Chapter 4

described how to configure the base station to setup different levels of diversity pilot and different "loading scenarios" for a cell; in particular, it was explained that the loading scenario specifies the ratio between the STS traffic power and total traffic power transmitted by the base station. In conjunction, the diversity pilot and the loading scenario completely specify the distribution of base station power between the two antennas.

In addition to the loading scenario, equations (5.22) and (5.25) show that the instantaneous post-demodulation SNR is also affected by the ratio I_{or}/I_{oc}, which appeared after normalization of other-cell interference and thermal noise to I_{or}. As defined in chapter 3, this ratio[39] determines the *geometry* for the mobile; like with the computer simulations, the lab experiments were also conducted for different geometry levels.

Given a combination of geometry, diversity pilot and loading scenario, the *performance loss* (P_L) is defined as:

$$P_L = \overline{\left(\frac{E_c^{(i)}}{I_{or}}\right)} - \overline{\left(\frac{E_c^{(0)}}{I_{or}}\right)} \qquad (5.28)$$

The first term in (5.28) is the mean traffic E_c/I_{or} required to achieve the target error rate under scenario i (scenario i refers to a combination of diversity pilot and loading scenario). The second term is the mean traffic E_c/I_{or} required to achieve the target error rate under loading 1 (regular NTD cell in which STS is not enabled), and serves as a reference: a positive value for P_L indicates an increase in required transmit power with respect to the NTD-cell case, implying performance degradation due to STS interference.

The motivation for using E_c/I_{or} as a performance metric can be easily traced to equations (5.22) and (5.25): as those equations show, E_c/I_{or} can be viewed as a measure of signal power. The equations also show that in-cell interference is dependent only on channel coefficients and the power ratio between the common and the diversity antenna. Finally, equations (5.22) and (5.25) show that other-cell interference plus thermal noise is scaled by the inverse of the geometry[40]: thus, in scenarios of high geometry both other-cell interference and thermal noise are dominated by in-cell interference. As a consequence, any degradation resulting from diversity-antenna power impact on in-cell interference becomes more pronounced under high geometry scenarios.

5.2.2 Setup

A basic sketch of the lab setup is shown in Figure 1.

[39] In conjunction with the channel gain.
[40] Assuming no large-scale path loss from the base-station to the mobile.

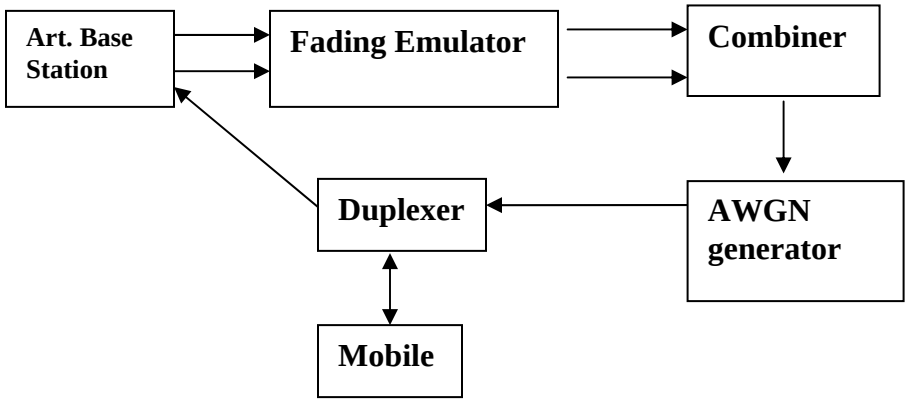

Figure 1: Lab setup

On the forward-link, the common and diversity signals from the base station are each wired to the channel fading emulator. The fading emulator specifies the multipath structure of the channel as well as the fading model and speed (which determines the time correlation of the fading coefficients). The two faded signals at the output are then fed to a combiner to emulate the over-the-air summation of the transmit diversity branch signals. The combined signal is subsequently fed to a noise generator so as to model other-cell interference and thermal noise; in particular, the AWGN generator is used to set the mobile geometry. The output of the AWGN generator is the sent to the NTD mobile. The reverse-link signal, on the other hand, is sent directly to the base station[41].

The role of the duplexer is to isolate transmitter and receiver signals since they go through different channels. As can be seen in figure 1, the mobile-duplexer link is two-sided and carries both the forward and reverse-link signals. The duplexer gets the forward-link signal from its input port - which is connected to the AWGN generator in the figure - and sends it to the mobile via the duplex link; at the same time, it also gets the mobile reverse-link signal from the duplex link and sends it to the base station via its output port.

5.2.3 Results

The multipath structure and the emulated mobile speed are shown in table 1.

Table 1: Multipath structure and mobile speed for lab tests

Multipaths	P1	P2
Pow rel to P1 (dB)	0	0
Delay(us)	0	2

speed (km/h)	8

[41] There was no need to emulate channels on the reverse-link since the experiment is concerned with receiver performance on the forward-link.

The multipath structure is the same for both the common and the diversity antenna, and the Rayleigh fading processes between any two of the four paths are uncorrelated.

The call parameters are the same as described in the last paragraph of section "Test Calls" in chapter 4; in particular, the target frame error-rate (FER) was 1%. In addition, the traffic-channel signals were coded and modulated under Radio Configuration 3 (RC3). Each test was run until the mobile received a total of 400 frame errors.

The channel was tested for:

1) two levels of diversity pilot: –3dB and –6dB (denoted as "TD-3" and "TD-6")
2) three loading scenarios: 1, 4 and 5 (as defined in chapter 4, these respectively correspond to a regular NTD cell, an STS cell where half the traffic power is STS power, and a cell where all traffic power is STS power).
3) five geometries: 0dB, 3dB, 6dB, 9dB and 12dB.

Table 2 shows the mean required E_c/I_{or} to achieve the target error rate in each case:

Table 2: Lab results for two-path Rayleigh channel

Ec/Ior (dB)	Geometry (dB)				
	0	3	6	9	12
loading0	-9.67	-12.47	-15.09	-16.71	-17.87
loading4_TD-3	-8.81	-11.89	-14.22	-15.74	-16.54
loading4_TD-6	-9.19	-11.81	-14.41	-15.78	-16.51
loading5_TD-3	-8.57	-11.72	-13.52	-15.21	-15.64
loading5_TD-6	-8.9	-12.21	-13.59	-15.22	-15.88

Figure 2 plots the NTD performance loss, or required increase in E_c/I_{or} relative to the NTD-only case.

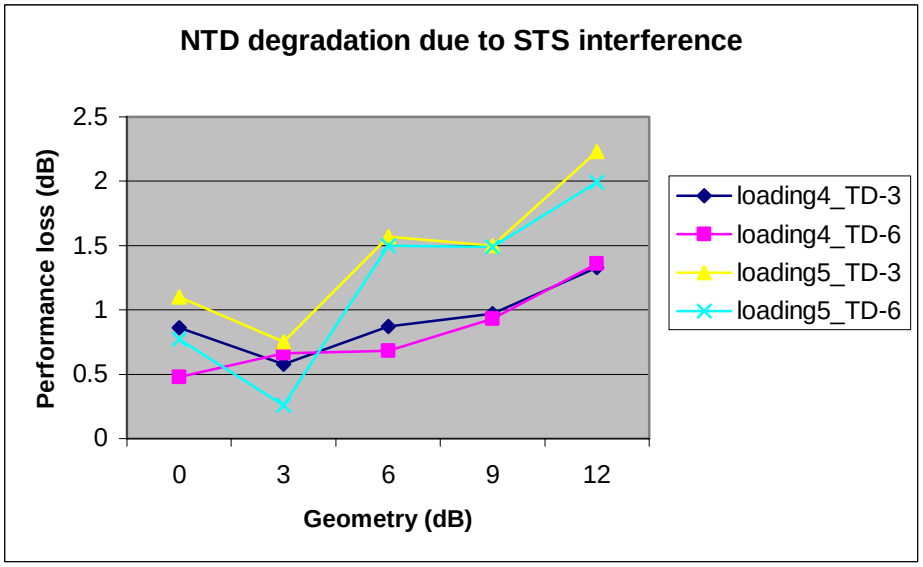

Figure 2: Lab results for two-path Rayleigh channel

As expected, larger degradation occurs in loading 5, the scenario that corresponds to the largest diversity-antenna power level. It can also be seen that the -3dB diversity pilot causes higher degradation than the –6dB diversity pilot, though the difference is slight since most of the diversity antenna power is STS traffic power. Finally, the losses increase with geometry, since at higher geometries in-cell interference – which is the source of the degradation with respect to NTD - dominates other-cell interference and thermal noise.

From figure 14, it can be seen that enabling STS on a cell can cause a degradation of 1.5dB to a NTD mobile[42]. This degradation can significantly impact cell capacity, as will be seen in the next chapter.

[42] The degradation of over 2dB for the 12dB geometry is downplayed since a geometry of 12dB is unrealistically high.

Chapter 6: Field measurements

Chapter 4 described various metrics computed in order to evaluate the performance of cdma2000 mobiles in cells using transmit diversity techniques (NTD, STS, PSTD). This chapter presents the results of field tests, and concludes with an estimate of the possible increase in base station capacity brought by the use of transmit diversity.

Section 6.1 explains how the field routes were selected. Section 6.2 explains the mechanics of field testing. Section 6.3 presents the results of the metrics computed from the field data, and draws important conclusions. Section 6.4 computes an estimate of cell-capacity improvement in terms of the increase in number of supported users.

6.1 Drive route design

Each field test consisted of setting up a call on each mobile being tested, traversing a particular field route, and logging various bits of information related to the physical layer. Based on information in the logs, various metrics were computed in order to assess the average call performance for the route.

All routes consisted of drive routes and were conducted outdoors[43]. The routes encompassed different ranges of mobile speed and mobile geometry, as explained in the next two subsections.

6.1.1 Speed

Ideally, the results from field tests should encompass the effects of different mobile speeds, as the speed determines the Doppler spread and hence the coherence time of the channel. However, it is generally not possible to achieve a constant mobile speed in a drive test. As a consequence, only two speed ranges were tested:

1) Walking speeds (less than 5 km/h).
2) City-driving speeds (between 10 km/h and 70 km/h).

Field testing was not done at highway speeds because of time and resource restrictions.

[43] Indoor channels have characteristics that differ significantly from outdoor channels. Unfortunately, indoor testing was impractical due to logistical reasons related to the test setup.

6.1.2 Geometry

The mobile geometry is not directly measurable, but can be inferred from the received common-pilot power. As shown in chapter 4 and repeated here for convenience, mobile geometry and received common-pilot E_c'/I_o are related by:

$$\frac{I_{or}'}{I_{oc}} = \left(\frac{E_c / I_{or}}{E_c' / I_o} - 1 \right)^{-1} \qquad (6.1)$$

Hence, given the transmitted E_c/I_{or} of the common-pilot channel, the received pilot E_c'/I_o uniquely determines the geometry (I_{or}'/I_{oc}).

A cell-coverage map was the starting point for the design of routes covering cell areas with different geometries. The map was obtained by setting the transmitted common-pilot E_c/I_{or} to -6dB and measuring the received common-pilot E_c'/I_o in different regions of the cell. The drive routes were then designed so that the E_c'/I_o would always be larger than -12dB at every point in the route; in addition, unrealistically high or low geometry values were avoided by ensuring that the routes were never too close or too far from the base-station antenna. With a transmitted common-pilot E_c/I_{or} of -6dB and assuming that the received common-pilot E_c'/I_o always lies between -6.5dB and -10dB (thus avoiding values close to the -6dB or -12dB), equation (6.1) shows that the geometry ranges between 0dB and 9dB.

Figures 1, 2 and 3 show the routes used for city-driving speeds, along with the received common-pilot E_c'/I_o values at different points in the route; in addition to satisfying the above constraints, the three routes were also designed to cover different geographic regions of the cell. Finally, a small and confined route was used for the walking-speed tests (route 4, not pictured).

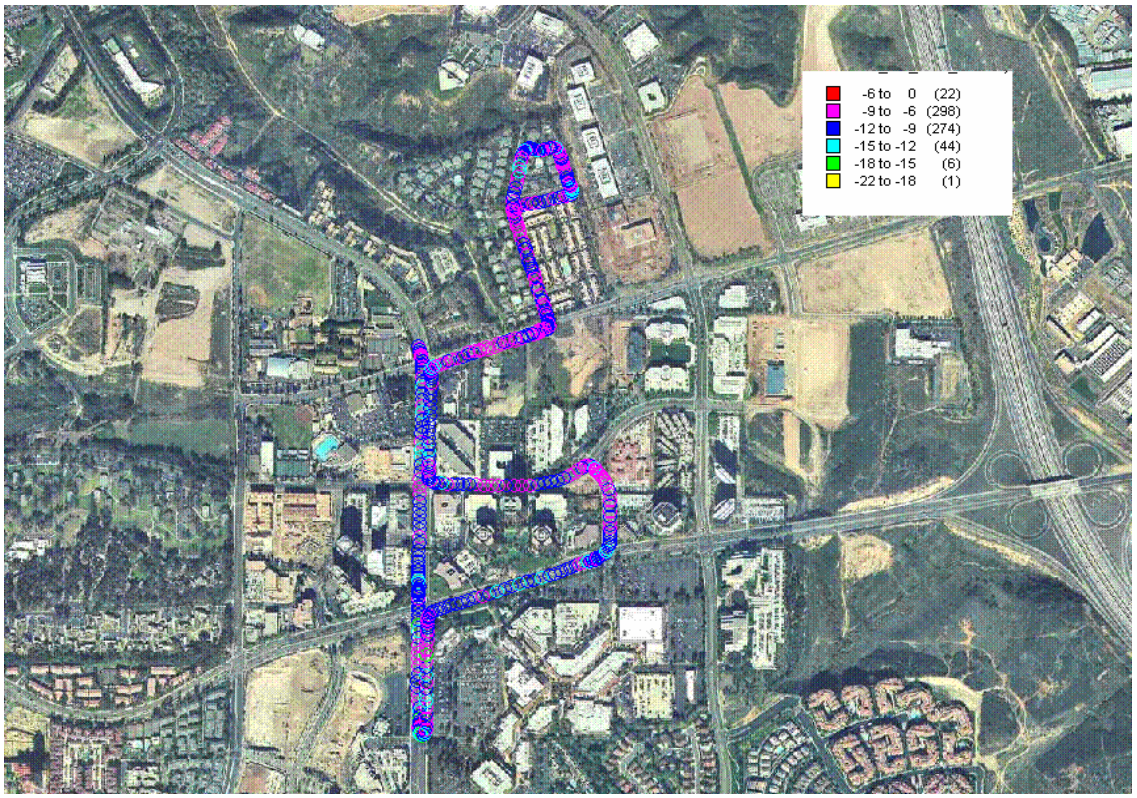

Figure 1: Drive route 1

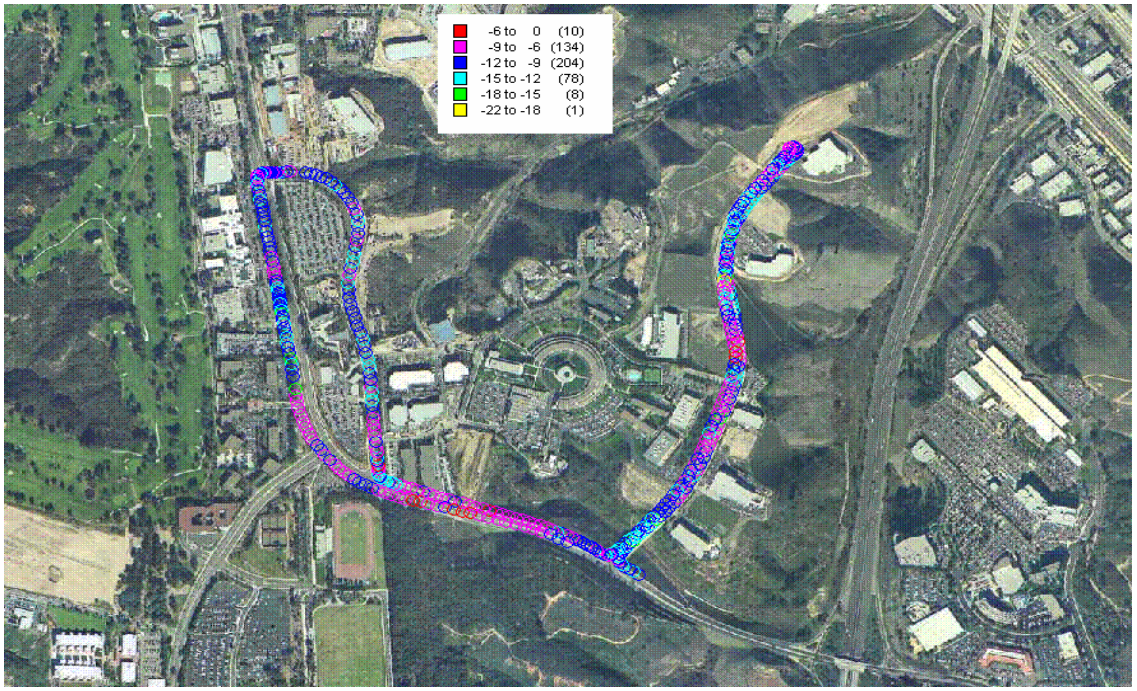

Figure 2: Drive route 2

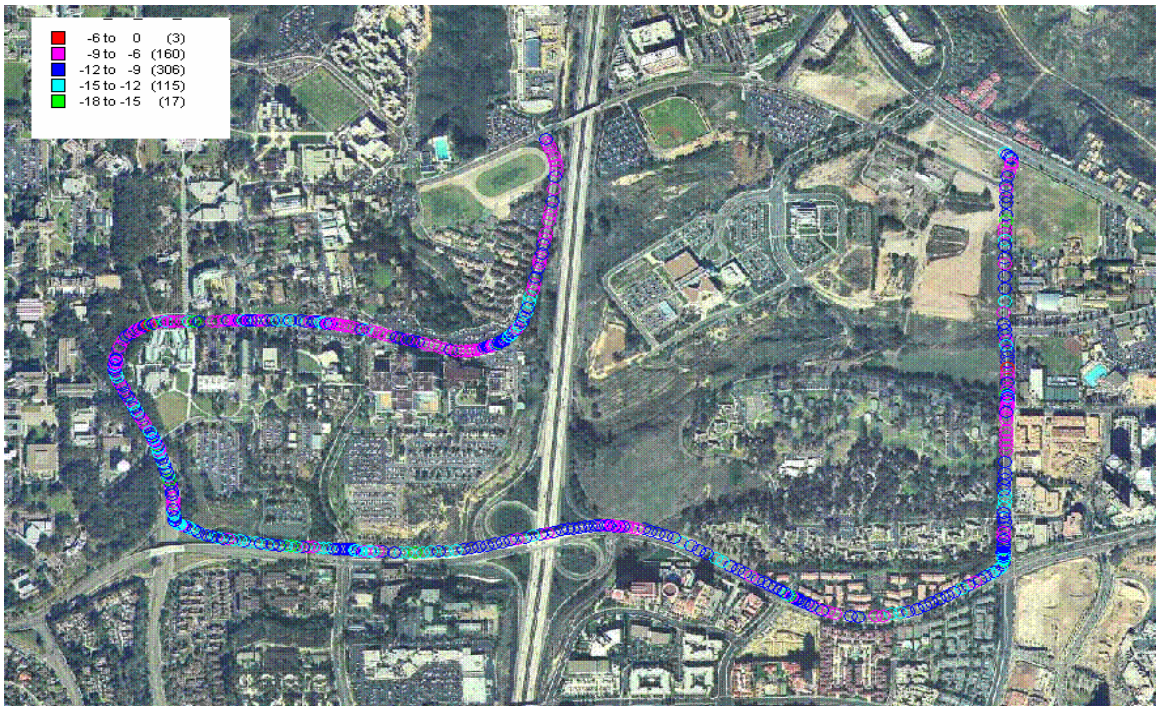

Figure 3: Drive route 3

6.2 Field testing mechanics

Before conducting any field tests, various checks were performed on the equipment to ensure proper functioning. Of particular importance was the verification of time-alignment between the common and diversity antennas: as explained in chapter 2, STS relies on this time-alignment to ensure the orthogonality of common-antenna and diversity-antenna signals arriving at the same delay (equivalently, the same finger). This orthogonality helps reduce in-cell interference and improve backward-compatibility with NTD.

It was verified that the two transmit antennas were time-aligned within ¼ of a cdma chip. Since the resolvability of a cdma2000 receiver is 1 cdma chip, this time alignment ensures the orthogonality of signals from the common and diversity antennas in a 1-tap delay channel. Furthermore, since the receiver phase coherence works at a ¼ chip granularity, the small timing misalignments introduced by the setup are undetectable at the receiver.

Once it was ascertained that the setup was satisfactory, the ground was set for the field tests. Each test consisted of:

1. Configuring the base-station. This includes setting the power levels for the common pilot, paging and synchronization channels; for STS testing, it also includes setting up the diversity pilot and the loading scenario.

2. Setting up test calls on each mobile being tested.
3. Traversing the mobile(s) along the drive route.

Incidentally, all calls were performed in a single isolated cell sector; thus, no neighboring pilot signal was present and no handoff was possible.

Figure 4 illustrates the setup for testing of an STS-enabled cell. Two mobiles - one NTD, one STS – were used in each test. In order to better compare the performance of the two phones, they were subjected to the same channel by sharing the same transmit/receive antenna. Hence, it is expected that any difference in performance results from the effects of transmit diversity.

The setup for NTD-cell and PSTD-cell testing is the same as figure 4 but without the STS phone; since an STS mobile behaves like a NTD mobile in a non-STS-enabled cell, only one phone was needed in those tests. Another difference is that in NTD-cell testing there is no signal from the diversity antenna.

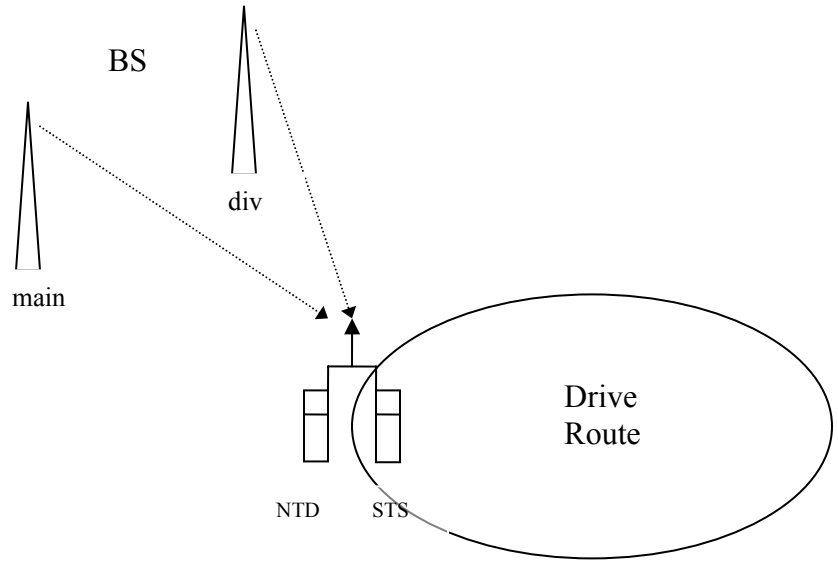

Figure 4: Field test setup. The dashed lines represent the wireless channel from each base station antenna to the shared mobile antenna.

6.3 Results

Table 1 summarizes the test cases for each drive route. The first column lists the transmit diversity (TD) techniques tested: NTD, PSTD and STS. For the STS cells, the second and third columns specify the level of diversity pilot and the loading scenario, respectively. The table also illustrates that both NTD and STS mobiles were tested in the STS-cell cases, whereas only a NTD phone was tested in NTD and PSTD cells.

Table 1: Test cases

TD technique	TD pilot	loading scenario	mobile	
			NTD	STS
NTD	N/A	1		N/A
PSTD	N/A	N/A		N/A
STS	TD-3dB	2		
		3		
		4		
		5		
	TD-6dB	2		
		3		
		4		
		5		

The matching between loading scenarios and STS/NTD traffic-power distribution was introduced in chapter 4. It is repeated in table 2 for reference.

Table 2: Loading scenarios and *Z* ratios

Loading scenario	Z = (STS traffic)/(total traffic)	Diversity pilot
1	0	Absent
2	0	Present
3	0.1	Present
4	0.5	Present
5	1	Present

The call parameters were the same as described in chapter 4; in particular, all were full-rate (9.6 kbps) calls with forward-link power control at 800Hz and a target frame error-rate (FER) of 1%. The calls used Radio Configuration (RC4) in the standard, which specifies a Walsh-code length of 128 chips. Since an RC4 cell has twice as many available Walsh codes as an RC3 cell, it can normally support many more users – a feature that will be important in the analysis of base station capacity in section 6.4.

The following subsections detail the results obtained for the different metrics described in chapter 4. For statistical consistency, three tests were performed for each combination of drive route, TD technique and - if applicable - diversity pilot and loading scenario; the results of the three tests were subsequently averaged to get the final metrics for each combination.

6.3.1 Forward-link and reverse-link frame error rates

For all test cases, both forward-link and reverse-link frame error rates successfully converged to 1%.

6.3.2 Received pilot E_c'/I_o

Tables 3 and 4 show the mean received pilot E_c'/I_o for the different test cases:

Table 3: Received pilot E_c'/I_o for NTD and PSTD cells

		Received pilot Ec'/Io (dB)	
		NTD cell	PSTD cell
route	1	-7.6	-7.6
	2	-7.3	-7.4
	3	-8.2	-8.2
	4	-7.4	-7.7

As can be seen from table 3, the E_c'/I_o values are similar for NTD and PSTD cells. Since the E_c'/I_o is a measure of channel conditions, these values indicate that the downlink channel statistics are the same regardless of whether one or two antennas are used for transmission. This corroborates the assumption that the individual wireless channels from each base-station antenna to the mobile antenna have the same statistics.

Table 4: Received pilot E_c'/I_o for STS cells

Received pilot Ec'/Io (dB)									
		STS cell							
		TD -3dB				TD -6dB			
		load 2	load 3	load 4	load 5	load 2	load 3	load 4	load 5
route	mobile								
1	NTD	-7.8	-7.7	-7.9	-7.4	-7.9	-7.9	-7.7	-7.4
	STS	-8.1	-7.8	-7.6	-7.6	-8.0	-7.6	-7.4	-7.6
2	NTD	-7.5	-7.4	-7.8	-7.7	-7.4	-7.4	-7.6	-7.8
	STS	-6.9	-7.0	-6.8	-7.2	-6.9	-6.8	-6.7	-7.0
3	NTD	-8.4	-8.3	-8.4	-8.3	-8.4	-8.3	-8.3	-8.3
	STS	-8.1	-8.3	-7.7	-7.9	-8.2	-8.0	-7.7	-7.8
4	NTD	-7.4	-7.3	-7.2	-7.0	-7.5	-7.4	-7.3	-7.0
	STS	-7.7	-7.7	-7.7	-7.6	-7.8	-7.7	-7.7	-7.6

Looking at the NTD-mobile numbers in table 3 and 4, it can be seen that most of the E_c'/I_o values are close to the transmitted common-pilot E_c/I_{or} (-7dB). This indicates that the average geometry for each route is fairly high. From the tables, a reasonable approximation for received pilot E_c'/I_o is -7.5dB for the stronger routes and -8.2dB for the weaker route 3. According to equation 6.1, these correspond to geometries of approximately 9dB and 5dB (respectively).

As explained in chapter 4, the pilot E_c'/I_o for an STS mobile is a combination of common-pilot and diversity-pilot energy, and its value is used as a weight in the combiner stage of the RAKE receiver. The pilot E_c'/I_o is also used as the weight for finger

recombination for a NTD mobile, but in this case the E_c'/I_o only includes the common pilot power. Therefore, the relative value of the STS-mobile E_c'/I_o with respect to the NTD-mobile E_c'/I_o gives an indication of the influence of the diversity-antenna signal in the demodulation process. In this regard, table 4 shows that the received pilot E_c'/I_o is consistently higher for the STS mobile in routes 2 and 3, whereas the opposite holds for route 4; therefore, the data in table 4 suggests that the diversity-antenna signal had the highest influence in routes 2 and 3, and the lowest influence in route 4.

The values in table 4 present no consistent trend between values across different loading scenarios, suggesting that the loading scenario has little influence on pilot acquisition.

6.3.3 Number of locking fingers

Tables 5 and 6 show the mean number of locking fingers for the different cases:

Table 5: Number of locking fingers, NTD and PSTD cells

		Locking fingers	
		NTD cell	PSTD cell
route	1	4.0	3.9
	2	3.9	3.9
	3	4.3	4.2
	4	4.8	5.0

Table 6: Number of locking fingers, STS cells

Locking fingers									
		STS cell							
		TD -3dB				TD -6dB			
		load 2	load 3	load 4	load 5	load 2	load 3	load 4	load 5
route	mobile								
1	NTD	3.8	3.8	3.7	3.9	3.7	3.7	3.8	3.9
	STS	3.7	3.7	3.7	3.8	3.3	3.5	3.6	3.7
2	NTD	3.8	3.8	3.7	3.7	3.8	3.8	3.7	3.7
	STS	3.8	3.7	3.8	3.8	3.6	3.6	3.7	3.6
3	NTD	4.1	4.0	4.0	3.9	4.0	4.0	4.1	4.0
	STS	4.1	3.9	4.0	4.1	3.6	3.5	3.8	3.7
4	NTD	4.7	4.8	4.9	4.9	4.8	4.9	4.9	4.9
	STS	4.8	4.8	4.8	4.9	4.3	4.3	4.4	4.3

As tables 5 and 6 show, the number of locking fingers was high for all cases, suggesting a field scenario with many resolvable multipaths. Inspection of the log files showed, however, that only one or two paths were strong at any given time, with the other three or four paths being much weaker. A possibility is that the weaker paths were the result of noise but were treated as weak fingers; unfortunately, it was not possible to

confirm this hypothesis based on the existing data. In any case, the data suggests that one-tap channels are unlikely in urban or suburban areas; in other words, multipath diversity is already present, potentially limiting additional benefits provided by transmit diversity.

Table 6 shows that the number of locking fingers detected by the NTD mobile is virtually constant across all STS test cases; this is expected since common-pilot transmitted power is always the same and the diversity pilot is ignored. On the other hand, the number of fingers detected by the STS phone is consistently smaller for the TD-6dB than for the TD-3dB cases: the weaker diversity pilot causes fewer paths to be detected and assigned to fingers.

It was originally expected that the number of fingers would be larger for a PSTD cell when compared to a NTD cell due to multipaths from the second antenna. Table 5, however, shows little difference between the two cell types. This indicates that in the PSTD cell, the paths from the diversity antenna tend to occur at the same delays as the paths from the common antenna. In other words, there appears to be a high correlation between the multipath structures of the channels from each antenna. The following section discusses this topic further.

6.3.4 Probability of common searcher peaks from the main and diversity antenna.

Chapter 4 explained that the following probabilities were computed from the STS mobile logs:

1. Probability of finding a searcher peak from the diversity antenna "near" a searcher peak from the main antenna.
2. Probability of finding a searcher peak from the main antenna "near" a searcher peak from the diversity antenna.

In both cases, the term "near" means within a threshold of either ½ or 1 cdma chip.

The purpose of this metric is to get an idea of the correlation between the multipaths delays in the channels from each base-station antenna to the mobile.
The numbers obtained are more accurate for stronger diversity-pilot levels since the tracking of the diversity-antenna pilot becomes more accurate.

Table 7 shows the results for loading scenario 2 and a diversity pilot of -3dB with respect to the main pilot (the results for other loading scenarios were virtually identical)[44]:

[44] The TD-6dB values are also similar, albeit likely to be less accurate, and are thus not shown.

Table 7: Probability of common searcher peaks from the main and diversity antennas. The "main" column contains the probability of a diversity searcher peak within either 0.5 chip or 1 chip from a main searcher peak, and conversely for the "td" column.

	Prob (%) comm srch peak w/in			
	0.5 chip		1 chip	
	main	td	main	td
route 1	69	75	90	96
route 2	72	78	91	96
route 3	74	82	89	95
route 4	60	75	76	90

These numbers indicate a high correlation between the main-antenna and diversity-antenna multipath delays. In particular, the table shows that given a searcher peak from the diversity antenna, the probability of a main-antenna searcher peak within ½ chip is greater than 75%. Since the multipath resolvability of the receiver is 1 chip, this statistic indicates a high likelihood of main and diversity multipaths being demodulated by the same finger.

6.3.5 Mobile setpoint

Tables 8 and 9 show the mean mobile setpoint for the different cases:

Table 8: Mobile setpoint, NTD and PSTD cells

		Mobile setpoint (dB)	
		NTD cell	PSTD cell
route	1	5.8	5.6
	2	5.7	5.6
	3	5.9	6.0
	4	5.8	5.5

Table 9: Mobile setpoint, STS cells

Mobile setpoint (dB)									
		STS cell							
		TD -3dB				TD -6dB			
		load 2	load 3	load 4	load 5	load 2	load 3	load 4	load 5
route	mobile								
1	NTD	6.0	5.8	5.9	6.3	5.8	5.8	5.9	6.4
	STS	5.6	5.5	5.5	5.6	5.9	5.8	5.7	5.8
2	NTD	5.9	5.8	6.0	6.5	5.9	5.8	6.0	6.5
	STS	5.7	5.6	5.7	5.7	6.2	6.0	5.7	5.8
3	NTD	6.3	6.1	6.1	6.4	6.5	6.0	6.3	6.7
	STS	5.8	5.7	5.6	5.6	6.2	6.0	5.8	5.9
4	NTD	5.7	5.8	5.7	5.9	5.8	5.9	5.9	5.9
	STS	5.4	5.5	5.4	5.4	5.9	5.8	5.7	5.6

Initial inspection of table 8 shows that the setpoint values are approximately the same across different routes, with an upward bias for route 3 due to higher speeds/faster fading. As explained in chapter 4, the setpoint should be independent of the channel assuming perfect power control; in practice, however, fast-fading channel conditions exacerbate power control imperfections and typically induce higher setpoint values.

Table 9 illustrates some of the negative effects of STS on a NTD mobile. Compared to table 8, the setpoint values for the NTD mobile are generally higher - with the exception of the slow route 4. In addition, the effect is most pronounced for loading scenario 5, which corresponds to the highest power level from the diversity antenna. The data thus suggests that the combination of a faster-fading channel and higher levels of in-cell interference result in a significant increase in the NTD-mobile setpoint, therefore degraded power-control performance for a legacy NTD phone on an STS-enabled cell.

Inspection of table 9 also shows that the STS-mobile setpoint values are generally lower than the NTD-mobile setpoint values, suggesting that power control is more effective under STS than under NTD. In addition, the STS-mobile setpoint is less sensitive to the loading scenario than the NTD-mobile setpoint. Finally, the STS-mobile setpoint is consistently lower for TD-3dB as compared to TD-6dB, indicating that better phase acquisition results in improved power control performance.

6.3.6 Mobile transmit-adjust: mean and standard deviation

Compared to the forward-link, reverse-link statistics are typically more volatile because the mobile-transmitted pilot signal is weaker than the base-station pilot signal. As a consequence, reverse-link metrics are less comparable since results differ significantly based on changes in channel conditions and sources of interference across different tests. For a given test, however, the NTD-mobile and STS-mobile values are still comparable since the two phones were subjected to identical channels; the analysis in this section thus focuses on the relative STS-mobile values with respect to the NTD-mobile instead of the absolute values.

Table 10 shows the mean mobile transmit adjust for the different STS-cell configurations, while table 11 shows the standard deviations. None of the table numbers suggest any particular pattern, indicating that forward-link improvements have little bearing on the reverse-link.

On a different note, table 11 shows that the standard deviation is highest for route 3, and smallest for route 4. This shows that the faster-fading channel presented by route 3 implies a higher volatility on the reverse-link metrics as well as on the forward-link. Reciprocal statements can be made about the slower-fading channel presented by route 4.

Table 10: Mean mobile transmit adjust, STS cells

Mobile transmit adjust: mean (dBm)									
		STS cell							
		TD -3dB				TD -6dB			
		load 2	load 3	load 4	load 5	load 2	load 3	load 4	load 5
route	mobile								
1	NTD	-19.4	-19.4	-16.6	-16.2	-19.3	-19.3	-16.1	-16.4
	STS	-18.4	-18.0	-17.1	-16.2	-18.9	-17.6	-16.3	-16.5
2	NTD	-21.0	-21.1	-17.9	-18.3	-21.2	-21.4	-18.6	-18.0
	STS	-20.0	-19.7	-18.1	-18.4	-20.9	-19.6	-18.8	-18.2
3	NTD	-18.8	-18.8	-17.1	-16.4	-18.7	-18.8	-15.7	-16.3
	STS	-17.9	-17.6	-17.2	-16.5	-18.4	-17.2	-16.0	-16.3
4	NTD	-19.1	-19.4	-19.6	-19.6	-18.7	-19.3	-19.4	-19.6
	STS	-19.5	-19.3	-19.6	-19.4	-19.4	-19.1	-19.3	-19.5

Table 11: Standard deviation of mobile transmit adjust, STS cells

Mobile transmit adjust: standard deviation (dBm)									
		STS cell							
		TD -3dB				TD -6dB			
		load 2	load 3	load 4	load 5	load 2	load 3	load 4	load 5
route	mobile								
1	NTD	3.9	3.8	3.7	3.9	3.9	3.9	3.6	3.7
	STS	3.9	3.8	3.7	3.9	3.9	4.0	3.6	3.8
2	NTD	3.6	4.0	3.7	3.8	3.9	4.0	4.0	3.6
	STS	3.6	3.9	3.6	3.8	3.9	3.9	3.9	3.6
3	NTD	4.2	4.2	4.7	4.4	4.6	4.0	4.0	4.7
	STS	4.2	4.2	4.7	4.5	4.6	4.0	4.0	4.7
4	NTD	3.4	3.4	3.4	3.3	3.5	3.5	3.4	3.4
	STS	3.4	3.4	3.4	3.3	3.6	3.5	3.5	3.4

6.3.7 Transmitted forward-link fundamental channel E_c/I_{or}: mean and standard deviation

6.3.7.1 NTD vs. PSTD

Tables (12.a) and (12.b) show the mean and standard deviation of the forward-link fundamental channel (F-FCH) E_c/I_{or} for the NTD and PSTD cells:

Table 12.a: Mean F-FCH E_c/I_{or} , NTD and PSTD cells

		F-FCH Ec/Ior: mean (dB)	
		NTD cell	PSTD cell
route	1	-16.4	-16.6
	2	-17.2	-17.3
	3	-14.9	-14.2
	4	-16.1	-16.2

Table 12.b: Mean F-FCH E_c/I_{or} , NTD and PSTD cells

		F-FCH Ec/Ior: standard deviation (dB)	
		NTD cell	PSTD cell
route	1	2.2	2.0
	2	2.4	2.1
	3	2.9	3.4
	4	2.3	1.8

Comparing tables 12.a and 12.b, there does not appear to be a correlation between mean and standard deviation of F-FCH E_c/I_{or}. Table 12.b does suggest, however, that PSTD reduces the variance of the required E_c/I_{or} for slower channel conditions (route 4) but increases the same variance for faster channels (route 3).

As can been in table 12.a, PSTD offers small improvement for routes 1, 2 and 4 but appears to hamper performance in route 3. The ineffectiveness of PSTD in route 3 is expected: PSTD works best in slow fading channels, whereas channel 3 corresponds to the fastest fading channel among the four routes.

As explained in chapter 1, PSTD was designed to improve time diversity in scenarios of slow and flat fading, where neither time nor frequency (multipath) diversity are present. The data in section 6.3.3 suggests, however, that many resolvable paths were present in all routes; therefore, there appears to be less scope for PSTD improvement since the channels encountered were not flat-faded channels. In addition, it is worth noting that route 4, being the slowest-fading channel, would be best suited for PSTD improvement; at the same time, route 4 was also the route with the largest number of resolvable multipaths, therefore limiting the possible benefits of PSTD.

Two lab experiments were conducted in an attempt to validate the assertions that PSTD offers the best benefit in slow and flat fading channels. Like was done in chapter 5, these experiments consisted in setting up test calls under well-known channel models and comparing performance by measuring the required F-FCH E_c/I_{or} required to achieve a 1% FER. The call parameters are the same as described in chapters 4 and 5, differing from the field parameters only by the use of Radio Configuration 3 (RC3) for the forward-link channels.

The channel models used are shown in tables 13 and 14. Table 13 represents a low-speed, 2-path Rayleigh-faded channel while table 14 represents a high-speed, 3-path Rayleigh-faded channel. The multipath structures were the same for the common and diversity antenna, with fading uncorrelated across all paths.

Table 13: 2-path Rayleigh-fading channel model

Multipaths	P1	P2
Fraction of Tx power	0.5	0.5
delay (us)	0	2
speed (km/h)	3	

Table 14: 3-path Rayleigh-fading channel model

Multipaths	P1	P2	P3
Fraction of Tx power	0.4	0.4	0.2
delay (us)	0	2	14.5
speed (km/h)	100		

Both NTD and PSTD were tested under both models. The 2-path model was tested for geometries of 3dB and 9dB, whereas the 3-path model was tested for a 9dB geometry.

Table 15 shows the results:

Table 15: F-FCH E_c/I_{or} (dB) required for a 1% FER

	2-path		3-path
Geometry	3dB	9dB	9dB
NTD	-11.38	-12.39	-13.78
PSTD	-14.7	-16.15	-14.41

The use of PSTD results in an improvement of 3.5dB for the slow, 2-path fading channel for both geometries. For the high-speed 3-path channel, however, the improvement is only 0.63 dB. These results appear to validate the fact that PSTD provides the largest improvement in slow and flat fading scenarios; since such a scenario was not seen in the field, the observed PSTD improvements were small.

6.3.7.2 NTD vs. STS

Table 16.b shows the field results for the STS-cell tests; the NTD-only values from table 12 are repeated in table 16.a for easy reference:

Table 16.a: Mean and standard deviation of F-FCH E_c/I_{or}, NTD-only cell

		FCH Ec/Ior (dB), NTD cell	
		mean	st dev
route	1	-16.4	2.2
	2	-17.2	2.4
	3	-14.9	2.9
	4	-16.1	2.3

Table 16.b: Mean F-FCH E_c/I_{or}, STS cells

F-FCH Ec/Ior: mean (dB)									
		STS cell							
		TD -3dB				TD -6dB			
		load 2	load 3	load 4	load 5	load 2	load 3	load 4	load 5
route	mobile								
1	NTD	-15.3	-15.7	-15.5	-15.5	-15.7	-15.4	-15.8	-15.5
	STS	-18.2	-18.9	-19.3	-19.4	-17.9	-18.5	-19.0	-19.1
2	NTD	-16.9	-16.9	-16.1	-15.1	-17.0	-17.0	-16.3	-15.3
	STS	-20.2	-20.3	-20.7	-20.6	-19.4	-19.9	-20.4	-20.5
3	NTD	-14.0	-14.0	-14.4	-14.0	-13.9	-14.5	-14.4	-14.1
	STS	-17.6	-16.8	-18.4	-18.5	-16.8	-17.1	-17.8	-18.1
4	NTD	-16.1	-16.0	-16.0	-15.8	-15.9	-16.0	-15.9	-15.9
	STS	-18.8	-18.8	-19.0	-19.2	-17.7	-18.0	-18.3	-18.8

Table 16.c: Standard deviation of F-FCH E_c/I_{or}, STS cells

F-FCH Ec/Ior: standard deviation (dB)									
		STS cell							
		TD -3dB				TD -6dB			
		load 2	load 3	load 4	load 5	load 2	load 3	load 4	load 5
route	mobile								
1	NTD	2.6	2.6	2.6	2.8	2.6	2.8	2.5	2.8
	STS	2.6	2.4	2.3	2.2	2.6	2.4	2.4	2.2
2	NTD	2.6	2.9	2.9	3.2	2.6	2.6	2.8	3.2
	STS	2.8	2.8	2.5	2.5	2.8	2.7	2.5	2.3
3	NTD	3.3	3.6	3.3	3.7	3.4	3.3	3.2	3.3
	STS	3.2	4.0	3.4	3.6	3.3	3.4	3.4	3.5
4	NTD	2.4	2.4	2.5	2.7	2.3	2.3	2.4	2.7
	STS	2.4	2.3	2.2	2.2	2.4	2.4	2.3	2.3

The results in table 16.b show that the mean required E_c/I_{or} is 2-3dB lower for STS when compared to NTD. This relative improvement is the result of two factors:

1. NTD degradation due to the power from the diversity antenna.
2. STS improvement due to transmit diversity.

The next two subsections examine each of these in turn.

6.3.7.2.1 NTD degradation due to power from the diversity antenna

As explained in chapter 5, the higher levels of NTD degradation should correspond to higher diversity-antenna power levels, or equivalently, higher loading scenarios. Therefore, loading 5 should correspond to the highest levels of NTD degradation; the values in table 16.b show that this is generally the case.

Comparing the NTD-mobile values for loading 5 in table 16.b to the reference value in table 16.a, it can be seen that:

1. A degradation of approximately 1 dB is observed for routes 1 and 3.
2. Route 2 presents a degradation of almost 2 dB.
3. Route 4 does not present a significant degradation.

To some extent, these results corroborate what had already been observed in section 6.3.2. As mentioned in that section, route 2 presented the highest geometry, so a high degradation was expected. It was also mentioned that the diversity signal appeared to have a smaller impact in signal demodulation for route 4; since the diversity signal is responsible for NTD degradation, this result might partially justify the lack of degradation for that route.

Further inspection of table 16.b indicates that the NTD degradation is independent of the diversity-pilot level. In addition, the 1 dB degradation in routes 1 and 3 is independent of the loading scenario, whereas the degradation in route 2 is only significant for loading scenarios 4 and 5. These results suggest that the power distribution across the two antennas plays a bigger role in degradation for higher-geometry scenarios.

Comparison between the NTD-mobile values in table 16.c and the reference values in table 16.a shows that the standard deviation of the E_c/I_{or} increases for an NTD mobile when STS is enabled in the cell. These results are in line with the models developed in chapter 5: as explained in that chapter, post-demodulation SNR is given by:

$$SNR = 2N_c^{\,2}\frac{E_c}{I_{or}}\frac{H^2}{a^2 H_{cr,1}^{\,2} + \frac{I_{oc}}{I_{or}} H_N^{\,2}} \qquad (6.2)$$

for a NTD mobile in a NTD-only cell, and:

$$SNR = 2N_c^2 \frac{E_c}{I_{or}} \frac{H^2}{a^2\left[f{H_{cr,1}}^2 + (1-f)\left|H_{cr,2}\right|^2 + 2\sqrt{f(1-f)}H_{cr,1}\,\mathrm{Re}\{H_{cr,2}^*\}\right] + \frac{I_{oc}}{I_{or}}{H_N}^2}$$

(6.3)

for a NTD mobile in an STS-enabled cell.

In equation (6.2), H, H_N and $H_{cr,1}$ are constants depending only on the channel coefficients from the common antenna to the mobile. On the other hand, $H_{cr,2}$ in equation (6.3) depends on the channel coefficients from both the common and the diversity antennas. The right-most fraction of (6.3) thus has a larger number of degrees of freedom than the last fraction in (6.2).

Since the E_c/I_{or} has to compensate for the larger variance in (6.3) in order to achieve a constant signal-to-noise ratio at the receiver, the E_c/I_{or} itself has a larger variance for a NTD mobile in an STS cell. In addition, since the channel coefficients from the diversity antenna are scaled by the power coming from the diversity antenna, a larger loading scenario results in higher variance for F-FCH E_c/I_{or} - a trend that can also be seen in table 16.c.

6.3.7.2.2 STS improvement due to transmit diversity

Comparing the required E_c/I_{or} values for the STS mobile with the reference value for a NTD mobile in table 16.a, it can be seen that STS provides a benefit of approximately 2-3dB in all cases. In addition, comparing values for the TD-3dB and TD-6dB for the same route and loading scenario, it can be seen that TD-3 pilot provides an additional benefit between 0.3dB and 0.8dB in most cases.

The data in table 16.b also suggests that STS performance improves with increasing loading scenarios; in fact, the STS-mobile E_c/I_{or} is smallest for loading scenario 5 under almost all combinations of route and diversity pilot. It appears that given a fixed base-station transmit power, the post-demodulation in-cell interference for an STS mobile is lower when the transmit power is more evenly distributed across the two antennas.

Examination of the values in 16.c does not indicate any consistent trend for the FCH E_c/I_{or} standard deviation for STS mobiles.

6.3.8 Field results: conclusions

The following is a summary of the most significant trends observed in sections 6.3.1 to 6.3.7:

1. The average geometry in the field ranged between 5dB and 9dB.

2. The channel presented a large number of resolvable paths, with 1-2 strong paths and 2-3 weaker paths for each route; therefore, multipath diversity was present in the field and possibly reduced the potential improvements brought by transmit diversity.

3. Path delays were highly correlated between the two antennas.

4. Mobile setpoint was slightly lower for STS than for NTD, with the -3dB diversity pilot resulting in lower setpoint values. In addition, NTD-mobile setpoint increased with faster fading channels and higher levels of diversity-antenna power.

5. NTD mobiles suffered a degradation of 1-2dB in F-FCH E_c/I_{or} when in an STS-enabled cell at city-driving speeds. In addition, the F-FCH E_c/I_{or} values for an STS mobile on an STS cell were generally 2-3dB lower than those of a NTD-mobile in a standard NTD-cell.

The difference between NTD and PSTD was small for all the metrics.

6.4 Cell capacity estimation

This section attempts to obtain an estimate of cell capacity for each transmit diversity technique (STS-3dB, STS-6dB, PSTD) and each loading scenario (if applicable). The approach used is similar to the one in chapter 3 and relies on the transmitted F-FCH E_c/I_{or} values; in particular, it is assumed that total base-station transmit power is fixed at a certain I_{or} value.

For each combination of transmit diversity technique and loading scenario, a single E_c/I_{or} value was computed by averaging the E_c/I_{or} for the individual tests[45]; this unified value corresponds to the required E_c/I_{or} for full-rate calls. The cell capacity is estimated by assuming that this unified E_c/I_{or} value is a good estimate of the average E_c/I_{or} required for a full-rate voice call by a typical mobile in the cell.

To obtain the final capacity estimate, an "average-rate" E_c/I_{or} is computed from the full-rate E_c/I_{or}. Section 6.4.1 explains how this average-rate E_c/I_{or} is computed; section 6.4.2 explains how the average-rate E_c/I_{or} is used to compute the cell capacity, and presents the results.

6.4.1 Average voice rate

The E_c/I_{or} values computed from the field correspond to full-rate calls. In practice, voice calls do not use full-rate all the time, but instead use variable rates to account for varying levels of voice activity. Based on the study performed in [14], the following rate probabilities will be assumed for a typical voice call:

[45] 12 tests total, corresponding to 3 runs for each of the 4 routes.

Table 17: Probabilities of different rates during a voice call

	Prob	Ec/Ior (dB)
Full rate	0.438	X
1/2 rate	0.057	X-3
1/8 rate	0.505	X-9

In a half-rate call, each symbol is repeated twice; therefore, for a given the F-FCH E_c/I_{or}, the energy-per-bit for a half-rate call is twice that of a full-rate call. It will be assumed that the energy-per-bit required to achieve a target FER is the same regardless of the data rate; this implies that for a half-rate call the required E_c/I_{or} to achieve a target FER is half that required for a full-rate call. For similar reasons, the E_c/I_{or} required for a 1/8-rate call is also 9dB lower than that required for a full-rate call. The second column in table 17 uses these assumptions.

From the values in table 4, the average-rate E_c/I_{or} (expressed in dB) is computed to be:

$$\left(\frac{E_c}{I_{or}}\right)_{avg} = 10 * \log\left(0.438 * 10^{X/10} + 0.057 * 10^{(X-3)/10} + 0.505 * 10^{(X-9)/10}\right)$$

6.4.2 Computing sector capacity

Using the same notation defined in chapter 3, let X be total transmitted STS traffic power and Y be total transmitted NTD traffic power. The number of NTD and STS users supported by the cell is given by:

$$n_{NTD} = \frac{Y}{\left(\frac{E_c}{I_{or}}\right)_{avg,NTD}}$$

$$n_{STS} = \frac{X}{\left(\frac{E_c}{I_{or}}\right)_{avg,STS}}$$

Table 18 shows the numbers obtained.

Table 18: Cell sector capacity for different field scenarios

			TD PICH -3 dB					TD PICH -6 dB			
	load 1		**load 2**	**load 3**	**load 4**	**load 5**		**load 2**	**load 3**	**load 4**	**load 5**
NTD users	50		36	33	17	1		44	40	20	1
STS users	0		1	8	46	90		1	8	44	92
Total users	50		37	41	63	91		45	48	64	93

In addition, this method estimated a capacity of 56 users for a PSTD cell.

The absolute numbers presented in table 18 are likely to be higher than what is achievable in commercial CDMA networks, primarily because all testing was done in a single isolated cell. As explained in chapter 2, in a real cell a fraction of the traffic channels is reserved for handoff activities; this overhead was not captured in the estimates. In addition, the method used for estimation of base-station capacity is overly simplistic as it attempts to encompass the cell variability into a single metric - namely a single F-FCH E_c/I_{or} for all mobiles in a cell. A more realistic estimate would have to consider the distribution of mobiles across different regions of the cell, and include the impact of handoff on required F-FCH E_c/I_{or}.

At the same time, since these limitations were the same across all cases, the numbers in table 18 should still present a good basis for comparing the different techniques. Therefore, the analysis of cell capacity will focus on the ratio between the capacity for a certain technique and the capacity for load 1 (reference NTD-only cell); this ratio will be denominated *relative forward-link capacity*.

The results indicate that PSTD provides a relative forward-link capacity of only 12%. Despite the small improvement, PSTD may be worthwhile because it can potentially improve performance of all mobiles in a cell. Since the technique does not require changes to the mobile receiver, it does not require users to upgrade their mobile phones - making the technique easier to deploy.

For the STS tests, figure 5 plots the relative forward-link capacity as a function of the STS user penetration ratio, defined as the ratio of STS to NTD users in the cell.

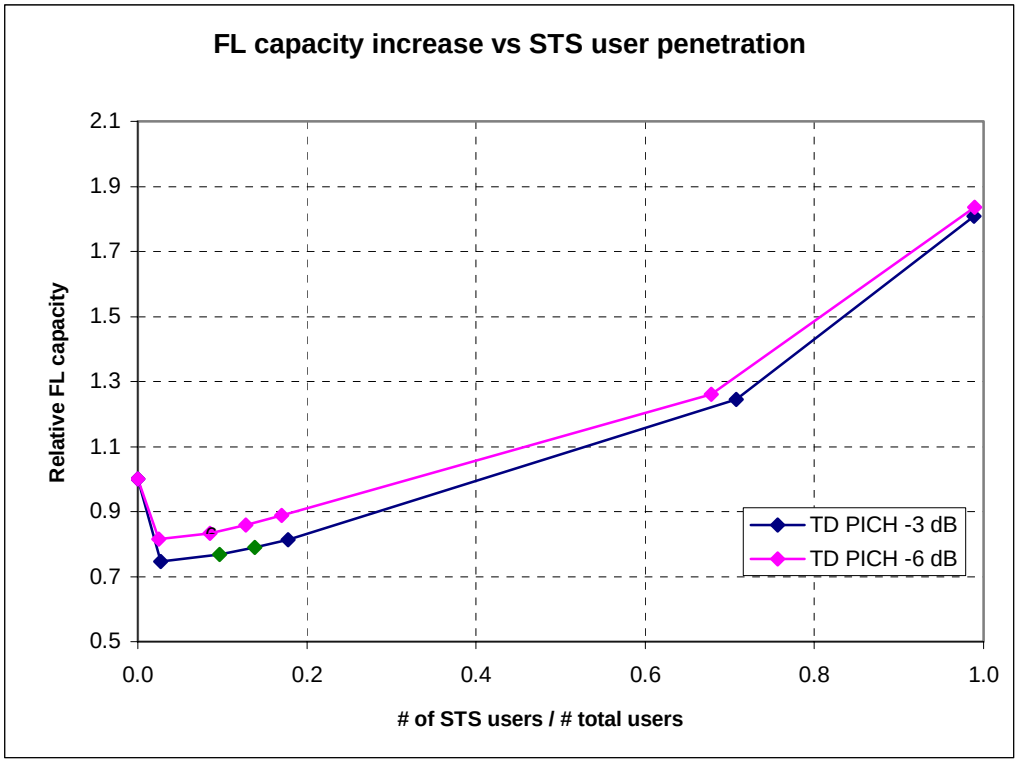

Figure 5: Plot of relative forward-link capacity vs. STS user penetration

The plot suggests that a diversity pilot of –6dB results in greater capacity than a diversity pilot of –3dB for all user penetrations. The plot also suggests that STS is a worthwhile technique at high STS user penetrations: in particular, as the user penetration approaches 1 – equivalently, as all mobiles upgrade to STS – cell capacity increases by 80%.

At the same time, the plot illustrates that at low STS user penetrations there is actually a capacity loss. This capacity loss results from the NTD performance degradation in an STS cell; at low STS user penetrations, the improved performance of the small number of STS users is not enough to counter the performance degradation suffered by the majority NTD users. More precisely, the plot shows that there is a 20% capacity loss just by turning on the diversity pilot. In addition, the plot suggests that a cell requires at least 35% STS users just to break even and reach the capacity of a legacy NTD cell.

It can be seen that STS deployment involves a tradeoff: while the potential benefits are high for high user penetrations, early stages of deployment would likely result in capacity losses. It is an open question whether the potential benefits compensate for the losses incurred in early deployment stages.

Conclusion

This dissertation presented an evaluation of the performance improvements of two transmit diversity schemes for cdma2000: *Space-Time Spreading* (STS) and *Phase-Sweep Transmit Diversity* (PSTD). These improvements were determined relative to the performance of *No Transmit Diversity* (NTD).

Preliminary simulation results indicated that both STS and PSTD provide significant link-level improvement compared to NTD, particularly in low-speed channels. For these low-speed scenarios, the link-level improvements translated into cell-capacity increases of over 100% for both STS and PSTD; in addition, capacity improvements on the order of 20% were observed even for high-speed channels. In the case of STS, the capacity improvement was significantly influenced by the diversity-pilot level. More specifically, the simulations showed that diversity pilots of -3dB and -6dB with respect to the main pilot provided the greatest increases in cell capacity. Simulations therefore suggested that these two diversity pilot levels represented the optimal tradeoff between diversity-pilot channel acquisition and overhead power consumption.

It was also shown that in cells with a mix of NTD and STS mobiles, the signal from the diversity antenna imposes significant interference to legacy NTD mobiles. This interference was shown to increase with higher ratios of STS to NTD mobiles in the cell. In addition, this interference was shown to increase with mobile geometry because in higher geometry scenarios the interference from the diversity-antenna signal dominates other-cell interference. Lab experiments concluded that STS interference on NTD can be responsible for increases of up to 1.5 dB in required transmit power to achieve a target receiver error-rate for NTD mobiles.

The field results did not indicate a large improvement for PSTD over NTD, suggesting only a 12% capacity increase. A possible explanation for this phenomenon might be the large number of multipaths present in the field; these multipaths provide significant frequency diversity to the receiver, therefore reducing the potential benefits of PSTD-induced time diversity.

The field results suggest that STS provides a performance improvement of 2-3dB over NTD in required transmit power, resulting in capacity increases of over 80% for cells in which all mobiles support STS. At the same time, enabling STS results in reduced capacity in cells where fewer than 35% of the mobiles support STS; this reduction in capacity is due to the degradation caused by STS interference on the majority NTD mobiles present in the cell. It is an open question whether the potential capacity increases compensate for any transitional losses incurred while users upgrade their mobile phones.

References

[1] J. Proakis, “Digital Communications”, Fourth Edition, McGraw-Hill, 2000.

[2] D. Tse, P. Viswanath, “Fundamentals of Wireless Communications”, 2003.

[3] T. S. Rappaport, “Wireless Communications, Principles & Practice”, First Edition, Prentice hall, 1996.

[4] V. Garg, “IS-95 CDMA and CDMA2000 – Cellular/PCS Systems Implementation”, Prentice Hall, 2000.

[5] V. Vanghi, A. Damjanovic, B. Vojcic, “The CDMA2000 System for Mobile Communications”, Prentice Hall, 2004.

[6] 3GPP2, Physical Layer Standard for CDMA2000 Spread Spectrum Systems, October 2000.

[7] V. Roussel, “Adaptive Antennas”, Industrial Thesis, Qualcomm Inc/Eurecom Institute, July 2000.

[8] S. Alamouti, “A Simple Transmit Diversity Scheme for Wireless Communications”, IEEE Journal for Select Areas in Communications, Vol. 16, No. 8, October 1998.

[9] A. Kogiantis, R. Soni, B. HochWald, C. Papadias, “Downlink Improvement through Space-Time Spreading”, Lucent Technologies, 1999

[10] H. Hochwald, T. Marzetta, C. Papadias, “A Transmitter Diversity Scheme for Wideband CDMA Systems Based on Space-Time Spreading”, IEEE Journal on Selected Areas in Communications, Vol. 19, No.1, January 2001.

[11] R.M. Buehrer, R. A. Soni, R.D. Benning, “Transmit Diversity for Combined 2G and 3G CDMA Systems”, Lucent Technologies, 2002.

[12] “DV Strawman”, Qualcomm Internal Memo, 3GPP2 (1x-EVDV) group.

[13] S. Patel, “STS vs. PSTD Performance Comparison”, Qualcomm Internal Memo, 02/04/03

[14] J. Yeh, “Forward and Reverse Link Capacity Gains of SMV”, Qualcomm Internal Memo, 05/22/03